UPPER CRITICAL FIELD OF INHOMOGENEOUS SUPERCONDUCTORS

BOJIONG YUAN

UPPER CRITICAL FIELD OF INHOMOGENEOUS SUPERCONDUCTORS

By

Bojiong Yuan

M. Sc., Memorial University of Newfoundland

A THESIS SUBMITTED IN PARTIAL FULFILLMENT OF

THE REQUIREMENTS FOR THE DEGREE OF

DOCTOR OF PHILOSOPHY

in

THE FACULTY OF GRADUATE STUDIES

DEPARTMENT OF PHYSICS

We accept this thesis as conforming

to the required standard

MEMORIAL UNIVERSITY OF NEWFOUNDLAND

1994

Abstract

The thesis consists of two distinct but closely related parts. In the first part we present an analysis of the angular dependence of the upper critical field of a type II superconducting film, using the de Gennes-Werthamer formalism. The results are presented for a range of thicknesses, which includes the special case of the semi-infinite geometry, and for all orientations $0 < \theta < \pi/2$. It is shown that careful consideration is required to recover the limiting parallel field case ($\theta \rightarrow 0$) from the finite θ calculation. A comparison with earlier work in this area is given and it is shown that more detailed and systematic experimental studies are required in order to resolve the differences between experiment and theory. In the second part, the temperature dependence of the parallel upper critical field for a layered superconductor is investigated within the framework of de Gennes-Werthamer theory. The resultant upper critical field curves are shown to be strongly dependent upon the presence of the free surface and the character of the initial layer deposited on an insulated substrate. A direct comparison of the calculated upper critical field curves with the experimental results on Nb/NbZr layered structures is given. The results are in good agreement provided the pair-breaking effect of the spin paramagnetism is included.

Acknowledgements

It is my great pleasure to thank all those who contributed to this dissertation. I wish to thank my thesis supervisor, Dr. J. P. Whitehead, for his knowledgeable and skillful direction of my research, encouragement for me to explore new phenomena in superconductivity, guidance of an interesting research topic, and helpful assistance in completing this thesis.

I am indebted to Professor M. D. Whitmore for his supervision during the year when Dr. J. P. Whitehead was on sabbatical leave. The tremendous amount of time Professor Whitmore spent in many stimulating and valuable discussions on my research topic provided great help for completing the research work contained in this thesis. I also wish to thank Dr. J. de Bruyn for his participation in my Supervisor's Committee. I thank Dr. N. H. Rich for his remarkable service as Graduate Officer in the Department of Physics.

I am grateful to Mrs. J. Barron for her efficient and kind service concerning the needs of a foreign student.

I gratefully acknowledge the financial assistance provided by the School of Graduate Studies and Department of Physics in the form of Graduate Fellowships and Teaching Assistantships.

I would like to thank my fellow graduate students Mr. A. B. MacIsaac, Mr. R. Baranowski, Mr. T. Andrews, Mr. Y. R. Kuang and Mr. D. Lu for sharing their knowledge and helping in many ways during my stay in St. John's.

Particularly, I would like to sincerely thank to my wife, Jun Ren, for her interest,

support, and encouragement during my Ph. D. program and staying with me in Newfoundland, and my son, Francis, who gave me the motivation, strength and courage to accomplish this dissertation.

Table of Contents

List of Tables

List of Figures

Chapter 1

Introduction

In 1911, Kamerlingh Onnes [1] discovered the superconducting state characterized by the appearance of zero electrical resistance of a metal, below a certain temperature, referred to as the transition temperature T_c. The subsequent discovery of the Meissner effect [2] revealed a more fundamental aspect of superconductivity. The Meissner effect is idealized as a total expulsion of the magnetic flux from a metal in the superconducting state placed in a weak magnetic field.

In the class of materials referred to as type I superconductors, the total expulsion of the magnetic flux from the superconductor, referred to as the Meissner state, persists up to some critical field $H_c(T)$, above which the metal makes a first order transition to the normal state. The reversibility of the Meissner effect indicates that the superconducting Meissner state is a thermodynamic state. The difference in free energy between the normal state and the superconducting state in zero field may be expressed in terms of the critical field as $H_c^2(T)/(8\pi)$. This free energy difference is typically referred to as the condensation energy and $H_c(T)$ as the thermodynamical critical field. Early experiments [3] further showed that the condensation energy goes to zero as $T \to T_c$, indicating that the transition to the superconducting state in zero field is a continuous transition.

One of earliest theoretical descriptions of the superconducting state, proposed by Ginzburg and Landau (GL) [4], was based on the premise that the superconducting state was characterized by the appearance of an order parameter described

by a complex macroscopic quantum mechanical wave function, $|\Psi(\mathbf{x})|e^{i\varphi(\mathbf{x})}$, where $|\Psi(\mathbf{x})|^2$ is identified as the number density of superconducting carriers with charge $e^* = 2e$. Due to the continuous nature of the transition at $T = T_c$, it was further assumed that the order parameter went to zero in the limit $T \to T_c$. This implies that the condensation energy could be expanded as a functional Taylor series in powers of the order parameter and its spatial derivatives, subject to the basic requirements of symmetry, such as translational invariance and phase invariance, of the free energy functional. It was shown that the qualitative description of the superconducting state close to T_c required that only quadratic terms in the spatial derivatives of the order parameter, and quadratic and quartic terms in the order parameter, need be retained. The response of the superconductor to an applied magnetic field is accomplished, in the GL theory, by the gauge invariant replacement $\nabla \to (\nabla - i\frac{2\pi}{\phi_o}\mathbf{A})$, where $\mathbf{A}$ denotes the vector potential ($\mathbf{h} = \nabla \times \mathbf{A}$) and ϕ_o denotes the flux quantum $\phi_o = \frac{hc}{e^*}$.

The contribution of the gauge invariant derivative of the complex wave function, $|\Psi(\mathbf{x})|e^{i\varphi(\mathbf{x})}$, to the free energy in GL theory may be separated into two distinct parts. The first part relates to the spatial variation of the amplitude, $(\nabla|\Psi(\mathbf{x})|)^2$, while the second part relates to the spatial variation of the phase, which appears through the gauge invariant contribution $\frac{1}{2m^*}[\nabla\varphi - \frac{2\pi}{\phi_o}\mathbf{A}]^2$. This second part can be identified as the contribution of the Meissner current [5]. An analysis of the electromagnetic response of the superconducting state in the framework of the GL theory recovers the earlier result obtained by the phenomenological London theory [6] that the magnetic flux in a superconducting metal is quantized with a flux quantum ϕ_o.

The minimization of the GL free energy, to obtain the equilibrium state, yields a set of coupled non-linear partial differential equations for the spatial variation of the order parameter $\Psi(\mathbf{x})$ and the magnetic field. The equations are expressed in terms

of two distinct length scales $\xi(T)$ and $\lambda(T)$, where $\xi(T)$ is the GL coherence length which describes the length scale associated with the spatial variation of the order parameter and $\lambda(T)$ is the penetration depth associated with the spatial variation the internal magnetic field $h(\mathbf{x})$. It is possible to rescale the GL free energy, order parameter and length scales such that the resultant equations depend only on a single temperature-independent parameter $\kappa = \lambda/\xi$.

Abrikosov pointed out [7] that for metals such that $\kappa > \frac{1}{\sqrt{2}}$, the Meissner state is thermodynamically unstable above a certain value of the applied external field, referred to as lower critical field H_{c1}. This instability arises as a consequence of the negative surface energy associated with the interface between superconducting and normal domains in the GL theory for $\kappa > \frac{1}{\sqrt{2}}$. At the lower critical field, the Meissner state collapses, allowing magnetic flux to enter the bulk of the superconductor in the form of vortices. Each vortex carries a single quantum of flux. As the applied field further increases, more flux quanta enter the superconductor and form a magnetic vortex lattice. At a particular value of the applied field, referred to as the upper critical field H_{c2}, the superconductor undergoes a continuous phase transition to the normal phase. The superconducting state at H_{c2} is characterized by the vanishing magnitude of the order parameter $|\Psi| \rightarrow 0$ and an uniform internal field $h(\mathbf{x}) \rightarrow H$. The superconducting state existing between H_{c1} and H_{c2}, with the vortex lattice structure, is referred to as the mixed state. A metal with $\kappa > \frac{1}{\sqrt{2}}$ is identified as a type II superconductor. It is possible to introduce a third length scale associated with the vortex lattice defined by $\xi_H = \sqrt{\frac{\phi_o}{2\pi H}}$, where ξ_H^{-2} may be identified as the number density of magnetic flux quanta in units of $\frac{\phi_o}{2\pi}$.

For $\kappa < \frac{1}{\sqrt{2}}$, the surface energy associated with the interface between superconducting and normal domains is positive and the superconducting state is dominated by the Meissner effect. Nevertheless, instead of a total expulsion of the magnetic flux

as expected, the superconductor may exhibit a domain structure consisting of distinct superconducting and normal regions, due to demagnetization effects associated with the shape of the specimen. This state is usually referred to as the intermediate state. The particular value $\kappa = \frac{1}{\sqrt{2}}$ thus provides a criterion for distinguishing between a type I and a type II superconductor. While GL theory gives rise to an impressive description of superconductivity, the superconducting order parameter in the GL theory was nevertheless introduced phenomenologically and provides no information as to the microscopic nature of the superconducting state. The validity of the GL theory was later verified by Gor'kov's [8] work in connecting the GL order parameter to the pair amplitude of the microscopic BCS theory [9].

The microscopic origin of superconductivity was first given in a model proposed by Bardeen, Cooper and Schrieffer [9] (BCS). In the BCS theory, the phonon mediated attractive interaction among the electrons in a metal gives rise to an instability of the Fermi surface in the normal phase and a new microscopic state appears corresponding to a lower ground state energy, in which the electrons near the Fermi surface with opposite momenta and spin bind to form Cooper pairs. At low temperature, the pairs are correlated within the BCS coherence length ξ_o. The study of the excitation spectrum in a self-consistent mean field approximation reveals the existence of an energy gap $\Delta(T)$ in the quasi-electron spectrum, which increases continuously from zero at $T = T_c$ to a saturated value $\Delta(0)$ at $T \ll T_c$. Many of the superconducting properties can be interpreted in terms of the BCS theory by virtue of the existence of this energy gap. The superconducting transition temperature T_c of a metal relates to the energy gap at zero temperature through $\frac{\Delta(0)}{k_B T_c} = 1.764$ and the relative finite difference of specific heat of the electrons at T_c is expressed as $\frac{(C_s - C_n)}{C_n}\Big|_{T_c} = \frac{12}{7\zeta(3)} = 1.43$ with ζ denoting the Riemman zeta function. These

relations, which BCS theory predicts are universal, are satisfied to a good approximation by a large class of superconducting materials and deviations from them can be accounted for by generalizations of BCS theory, e.g. strong coupling theory. It is nevertheless difficult to apply the BCS theory to an inhomogeneous superconducting system due to the complex self-consistency condition required by the microscopic theory.

Gor'kov [8] successfully derived the Ginzburg-Landau equations from the microscopic BCS theory [9] close to the transition temperature, T_c, by means of a Green's function method. He showed that the fact that the charge e^* in the phenomenological GL theory equals $2e$ is consistent with the microscopic pairing mechanism, and that the spatially varying microscopic pair amplitude, $\mathcal{F} \equiv \langle \psi_\uparrow(\mathbf{x})\psi_\downarrow(\mathbf{x}')\rangle$, where $\psi_\alpha(\mathbf{x})$ denotes the wave function of an electron with spin α, was proportional to the GL macroscopic quantum wave function $\Psi(\mathbf{x})$. In particular, $\langle \psi_\uparrow(\mathbf{x})\psi_\downarrow(\mathbf{x}')\rangle \neq 0$ indicates the appearance of off-diagonal long range order in the superconducting state and that the phase symmetry of the Hamiltonian is broken in the superconducting state. The equivalence of the spatial variation of the pair amplitude in the BCS theory and the phenomenological order parameter in the GL theory allows a definition of the GL coherence length and penetration depth in terms of the microscopic parameters of the BCS theory.

The microscopically derived GL theory is usually referred to as Ginzburg-Landau-Abrikosov-Gor'kov (GLAG) theory. This derivation later was extended by Maki [10] and de Gennes [11] to include the entire temperature range close to the upper critical field $H \lesssim H_{c2}$ in the dirty limit $l \ll \xi_o$ where l denotes the mean free path. A further generalization of the GLAG theory for arbitrary mean free path was proposed by Helfand-Werthamer-Maki-Tsuzuki-Eilenberger [12, 13, 14, 15], referred to as HWMTE theory. It is important to note, however, that the HWMTE theory is

derived only for the case of a homogeneous superconducting sample in a constant magnetic field, while the dirty limit theory proposed by Maki and de Gennes is valid for samples of arbitrary shape [16].

In addition to its importance in determining the electromagnetic properties of type II superconductors in the mixed state, the spatial variation of the GL order parameter plays an important role in properties associated with geometry, in which the length scale is comparable with those length scales in GL theory. Earlier experimental evidence, which serves to illustrate the importance of the geometry, was given by Khukhareva [17] in his experiments on the critical field of a superconducting mercury film in a parallel applied field. Khukhareva showed that the critical field varies inversely as the thickness of the film d and that, close to the transition temperature T_c, the critical field varies as $H_c \propto \sqrt{T_c - T}$, in contrast to what is observed in a bulk sample, in which case $H_c \propto (T_c - T)$. The theoretical description of the thickness-dependent critical field behavior may be obtained within the framework of the linearized GL theory in the thin film limit [10], together with the GL boundary condition that $(\nabla - i\frac{2\pi}{\phi_o}\mathbf{A})_n \Psi = 0$, where n denotes the component normal to the film surface. It should be noted that this choice of boundary condition is based on the experimental observation that the superconducting film has the same transition temperature T_c at zero applied field as the bulk material. In contrast, the other possible boundary condition, $\Psi = 0$ at the surface, yields a zero transition temperature in the thin film limit [18], in contradiction with experimental observation.

The studies of the upper critical field for this simple film geometry with arbitrary thickness d were then extended by Saint-James and de Gennes [19], and Tinkham [20] using the linearized GL theory. In the former case, Saint-James and de Gennes showed that when the field is applied parallel to the film, then, for moderately thick

films, the order parameter at the upper critical field was confined to a region $\sim \xi_H$ near the surface. This surface superconducting state results in an enhancement of the upper critical field even in the limit $d \to \infty$. The upper critical field is generally referred to as H_{c3} and satisfies the relation $H_{c3}/H_{c2} = 1.69$. In the thin film limit, $d \to 0$, Tinkham derived an approximate analytical expression for the angular dependence of the upper critical field, $H(\theta)$, at fixed temperature T and thus related the experimental measurement of the angle-dependent upper critical field to the geometrical anisotropy of the sample.

Saint-James [21] later studied the angular dependence of the upper critical field for films with arbitrary thickness in the limit $\theta \to 0$, within the framework of GL theory, by means of a perturbation expansion with respect to θ. In particular, Saint-James pointed out that the logarithmic derivative of the upper critical field with respect to θ, $\lim_{\theta \to 0} \frac{1}{H} \frac{\partial H(\theta)}{\partial \theta}\Big|_T$, as a function of $\frac{(d/2)^2}{\xi_H^2}$ exhibits a cusp at $d = 2.55\xi_H$, a qualitatively different result from that obtained earlier by Tinkham. The theoretical prediction of this cusp was subsequently confirmed experimentally [22, 23]. However, Thompson [24] pointed out that there was a mathematical error in Saint-James' perturbation expansion.

The existence of the finite slope in $H(\theta)$, in the limit $\theta \to 0$, and the cusp in the value of that slope at a particular value of reduced thickness, are the result of subtle and non-trivial aspects of the effects of geometry on the upper critical field and the crossover from two dimensional to three dimensional behavior. To understand this we note that in the parallel field case the magnetic field is screened by the persistent current in the surface of the superconductor. However, as the field is tilted the flux must penetrate the superconductor. This indicates that a qualitative change in the spatial distribution of the internal magnetic field and current must occur as the field is being tilted. It is this that underlies the appearance of the finite slope

in $\lim_{\theta\to 0} \frac{1}{H}\frac{\partial H(\theta)}{\partial \theta}\Big|_T \neq 0$ in the limit $\theta \to 0$. The existence of the cusp arises as a consequence of the fact that the nature of the screening in the parallel field case changes qualitatively with the appearance of vortex states for $d > 2.55\xi_H$. The value of the slope and the appearance of the cusp are therefore a sensitive indicator of the effects of geometry, and the discrepancy between the results of Thompson [24] and Saint-James [21] is therefore of some importance. While a major portion of this thesis is concerned with the evaluation of the θ dependence of the upper critical field for films of arbitrary thickness, we examine very carefully the behavior in the limit $\theta \to 0$.

Another aspect of superconductivity in which the spatial variation of the pair amplitude plays an important role is the superconducting proximity effect. The proximity effect describes the phenomenon that occurs when two distinct metals, at least one of which is superconducting, are superposed in such a way that electrons from one can tunnel into the other. This effect gives rise to a wide variety of interesting phenomena. Most notably it can induce a finite pair amplitude in an non-superconducting metal. The simplest geometry in which the proximity effect plays an important role is in a metallic bilayer consisting of a film comprised of two distinct metals separated by a planar interface usually denoted by *NS*. The superconducting properties of such systems, notably the transition temperature and the upper critical field, have been the subject of considerable experimental and theoretical study.

An obvious generalization of the metallic bilayers are multilamellar structures such as superlattice geometries consisting of alternating layers of different types of metals. Such systems are of particular interest as the proximity effect can give rise to a spatial coherence in the order parameter that extends across many distinct layers. Such systems can exhibit the characteristics of both two dimensional systems,

typically associated with thin films, or three dimensional systems. A wide variety of such systems has been studied experimentally and theoretically, as described in the review article [25] by Jin and Ketterson, and are the subject of a major portion of the research described in this thesis.

Much of the recent theoretical work on the superconducting properties of proximity coupled superlattices is concerned with the calculation of the transition temperature and upper critical field for various combinations of metals [25]. Many of these calculations are based on the formalism proposed by de Gennes [26] in the 1960's, derived from the linearized Gor'kov theory. Writing the kernel that appears in the linearized Gor'kov equation as a sum over Matsubara frequencies $\omega_n = (2n+1)\pi k_B T$ $(n = 0, \pm 1, \pm 2, \cdots)$, de Gennes postulated that each term in the series would satisfy a diffusion equation, in which the spatial variation of the kernel is characterized by a Matsubara-frequency-dependent coherence length, $\xi_n = \sqrt{\frac{\hbar D}{2\omega_n}}$, where D denotes the electron diffusion constant. In particular, de Gennes solved the diffusion equation for two geometries, an semi-infinite geometry with one free surface and an infinite bilayer system with one interface. In the former case, de Gennes derived the boundary condition that the normal derivative of the kernel goes to zero at the free surface. This leads to the result that the normal derivative of the pair amplitude must also go to zero at the free surface. This derivation provides the microscopic basis for the phenomenological GL boundary condition, $(\nabla - i\frac{2\pi}{\phi_o}\mathbf{A})_n \Psi = 0$. In the latter case, de Gennes derived continuity conditions for the normal derivative and the amplitude of the kernel at the interface in terms of the diffusion constants, density of states at the Fermi surface and the BCS constants of the component metals. This leads to the boundary conditions for the pair amplitude $\mathcal{F}$ at the interface that $\mathcal{F}(\mathbf{x})/N_i$ and $D_i(\nabla - i\frac{2\pi}{\phi_o}\mathbf{A})_n \mathcal{F}(\mathbf{x})$ are continuous, where N_i denotes the density of states at Fermi surface and D_i denotes the diffusion constant for $i = N, S$ respectively. In the

absence of an applied field, de Gennes also showed that the thickness dependence of the transition temperature of a thin bilayer system NS reduces to the earlier result of Cooper [27] for an NS bilayer.

Using a somewhat different approach, based on the Green's function method, Werthamer [28] derived an explicit expression for the kernel of a homogeneous superconductor of arbitrary shape in the dirty limit and long wavelength approximation. The linearized Gor'kov integral equation was then cast into a differential equation satisfied by the pair amplitude in the superconducting geometry. Werthamer argued that the differential form of the linearized Gor'kov equation may be directly applied to a bilayer system together with a properly chosen continuity condition imposed on the pair amplitude at the interface. While Werthamer's formalism may be obtained in terms of de Gennes' theory in the one-frequency approximation for a thick bilayer system, it is nevertheless important to note that, for a thin bilayer system, the Cooper limit [27] can not be recovered in the Werthamer formalism. It is well established [25] that the Werthamer formalism usually overestimates the transition temperature of a thin bilayer system at zero field [29]. The quantitative difference between the result obtained from de Gennes' theory and that obtained from Werthamer's formalism may be attributed to the approximation taken by Werthamer, in which the non-local nature of the linearized Gor'kov theory for a thin bilayer system was ignored, while de Gennes treated the non-locality in the dirty limit exactly by solving the diffusion equation of the kernel for a bilayer system with arbitrary thickness.

Despite the fact that Werthamer's formalism is an approximate theory, it has been applied to a wide variety of bilayer and sandwich systems, incorporated with de Gennes' boundary conditions [26]. The formalism has also been extended to multilayer systems, based on the assumption that de Gennes' boundary conditions,

derived for the single interface case, can be generalized to the multi-interface case. It is expected that for a multilayer system composed of moderately thick layers, both Werthamer's formalism and de Gennes' boundary conditions are applicable. This case is usually referred to as the de Gennes-Werthamer (DW) proximity coupling theory.

Menon and Arnold [30] were the first to apply the DW theory to a bimetallic superlattice to study the transition temperature at zero field and the temperature dependence of the upper critical field. They concluded that the application of the DW theory in a superlattice reduces to solving for the ground state of the Cooper pair amplitude in a periodic potential. In the absence of an applied field, they found that the transition temperature T_c is enhanced in comparison with the corresponding bilayer system. In the parallel field case, they found that the upper critical field exhibits a temperature dependence, at high temperatures, similar to that of a bulk material, while at low temperatures, the upper critical field is dramatically enhanced, in analogy with the case of a superconducting film. This theoretical result provided a qualitative interpretation of the experimental phenomena found earlier in the work of Chun et al. on an Nb/Cu superlattice [31], and later in Broussard and Geballe's work on an Nb/Ta superlattice [32]. The dramatic enhancement of the upper critical field exhibited in its temperature dependence in a superlattice is referred to as dimensional crossover.

Biagi et al. [33] studied the superconductor-normal-metal superlattice using the dirty limit version [34] of the Eilenberger theory [35]. With properly chosen parameters, their theoretical results showed good agreement with experimental data [31] for the perpendicular upper critical field. In particular, it exhibits a positive curvature, $\frac{d^2H_\perp}{dT^2}$, at high temperatures consistent with experimental observation. Nevertheless, the temperature dependence of the parallel upper critical field, and

thus the dimensional crossover, were not covered in their work.

A systematic method of applying the de Gennes theory to a superlattice was later proposed by Takahashi and Tachiki [36] (TT), in which the calculation for both perpendicular and parallel upper critical fields from the linearized Gor'kov equation is reduced to solving an eigenvalue equation, incorporating the de Gennes continuity conditions at the interfaces of the superlattice. One interesting application of the TT formalism was to a superlattice consisting of two superconducting metals, which share the same bulk transition temperature ($T_S = T_N$) but which have different diffusion constants ($D_S \neq D_N$). As we will show later, the TT formalism reduces exactly to the DW formalism for this particular system. For particular ranges of the ratio D_S/D_N and the modulation length, they show that the parallel upper critical field exhibits a discontinuous slope as a function of temperature. This effect, referred to as the Takahashi-Tachiki effect, provides a critical experimental test of the application of the de Gennes theory of proximity coupling to multilayer systems. The subsequent experimental work of Karkut et al. [37] on Nb/NbTi superlattices, Kuwasawa et al. [38] on Nb/NbZr superlattices, and Aarts et al. [39, 40, 41] on Nb/NbZr superlattices, qualitatively confirmed the effect predicted by Takahashi and Tachiki. The TT theory was later generalized by Auvil, Ketterson and Song [42] to include spin-orbital scattering and spin paramagnetism. The transition temperature of a superlattice at zero field in the thin layer and thick layer cases, and the upper critical field behavior, were experimentally examined by Ketterson's group [25, 29, 43, 44, 45, 46, 47], and various theoretical results obtained from the DW theory and the TT theory were compared with the experimental data. In the absence of an applied field, they showed [25] that the transition temperatures calculated for both the bilayer and the superlattice system using the TT formalism in the thin layer case are in good agreement with the experimental data. For the

thick layer case, the theoretical results obtained from both the TT and the DW formalism agree with the experimental data.

In addition to the development of the DW theory, the application of the dirty limit version of Eilenberger theory [34, 35] to superconductor-ferromagnet superlattices was further carried out by Radović et al. [48, 49] following the work of Biagi et al. [33]. This type of superlattice is characterized by the pair breaking mechanism in the ferromagnetic layer due to the strong exchange field. By a careful choice of parameters, Radović et al. were able to obtain good agreement with experimental data on the temperature dependence of the perpendicular and parallel upper critical field for a V/Fe multilayer system [44], except in a narrow region of temperature, in which the deviation of the calculated parallel upper critical field from the experimental data remains unexplained.

While the effect predicted by Takahashi and Tachiki was confirmed qualitatively by a number of experimental results, nevertheless, a quantitative comparison of the theoretical results with the experiment, which would provide a critical test of the existing theoretical model, was absent. Practically, the samples used in experiments are multilayer systems with two boundaries, which breaks the finite translational invariance assumed in a model of superlattice geometry. Saint-James and de Gennes' superconducting sheath theory [19] showed that the existence of a free surface could enhance the parallel upper critical field in a homogeneous sample. This surface effect may play an important role as well in a multilayer system with free boundaries. Therefore, a realistic model of a multilayer system should include the influence of the free surface in determining the parallel upper critical field. Yuan and Whitehead [50, 51] modeled a practical multilayer system as a superlattice with one free surface (semi-infinite superlattice). The two-component superlattice is assumed to satisfy the conditions $V_S = V_N$, $N_S = N_N$, $T_{cS} = T_{cN}$ and $D_S \neq D_N$, while the first layer

may be either S type superconductor or N type superconductor. This study led to a number of qualitative theoretical predictions that arise as a consequence of surface and the interfacial effects. Several of these predictions have been confirmed experimentally [41] and a systematic comparison of the theoretical results with the experimental data [37, 38, 39, 40, 41] showed excellent quantitative agreement. This work will form the second major part of this thesis and the various results will be detailed in the subsequent chapters. An elegant analysis and review article of the development of the DW theory in multilayer systems was recently given by Lodder and Koperdraad [52].

The outline of the thesis is as follows: In Chapter 2, we review the microscopic theory of inhomogeneous superconductors. Starting from the effective BCS Hamiltonian [9], we will derive the linearized Gor'kov integral equation [8] for the order parameter of superconductivity, following Gor'kov's work. We will then obtain the momentum space representation of the kernel in the Gor'kov equation using a Green's function method [18], including the effect of a randomly distributed impurity potential. In the long-wavelength approximation and the dirty limit, we will show that the spatial variation of the kernel satisfies a diffusion equation, as proposed by de Gennes [26]. Then we will follow de Gennes' work [26] to discuss the boundary and continuity conditions imposed on the kernel at a free surface and at the interface of a bilayer system. The introduction of a magnetic field and the calculation of the upper critical field in superconducting films and multilayer is based on the semi-classical phase integral approximation. It is shown how the de Gennes formalism may be applied in two particular cases, namely the evaluation of the upper critical field in the case of an infinite homogeneous superconductor and the case of a metallic multilayer consisting of two distinct types of metals, at least one of which is assumed to be superconducting. It is shown how the integral equation

in the linearized Gor'kov equation may be transformed into a differential equation for the pair amplitude, together with certain boundary and continuity conditions, derived from the de Gennes boundary and continuity conditions for the kernel. The resultant formalism is referred to as the de Gennes-Werthamer formalism. We show that while this is exact in the case of a homogeneous superconductor, it is, in general, only approximate in the case of multilayered systems. This, together with the recent developments of the de Gennes-Werthamer theory [30, 36, 43, 52, 53] are briefly discussed at the end of chapter 2.

In Chapter 3, we will apply the DW theory to a superconducting film to study the influence of the geometric inhomogeneity and anisotropy of the sample on the temperature dependence and the angular dependence of the upper critical field, respectively. The parallel applied field case will be studied in detail first [19], to show the importance of the nucleation site in determining the spatial distribution of the order parameter one obtains from the linearized GL equation [4] and the subsequent determination of the upper critical field. An approximate analytical expression for the upper critical field of a thin film will be obtained through a mean field approximation, and the phenomena of surface superconductivity will be discussed, within the framework of the de Gennes-Werthamer formalism. Moreover, the understanding of the importance of the nucleation site, based on detailed calculations in the parallel field case, will provide an intuitive physical picture for later discussion of the angle-dependent upper critical field. We will then present a detailed analysis of the angle-dependent upper critical field by various theories proposed in previous studies [20, 21, 24, 54, 55, 56]. This analysis will focus on the validity of the approximations and the mathematical methods employed by previous authors, and will explore the inconsistencies that exist in these earlier studies. A detailed numerical calculation of the angular dependence of the upper critical field in superconducting films, using an

eigenfunction expansion technique, will be presented. These results show explicitly the non-analytical nature of the upper critical field in the limit $\theta \rightarrow 0$, and also serve to verify the earlier results of Thompson regarding the slope $\frac{\partial H}{\partial \theta}\Big|_T$ in the limit $\theta \rightarrow 0$. Our results predict a new dimensional crossover, from single surface effects, dominated by the superconducting sheath, and double surface effects, dominated by the size of the sample for a thick film in the angular dependence of the upper critical field. A semi-infinite bulk superconducting sample is also included as a limiting case of thick film.

In Chapter 4, we focus on the parallel upper critical field of a metallic multilayer composed of alternating layers of different types of metal. In particular we will consider a class of superlattice structures in which the composite metals share the same transition temperature but which have a different electron mean free path. We show how the problem may be formulated within the de Gennes-Werthamer formalism, how the upper critical field for an infinite superlattice may be calculated and the effect of the modulation on the nucleation site examined. The Takahashi-Tachiki effect is obtained and discussed in some detail. We then go on to consider a more realistic model of a metallic superlattice, a semi-infinite superlattice, that includes a free surface. Particular attention is given to the subtle interplay between the surface effect and the effect of the modulation on the location of the nucleation center. In particular we will show that the upper critical field for such a system will depend on the sequence in which the layers are deposited [37, 38, 39, 40, 41]. This result has been confirmed experimentally by Maj and Aarts [41] who arrived at a similar conclusion independently, through their experimental studies. Our results also show that the ratio H_{c3}/H_{c2} can be significantly enhanced in a superlattice geometry by virtue of the modulation. Again this result has been confirmed experimentally [41].

In this work we also consider the effect of the free surface on the discontinuity

in the slope $\frac{\partial H}{\partial T}$, predicted by Takahashi and Tachiki. It is shown that both the appearance of the discontinuity and the temperature at which it occurs are dependent on the sequence in which the layers are deposited. It is also shown how the field H^*, at which this discontinuity occurs, satisfies a simple scaling law with respect to the modulation length. Several data sets are analyzed and are shown to satisfy this scaling law, and it is shown that the apparent discrepancies between different data sets may be attributed to the sequence in which the layers are deposited.

In the final part of chapter 4, we consider, in some detail, a particularly elegant set of experiments on a sequence of multilayer which differ only in the composition and thickness of the initial layer. It will be shown that, provided the effects of spin paramagnetism are included, the results obtained from the de Gennes theory are in excellent agreement with the experimental data.

In chapter 5 we present a number of conclusions that can be drawn from the research work presented in this thesis.

Chapter 2

The Microscopic Theory of Inhomogeneous Superconductors

In this chapter, we will review the de Gennes-Werthamer dirty-limit theory in detail. We start by introducing the effective BCS Hamiltonian, in Section 2.1, that arises as a result of the electron-phonon interaction [57]. In Section 2.2, this BCS Hamiltonian is transformed from momentum space to coordinate space by a Fourier transformation. Introducing the Matsubara Green's function and applying the mean field approximation, we obtain the Gor'kov equations [58] for the Green's functions. In Section 2.3, a linearization approximation is applied to the Gor'kov equation and thus a solution of the Gor'kov equation, in integral form, is obtained. The kernel of the integral equation is studied in detail for a dilute doped superconductor and an explicit form of the kernel is obtained. In Section 2.4, we show how the kernel may be evaluated in the long-wavelength approximation and expressed in terms of a differential equation. Then, following de Gennes' work, we discuss how the effect of surfaces and interfaces on the kernel may be introduced through appropriate boundary conditions. We then go on to discuss two important applications of the de Gennes formalism. The first involves the evaluation of the upper critical field of a homogeneous type II superconductor, while the second is the calculation of the transition temperature and the upper critical field of a metallic multilamellar system. The first example serves as a straightforward application of the de Gennes formalism while the second provides the theoretical framework for much of the subsequent analysis, and includes the superconducting film as a special case.

2.1 BCS Hamiltonian

2.1.1 The Electron-Phonon Interaction

In the second quantization representation, the model Hamiltonian of the electron-phonon system [1] may be written as [57]

$$H = H_0 + H_1 \,, \tag{2.1}$$

where H_0 is the Hamiltonian for free phonons and free electrons,

$$H_0 = \sum_{\mathbf{q}} \hbar\omega_{\mathbf{q}} a^+_{\mathbf{q}} a_{\mathbf{q}} + \sum_{\mathbf{k},\sigma} \epsilon_{\mathbf{k}} c^+_{\mathbf{k}\sigma} c_{\mathbf{k}\sigma} \,, \tag{2.2}$$

and H_1 is the interaction Hamiltonian of the electrons and the phonons,

$$H_1 = \sum_{\mathbf{k},\mathbf{q},\sigma} \left(D_{\mathbf{q}} a_{\mathbf{q}} c^+_{\mathbf{k}+\mathbf{q},\sigma} c_{\mathbf{k},\sigma} + D^*_{\mathbf{q}} a^+_{\mathbf{q}} c^+_{\mathbf{k}-\mathbf{q},\sigma} c_{\mathbf{k},\sigma} \right) . \tag{2.3}$$

The indices $\mathbf{q}$ and $\mathbf{k}$ denote the wave vectors of the phonons and the electrons respectively, $\epsilon_{\mathbf{k}} = \frac{k^2}{2m} - \mu$ is the energy of a single electron in the state $\mathbf{k}$ relative to the chemical potential μ, $\hbar\omega_{\mathbf{q}}$ denotes the energy of a phonon in the state $\mathbf{q}$ and σ is the spin index of an electron. $D_{\mathbf{q}}$ is the electron-phonon coupling constant while $D^*_{\mathbf{q}}$ is its complex conjugate, which depends on the interaction potential, and $a^+_{\mathbf{q}}$ ($a_{\mathbf{q}}$) and $c^+_{\mathbf{k},\sigma}$ ($c_{\mathbf{k},\sigma}$) are the creation (annihilation) operators of the phonons and electrons, which satisfy the algebra

$$[a^+_{\mathbf{q}}, a_{\mathbf{q}'}] = a^+_{\mathbf{q}} a_{\mathbf{q}'} - a_{\mathbf{q}'} a^+_{\mathbf{q}} = \delta_{\mathbf{q}\mathbf{q}'} \,, \tag{2.4}$$

and

$$\{c^+_{\mathbf{k},\sigma}, c_{\mathbf{k}',\sigma'}\} = c^+_{\mathbf{k},\sigma} c_{\mathbf{k}',\sigma'} + c_{\mathbf{k}',\sigma'} c^+_{\mathbf{k},\sigma} = \delta_{\mathbf{k}\mathbf{k}'}\, \delta_{\sigma\sigma'} \,, \tag{2.5}$$

respectively.

[1] We consider a "jellium" model for the metal, therefore, only the longitudinal phonon is included in the Hamiltonian H. We also neglect a constant part of the energy, $\sum_{\mathbf{q}} \frac{1}{2}\hbar\omega_{\mathbf{q}}$.

Starting from the Hamiltonian (2.1), Fröhlich [57] derived the effective Hamiltonian by means of the canonical transformation

$$H_S = e^{-S} H e^{S} \,, \tag{2.6}$$

where the operator S is chosen such that the transformed Hamiltonian H_S has the same eigenvalue spectrum as that of H.

Equation (2.6) may be expanded as

$$\begin{aligned} H_S &= H + [H,S] + \tfrac{1}{2}[[H,S],S] + \cdots \\ &= H_0 + (H_1 + [H_0,S]) + \tfrac{1}{2}[(H_1 + [H_0,S]),S] \\ &\quad + \tfrac{1}{2}[H_1,S] + \tfrac{1}{2}[H_1 + [H_1,S],S] + \cdots \,. \end{aligned} \tag{2.7}$$

We can eliminate the interaction to lowest order if we choose S to satisfy the equation

$$H_1 + [H_0,S] = 0 \,, \tag{2.8}$$

so that there is no first order electron-phonon interaction and we obtain the following expression for H_S,

$$\begin{aligned} H_S &= H_0 + \tfrac{1}{2}[H_1,S] + \tfrac{1}{2}[H_1 + [H_1,S],S] + \cdots \\ &\approx H_0 + \tfrac{1}{2}[H_1,S] \,. \end{aligned} \tag{2.9}$$

If the operator S is assumed to be of the form

$$S = \sum_{\mathbf{k},\mathbf{q},\sigma} (A_{\mathbf{q}} a_{\mathbf{q}} c^{+}_{\mathbf{k}+\mathbf{q},\sigma} c_{\mathbf{k},\sigma} + B_{\mathbf{q}} a^{+}_{\mathbf{q}} c^{+}_{\mathbf{k}-\mathbf{q},\sigma} c_{\mathbf{k},\sigma}) \,, \tag{2.10}$$

then using equation (2.8), we can determine the coefficients $A_{\mathbf{q}}$ and $B_{\mathbf{q}}$

$$\begin{cases} A_{\mathbf{q}} &= D_{\mathbf{q}} (\epsilon_{\mathbf{k}} + \hbar\omega_{\mathbf{q}} - \epsilon_{\mathbf{k}+\mathbf{q}})^{-1} \,, \\ B_{\mathbf{q}} &= D^{*}_{\mathbf{q}} (\epsilon_{\mathbf{k}} - \hbar\omega_{\mathbf{q}} - \epsilon_{\mathbf{k}-\mathbf{q}})^{-1} \,, \end{cases} \tag{2.11}$$

thus S can be expressed as

$$S = \sum_{\mathbf{k},\mathbf{q},\sigma} (D_{\mathbf{q}} \frac{a_{\mathbf{q}} c^{+}_{\mathbf{k}+\mathbf{q},\sigma} c_{\mathbf{k},\sigma}}{\epsilon_{\mathbf{k}} - \epsilon_{\mathbf{k}+\mathbf{q}} + \hbar\omega_{\mathbf{q}}} + D^{*}_{\mathbf{q}} \frac{a^{+}_{\mathbf{q}} c^{+}_{\mathbf{k}-\mathbf{q},\sigma} c_{\mathbf{k},\sigma}}{\epsilon_{\mathbf{k}} - \epsilon_{\mathbf{k}-\mathbf{q}} - \hbar\omega_{\mathbf{q}}}) \,. \tag{2.12}$$

To obtain the effective Hamiltonian which describes the scattering process of the electrons through exchange of one phonon, we can take the expectation value of the term H_S with respect to the phonon vacuum state $|0\rangle$, which is defined as

$$a_{\mathbf{q}}\,|0\rangle = 0, \tag{2.13}$$

to give

$$\begin{aligned} H_{eff} &= \langle 0|H_S|0\rangle \\ &= \frac{1}{2}\sum_{n_{\mathbf{q}}}\sum_{\mathbf{q}}\{\langle 0|H_1|n_{\mathbf{q}}\rangle\langle n_{\mathbf{q}}|S|0\rangle - \langle 0|S|n_{\mathbf{q}}\rangle\langle n_{\mathbf{q}}|H_1|0\rangle\} \\ &= \frac{1}{2}\sum_{\mathbf{q}}\{\langle 0|H_1|1_{\mathbf{q}}\rangle\langle 1_{\mathbf{q}}|S|0\rangle - \langle 0|S|1_{\mathbf{q}}\rangle\langle 1_{\mathbf{q}}|H_1|0\rangle\}\,. \end{aligned} \tag{2.14}$$

where we have used the completeness of the phonon eigenstates

$$\sum_{n_{\mathbf{q}},\mathbf{q}} |n_{\mathbf{q}}\rangle\langle n_{\mathbf{q}}| = 1\,, \tag{2.15}$$

and the property of the operator S

$$\langle n_{\mathbf{q}}|S|0\rangle = 0 \qquad \text{for} \qquad n_{\mathbf{q}} \neq 1_{\mathbf{q}}\,. \tag{2.16}$$

Substituting (2.12) and (2.3) into (2.14) and completing the algebraic calculation, we obtain the effective interaction Hamiltonian

$$H_{eff} = \frac{1}{2}\sum_{\mathbf{k},\mathbf{k}',\mathbf{q}}\sum_{\sigma,\sigma'}|D_{\mathbf{q}}|^2\frac{2\hbar\omega_{\mathbf{q}}}{(\epsilon_{\mathbf{k}}-\epsilon_{\mathbf{k}+\mathbf{q}})^2-(\hbar\omega_{\mathbf{q}})^2}c^{+}_{\mathbf{k}+\mathbf{q},\sigma}c^{+}_{\mathbf{k}'-\mathbf{q},\sigma'}c_{\mathbf{k}',\sigma'}c_{\mathbf{k},\sigma}\,. \tag{2.17}$$

which describes the interaction between two electrons through the one-phonon-exchange process. The other terms describing multiphonon processes can be omitted due to Migdal's theorem [59].

2.1.2 The Effective BCS Hamiltonian

The effective electron-phonon interaction may be written as

$$H_{eff} = \frac{1}{2}\sum_{\mathbf{k},\mathbf{k}',\mathbf{q}}\sum_{\sigma,\sigma'}V_{\mathbf{k},\mathbf{q}}c^{+}_{\mathbf{k}+\mathbf{q},\sigma}c^{+}_{\mathbf{k}'-\mathbf{q},\sigma'}c_{\mathbf{k}',\sigma'}c_{\mathbf{k},\sigma}\,, \tag{2.18}$$

where

$$V_{\mathbf{k},\mathbf{q}} = |D_{\mathbf{q}}|^2 \frac{2\hbar\omega_{\mathbf{q}}}{(\epsilon_{\mathbf{k}} - \epsilon_{\mathbf{k}+\mathbf{q}})^2 - (\hbar\omega_{\mathbf{q}})^2} \,. \tag{2.19}$$

When both of the electrons scattered by exchanging a phonon are sufficiently close to the Fermi surface, determined by chemical potential μ, that the difference in the energies satisfies the condition $|\epsilon_{\mathbf{k}} - \epsilon_{\mathbf{k}+\mathbf{q}}| < \hbar\omega_{\mathbf{q}} \approx \hbar\omega_D$ (ω_D is the Debye frequency), then the coupling constant $V_{\mathbf{k},\mathbf{q}} < 0$, which yields an attractive interaction. On the other hands, if the difference in the energies is larger than $\hbar\omega_D$, the coupling constant $V_{\mathbf{k},\mathbf{q}}$ is positive, and in that case, H_{eff} is a repulsive interaction, the strength of which decreases rapidly with increasing energy difference.

In the superconducting state, only the electrons occupying states with energy in the range of $\mu \pm \hbar\omega_D$ can be scattered to new states through the phonon-exchange process. Thus, in the application of (2.19) to superconductivity, Cooper [60] made the appropriate assumption that for the electrons in states with $\epsilon_{\mathbf{k}} < \hbar\omega_D$ the coupling induced by phonons is a constant, $V_{\mathbf{k},\mathbf{q}} = -V$ with $V > 0$, and for those in the states $\epsilon_{\mathbf{k}} > \hbar\omega_D$, the coupling vanishes. So the effective Hamiltonian becomes, in the BCS approximation,

$$H_{eff} = -\frac{1}{2} V \sum_{\mathbf{k},\mathbf{k}',\mathbf{q}} \sum_{\sigma,\sigma'} c^{+}_{\mathbf{k}+\mathbf{q},\sigma} c^{+}_{\mathbf{k}'-\mathbf{q},\sigma'} c_{\mathbf{k}',\sigma'} c_{\mathbf{k},\sigma} \,. \tag{2.20}$$

where $\mathbf{k}$ and $\mathbf{k}'$ are the momenta of electrons in a shell with width $2\hbar\omega_D$ at the Fermi sphere.

The approximation obtained here is valid only for a "weak coupling" superconductor, since the form of H_{eff} implies two assumptions:

(i) In assuming a coupling constant which is independent of the energy variables $\epsilon_{\mathbf{k}}$ and $\hbar\omega_{\mathbf{q}}$, we have neglected the effect of retardation.

(ii) All the processes of absorption and emission of phonons involving the creation

and annihilation of a pair of quasi-particles have been neglected so that the quasi-particles are treated as having infinite lifetime.

To consider both of the influences mentioned above, a theory of strong coupling superconductivity should be built, however, we will only discuss the weak coupling limit.

In applying the theory to the inhomogeneous geometry, it is necessary to transform H_{eff} into the coordinate representation by means of the transformation,

$$\begin{cases} \hat{\psi}_\sigma(\mathbf{x}) &= \sum_{\mathbf{k}} c_{\mathbf{k},\sigma} e^{i\mathbf{k}\cdot\mathbf{x}} , \\ \hat{\psi}^\dagger_\sigma(\mathbf{x}) &= \sum_{\mathbf{k}} c^+_{\mathbf{k},\sigma} e^{-i\mathbf{k}\cdot\mathbf{x}} , \end{cases} \tag{2.21}$$

which may be inverted to yield

$$\begin{cases} c_{\mathbf{k},\sigma} &= \int e^{-i\mathbf{k}\cdot\mathbf{x}} \hat{\psi}_\sigma(\mathbf{x})\, d^3x , \\ c^+_{\mathbf{k},\sigma} &= \int e^{i\mathbf{k}\cdot\mathbf{x}} \hat{\psi}^\dagger_\sigma(\mathbf{x})\, d^3x , \end{cases} \tag{2.22}$$

where we have chosen the volume to be unity. The operators $\hat{\psi}_\sigma(\mathbf{x})$ and $\hat{\psi}^\dagger_\sigma(\mathbf{x})$ can be shown to satisfy the anti-commutation algebra

$$\{\hat{\psi}_\sigma(\mathbf{x}) , \hat{\psi}^\dagger_{\sigma'}(\mathbf{x}')\} = \delta(\mathbf{x}-\mathbf{x}')\delta_{\sigma\sigma'}. \tag{2.23}$$

The effective interaction Hamiltonian in the BCS approximation may be written in terms of the operators $\hat{\psi}$ and $\hat{\psi}^\dagger$ as

$$\begin{aligned} H_{eff} \to \hat{V} &= -\frac{1}{2} V \sum_{\alpha,\beta} \int \hat{\psi}^\dagger_\alpha(\mathbf{x})\, \hat{\psi}^\dagger_\beta(\mathbf{x})\, \hat{\psi}_\beta(\mathbf{x})\, \hat{\psi}_\alpha(\mathbf{x})\, d^3x \\ &= -V \int \hat{\psi}^\dagger_\uparrow(\mathbf{x})\, \hat{\psi}^\dagger_\downarrow(\mathbf{x})\, \hat{\psi}_\downarrow(\mathbf{x})\, \hat{\psi}_\uparrow(\mathbf{x})\, d^3x , \end{aligned} \tag{2.24}$$

where we have further simplified the effective interaction Hamiltonian by considering the Pauli exclusion principle, which prohibits two electrons from occupying the same state, i.e.,

$$\hat{\psi}^\dagger_\uparrow(\mathbf{x})\, \hat{\psi}^\dagger_\uparrow(\mathbf{x}) = \hat{\psi}^\dagger_\downarrow(\mathbf{x})\, \hat{\psi}^\dagger_\downarrow(\mathbf{x}) = \hat{\psi}_\uparrow(\mathbf{x})\, \hat{\psi}_\uparrow(\mathbf{x}) = \hat{\psi}_\downarrow(\mathbf{x})\, \hat{\psi}_\downarrow(\mathbf{x}) = 0 . \tag{2.25}$$

In the Hamiltonian (2.2) for free phonons and electrons, we can omit the free phonon term, since in superconductivity, the physical properties of a superconducting state mainly depend on the behavior of the electrons, and consider the phonons only in a role which induces a new attractive interaction H_{eff}. The free part of the Hamiltonian, $\hat{H}_0$ may then be written as

$$H_0 \approx \hat{K}_0 = \int d^3x\, \hat{\psi}^\dagger_\sigma(\mathbf{x}) \epsilon(i\nabla) \hat{\psi}_\sigma(\mathbf{x}), \tag{2.26}$$

with

$$\epsilon(i\nabla) = \frac{-h^2\nabla^2}{2m} - \mu\ .$$

Combining Eq. (2.24) and (2.26), we finally obtain the BCS Hamiltonian

$$\hat{K} = \hat{K}_0 + \hat{V}\ , \tag{2.27}$$

which includes the phonon-induced attractive interaction among the electrons. Such a new mechanism enables one to calculate various parameters in superconductivity and explain experimental phenomena.

2.2 Gor'kov Equation

2.2.1 Mean Field Approximation

The theory obtained in the last section can be easily generalized to include both the influence of an external magnetic field and the existence of non-magnetic impurities. Following the method of A. L. Fetter and J. D. Walecka [61], we obtain

$$\hat{K} = \hat{K}_0 + \hat{V}\ , \tag{2.28}$$

$$\hat{K}_0 = \int d^3x\, \hat{\psi}^\dagger_\alpha(\mathbf{x}) \left\{ \frac{1}{2m}[-ih\nabla + \frac{e}{c}\mathbf{A}(\mathbf{x})]^2 - \mu + U(\mathbf{x}) \right\} \hat{\psi}_\alpha(\mathbf{x})\ , \tag{2.29}$$

$$\hat{V} = -\frac{1}{2} V \sum_{\alpha,\beta} \int \hat{\psi}^\dagger_\alpha(\mathbf{x})\, \hat{\psi}^\dagger_\beta(\mathbf{x})\ \hat{\psi}_\beta(\mathbf{x})\, \hat{\psi}_\alpha(\mathbf{x})\, d^3x\ , \tag{2.30}$$

where $\mathbf{A}(\mathbf{x})$ is the vector potential and $U(\mathbf{x})$ is the impurity potential which is of the form

$$U(\mathbf{x}) = \sum_a u(\mathbf{x} - \mathbf{x}_a) \,, \tag{2.31}$$

with $\mathbf{x}_a$ being the position of a^{th} impurity.

Generally, one can obtain a non-linear differential equation describing the spatial and temporal evolution of the operator fields, $\hat{\psi}_\sigma(\mathbf{x})$, by means of the Hamiltonian (2.28). However, this equation is too complicated to be solved completely, so a mean field approximation has to be taken. In this approximation, one can decompose the product of the four field operators in the interaction term, $\hat{V}$, into the following

$$\begin{aligned} \hat{V} &\approx \hat{V}_{eff} \\ &= -V \int d^3x \{ \langle \hat{\psi}_\downarrow^\dagger(\mathbf{x}) \hat{\psi}_\uparrow^\dagger(\mathbf{x}) \rangle \hat{\psi}_\uparrow(\mathbf{x}) \hat{\psi}_\downarrow(\mathbf{x}) + \hat{\psi}_\downarrow^\dagger(\mathbf{x}) \hat{\psi}_\uparrow^\dagger(\mathbf{x}) \langle \hat{\psi}_\uparrow(\mathbf{x}) \hat{\psi}_\downarrow(\mathbf{x}) \rangle \}. \end{aligned} \tag{2.32}$$

The reason for making such a decomposition is that an essential characteristic of superconductivity is the formation of Cooper pairs by two electrons with opposite spins, which results in the appearance of an order parameter $\langle \hat{\psi}\hat{\psi} \rangle \neq 0$. The other terms coming from the Hartree-Fock decomposition such as $\langle \hat{\psi}_\alpha^\dagger(\mathbf{x}) \hat{\psi}_\alpha(\mathbf{x}) \rangle$ and $\langle \hat{\psi}_\alpha^\dagger(\mathbf{x}) \hat{\psi}_\beta(\mathbf{x}) \rangle$ have been omitted since only the difference between the superconducting state and the normal state is of interest; these Hartree-Fock terms are assumed to be the same in both of states and hence have no influence on the differences between these two states.

With the mean field approximation, the effective Hamiltonian now becomes

$$\hat{K} \approx \hat{K}_{eff} = \hat{K}_0 + \hat{V}_{eff} \,. \tag{2.33}$$

and the pair amplitude in the decomposition is defined as

$$\langle \hat{\psi}_\downarrow^\dagger(\mathbf{x}) \hat{\psi}_\uparrow^\dagger(\mathbf{x}) \rangle = \frac{T_r[e^{-\beta \hat{K}_{eff}} \hat{\psi}_\downarrow^\dagger(\mathbf{x}) \hat{\psi}_\uparrow^\dagger(\mathbf{x})]}{T_r[e^{-\beta \hat{K}_{eff}}]} \,, \tag{2.34}$$

with

$$\beta^{-1} = k_B T .$$

Eq. (2.34) provides us with a self-consistent definition of the pair amplitude, which depends on the effective Hamiltonian, including the pair amplitude itself.

2.2.2 Gor'kov Equation

To calculate the pair amplitude, one needs to introduce the generalized Heisenberg field operators defined as

$$\hat{\psi}_{K\uparrow}(\mathbf{x},\tau) = e^{\hat{K}_{eff}\,\tau/\hbar}\,\hat{\psi}_{\uparrow}(\mathbf{x})\,e^{-\hat{K}_{eff}\,\tau/\hbar} , \tag{2.35}$$

$$\hat{\psi}^{\dagger}_{K\uparrow}(\mathbf{x},\tau) = e^{\hat{K}_{eff}\,\tau/\hbar}\,\hat{\psi}^{\dagger}_{\uparrow}(\mathbf{x})\,e^{-\hat{K}_{eff}\,\tau/\hbar} , \tag{2.36}$$

$$\hat{\psi}_{K\downarrow}(\mathbf{x},\tau) = e^{\hat{K}_{eff}\,\tau/\hbar}\,\hat{\psi}_{\downarrow}(\mathbf{x})\,e^{-\hat{K}_{eff}\,\tau/\hbar} , \tag{2.37}$$

$$\hat{\psi}^{\dagger}_{K\downarrow}(\mathbf{x},\tau) = e^{\hat{K}_{eff}\,\tau/\hbar}\,\hat{\psi}^{\dagger}_{\downarrow}(\mathbf{x})\,e^{-\hat{K}_{eff}\,\tau/\hbar} , \tag{2.38}$$

where we may regard τ as an the imaginary time. With this definition, one can establish the equations of motion for the field operators from the effective Hamiltonian, $\hat{K}_{eff}$, using the Heisenberg equation

$$\hbar\frac{\partial}{\partial\tau}\hat{O}_K = [\hat{O}_K\,,\,\hat{K}_{eff}] , \tag{2.39}$$

where $\hat{O}_K$ is a arbitrary operator defined by $\hat{O}_K = e^{\hat{K}_{eff}\,\tau/\hbar}\hat{O}e^{-\hat{K}_{eff}\,\tau/\hbar}$. By means of the anti-commutation algebra, Eq. (2.23), we obtain the equations of motion for the field operators as follows

$$\hbar\frac{\partial}{\partial\tau}\hat{\psi}_{K\uparrow} = -[\frac{1}{2m}(-i\hbar\nabla + \frac{e}{c}\mathbf{A}(\mathbf{x}))^2 - \mu + U(\mathbf{x})]\hat{\psi}_{K\uparrow} - V\langle\hat{\psi}_{\uparrow}\hat{\psi}_{\downarrow}\rangle\hat{\psi}^{\dagger}_{K\downarrow} , \tag{2.40}$$

$$\hbar\frac{\partial}{\partial\tau}\hat{\psi}^{\dagger}_{K\downarrow} = [\frac{1}{2m}(i\hbar\nabla + \frac{e}{c}\mathbf{A}(\mathbf{x}))^2 - \mu + U(\mathbf{x})]\hat{\psi}^{\dagger}_{K\downarrow} - V\langle\hat{\psi}^{\dagger}_{\downarrow}\hat{\psi}^{\dagger}_{\uparrow}\rangle\hat{\psi}_{K\uparrow} . \tag{2.41}$$

Note that the pair amplitudes may be expressed in terms of the Heisenberg field operators, i.e.

$$\begin{cases} \langle \hat{\psi}_\uparrow^\dagger \hat{\psi}_\downarrow^\dagger \rangle &= \langle \hat{\psi}_{K\uparrow}^\dagger(\tau) \hat{\psi}_{K\downarrow}^\dagger(\tau) \rangle \ , \\ \langle \hat{\psi}_\downarrow \hat{\psi}_\uparrow \rangle &= \langle \hat{\psi}_{K\downarrow}(\tau) \hat{\psi}_{K\uparrow}(\tau) \rangle \ . \end{cases} \tag{2.42}$$

Since we are only interested in finding the pair amplitude, which gives the order parameter in a superconductor, rather than the detailed representation of the quantized wave functions $\hat{\psi}$ and $\hat{\psi}^\dagger$ themselves, we introduce the Matsubara function, which is given by

$$\mathcal{G}(\mathbf{x}\tau, \mathbf{x}'\tau') = -\langle T_\tau[\hat{\psi}_{K\uparrow}(\mathbf{x}\tau)\hat{\psi}_{K\uparrow}^\dagger(\mathbf{x}'\tau')]\rangle \ , \tag{2.43}$$

together with the anomalous Matsubara function $\mathcal{F}(\mathbf{x}\tau, \mathbf{x}'\tau')$, which is closely related to the pair amplitude and is given by

$$\mathcal{F}(\mathbf{x}\tau, \mathbf{x}'\tau') = -\langle T_\tau[\hat{\psi}_{K\uparrow}(\mathbf{x}, \tau)\hat{\psi}_{K\downarrow}(\mathbf{x}', \tau')]\rangle \ , \tag{2.44}$$

$$\mathcal{F}^\dagger(\mathbf{x}\tau, \mathbf{x}'\tau') = -\langle T_\tau[\hat{\psi}_{K\downarrow}^\dagger(\mathbf{x}, \tau)\hat{\psi}_{K\uparrow}^\dagger(\mathbf{x}', \tau')]\rangle \ . \tag{2.45}$$

The self-consistent expression for the order parameter is

$$\Delta(\mathbf{x}) = V\mathcal{F}(\mathbf{x}\tau^{0^+}, \mathbf{x}\tau) = V\langle \hat{\psi}_\downarrow(\mathbf{x})\hat{\psi}_\uparrow(\mathbf{x})\rangle \ . \tag{2.46}$$

The time-order operator T_τ, which appears in the definition of the Matsubara functions, with respect to the imaginary time τ, is defined as

$$\langle T_\tau(\hat{A}(\tau)\hat{B}(\tau'))\rangle = \theta(\tau - \tau')\langle \hat{A}(\tau)\hat{B}(\tau')\rangle - \theta(\tau' - \tau)\langle \hat{B}(\tau')\hat{A}(\tau)\rangle, \tag{2.47}$$

where $\hat{A}$ and $\hat{B}$ are any fermion operators and $\theta(\tau)$ is the step function

$$\theta(\tau) = \begin{cases} 1, & \tau > 0, \\ 0, & \tau < 0. \end{cases} \tag{2.48}$$

If we use Eq. (2.41) and take the derivative with respect to imaginary time τ of the Matsubara functions defined by Eqs. (2.43) and (2.45), we obtain the Gor'kov equations

$$\left\{-\hbar\frac{\partial}{\partial\tau}-\frac{1}{2m}[-i\hbar\nabla+\frac{e}{c}\mathbf{A}(\mathbf{x})]^2+\mu-U(\mathbf{x})\right\}\mathcal{G}(\mathbf{x}\tau,\mathbf{x}'\tau') \quad +\Delta(\mathbf{x})\mathcal{F}^\dagger(\mathbf{x}\tau,\mathbf{x}'\tau') = h\delta(\mathbf{x}-\mathbf{x}')\,, \tag{2.49}$$

$$\left\{-\hbar\frac{\partial}{\partial\tau}-\frac{1}{2m}[-i\hbar\nabla+\frac{e}{c}\mathbf{A}(\mathbf{x})]^2+\mu-U(\mathbf{x})\right\}\mathcal{F}(\mathbf{x}\tau,\mathbf{x}'\tau') \quad -\Delta(\mathbf{x})\mathcal{G}(\mathbf{x}\tau,\mathbf{x}'\tau') = 0\,, \tag{2.50}$$

$$\left\{\hbar\frac{\partial}{\partial\tau}-\frac{1}{2m}[ih\nabla+\frac{e}{c}\mathbf{A}(\mathbf{x})]^2+\mu-U(\mathbf{x})\right\}\mathcal{F}^\dagger(\mathbf{x}\tau,\mathbf{x}'\tau') \quad -\Delta^\dagger(\mathbf{x})\mathcal{G}(\mathbf{x}\tau,\mathbf{x}'\tau') = 0\,. \tag{2.51}$$

In the case that the Hamiltonian is independent of τ, the Matsubara functions only depend on the time difference $(\tau-\tau')$. The Fourier transformation, in this case, of the Matsubara functions with respect to τ yields

$$\mathcal{G}(\mathbf{x}\tau,\mathbf{x}'\tau') = (\beta h)^{-1}\sum_n e^{-i\omega_n(\tau-\tau')}\mathcal{G}(\mathbf{x},\mathbf{x}',\omega_n)\,, \tag{2.52}$$

$$\mathcal{F}^\dagger(\mathbf{x}\tau,\mathbf{x}'\tau') = (\beta h)^{-1}\sum_n e^{-i\omega_n(\tau-\tau')}\mathcal{F}^\dagger(\mathbf{x},\mathbf{x}',\omega_n)\,, \tag{2.53}$$

where $\omega_n=(2n+1)\pi/\beta h$ and $n=0,\pm1,\pm2,\ldots$ and we have used the periodicity of the Matsubara function [61] given by

$$\mathcal{G}(\tau<0)=-\mathcal{G}(\tau+\beta>0)\,. \tag{2.54}$$

The equations of motion for the Fourier components can be written as

$$\left\{ih\omega_n - \frac{1}{2m}[-ih\nabla + \frac{e}{c}\mathbf{A}(\mathbf{x})]^2 + \mu - U(\mathbf{x})\right\}\mathcal{G}(\mathbf{x},\mathbf{x}'\omega_n) \quad +\Delta(\mathbf{x})\mathcal{F}^\dagger(\mathbf{x},\mathbf{x}',\omega_n) = h\delta(\mathbf{x}-\mathbf{x}')\,, \tag{2.55}$$

$$\left\{-ih\omega_n - \frac{1}{2m}[ih\nabla + \frac{e}{c}\mathbf{A}(\mathbf{x})]^2 + \mu - U(\mathbf{x})\right\}\mathcal{F}^\dagger(\mathbf{x},\mathbf{x}',\omega_n) \quad -\Delta^\dagger(\mathbf{x})\mathcal{G}(\mathbf{x},\mathbf{x}',\omega_n) = 0\,. \tag{2.56}$$

The self-consistency condition for the order parameter given by Eq. (2.46) becomes

$$\begin{aligned}\Delta(\mathbf{x}) &= V\langle\hat{\psi}_\downarrow(\mathbf{x})\hat{\psi}_\uparrow(\mathbf{x})\rangle \\ &= V\mathcal{F}(\mathbf{x}\tau^{0^+},\mathbf{x}\tau) \\ &= V(\beta h)^{-1}\sum_n e^{-i\omega_n 0^+}\mathcal{F}(\mathbf{x},\mathbf{x}',\omega_n)\,.\end{aligned} \tag{2.57}$$

The Gor'kov equations obtained above provide an effective basis for the self-consistent calculation of the order parameter. The theory obtained incorporates most of the early theories such as Ginzburg-Landau theory (GL) and BCS theory. Gor'kov [8] succeeded in deriving the GL equation near the critical temperature, T_c, from the Gor'kov equations. The derivation determines the phenomenological constants appearing in the GL theory in terms of the microscopic constants and the appropriate range for which the GL theory is applicable. Thus the GL theory has a firm basis in the microscopic theory, and hence can be generalized to much more complicated systems.

If one applies the Gor'kov equations to the spatially homogeneous bulk superconductor in the absence of an external magnetic field, one recovers the results obtained from the BCS [9] theory (see Appendix A).

2.3 Linearized Gor'kov Equation

We have discussed the theoretical description of an inhomogeneous superconductor based on the Gor'kov equations which includes the GL theory and BCS theory as special cases. The Gor'kov theory in principle allows one to consider more general situations, including the case of an applied magnetic field as well as both magnetic and nonmagnetic impurities, for example. However, it is very difficult to solve the Gor'kov equations directly, and further approximation methods have to be considered corresponding to specific conditions.

2.3.1 Linearization of Gap Equation

The differential equations, Eqs. (2.49) and (2.50), can be rewritten in terms of integral equations;

$$\mathcal{G}(\mathbf{x},\mathbf{x}',\omega) = \mathcal{G}_N(\mathbf{x},\mathbf{x}',\omega) - \int d^3x_1\, d^3x_2 \mathcal{G}_N(\mathbf{x},\mathbf{x}_1,\omega)\Delta(\mathbf{x}_1)\mathcal{G}_N(\mathbf{x}_2,\mathbf{x}_1,-\omega)\Delta^\dagger(\mathbf{x}_2)\mathcal{F}^\dagger(\mathbf{x}_2,\mathbf{x}',\omega), \quad (2.58)$$

$$\mathcal{F}^\dagger(\mathbf{x},\mathbf{x}',\omega) = \int d^3x_1\, \mathcal{G}_N(\mathbf{x}_1,\mathbf{x},-\omega)\Delta^\dagger(\mathbf{x}_1)\mathcal{G}_N(\mathbf{x}_1,\mathbf{x}',\omega) - \int d^3x_1 d^3x_2 \mathcal{G}_N(\mathbf{x}_1,\mathbf{x},-\omega)\Delta^\dagger(\mathbf{x}_1)\mathcal{G}_N(\mathbf{x}_1,\mathbf{x}_2,-\omega)\Delta(\mathbf{x}_2)\mathcal{F}^\dagger(\mathbf{x}_2,\mathbf{x}',\omega), \quad (2.59)$$

where $\mathcal{G}_N(\mathbf{x},\mathbf{x}',\omega)$ denotes the normal state Green's function, which satisfies the equation

$$\left[i\omega - \frac{1}{2m}\left(-i\nabla + \frac{e}{c}\mathbf{A}(\mathbf{x})\right)^2 + \mu - U(\mathbf{x})\right]\mathcal{G}_N(\mathbf{x},\mathbf{x}',\omega) = \delta(\mathbf{x}-\mathbf{x}')\,, \quad (2.60)$$

In order to calculate the upper critical field in a type II superconductor, it is sufficient to consider the linearized Gor'kov equation, since the order parameter goes

continuously to zero at the transition. Substituting the linear term in Eq. (2.59) into the self-consistent gap equation, Eq. (2.57), we obtain

$$\begin{aligned} \Delta^{\dagger}(\mathbf{x}) &= V\beta^{-1}\sum_{\omega}\int d^3y\, Q_{\omega}(\mathbf{x},\mathbf{y})\Delta^{\dagger}(\mathbf{y})\,, \\ &= V\int d^3y\, \mathcal{Q}(\mathbf{x},\mathbf{y})\Delta^{\dagger}(\mathbf{y})\,. \end{aligned} \tag{2.61}$$

The kernel $Q_{\omega}(\mathbf{x},\mathbf{y})$ with a single Matsubara frequency ω is defined as

$$Q_{\omega}(\mathbf{x},\mathbf{y}) = \langle \mathcal{G}_N(\mathbf{y},\mathbf{x},-\omega)\mathcal{G}_N(\mathbf{y},\mathbf{x},\omega)\rangle\ , \tag{2.62}$$

where the bracket denotes the average over the randomly distributed impurity configurations. We average over all possible distributions of impurities, since we are interested only in the large scale behavior of the electrons. The kernel $\mathcal{Q}(\mathbf{x},\mathbf{y})$ is defined as

$$\mathcal{Q}(\mathbf{x},\mathbf{y}) = \beta^{-1}\sum_{\omega} Q_{\omega}(\mathbf{x},\mathbf{y})\,. \tag{2.63}$$

It is important to note that the kernel is determined only by the Green's functions of the normal state electrons. Once the kernel $Q_{\omega}(\mathbf{x},\mathbf{y})$ has been determined for a given applied field then the dependence of the transition temperature on the field may be determined from the solution of Eq. (2.61).

In order to obtain the kernel, $Q_{\omega}(\mathbf{x},\mathbf{x}')$, appearing in the linearized gap equation Eq. (2.61), one has to solve Eq. (2.60) for the Matsubara function describing an electron in the normal state, and perform the average described in Eq. (2.62). It is quite difficult to solve such an equation exactly, so some further approximations are normally made.

In the next section we show how the kernel, $Q_{\omega}(\mathbf{x},\mathbf{y})$, may be evaluated in the case of a "dirty superconductor". First, assuming that the dependence of the Matsubara function on the impurity potential $U(\mathbf{x})$ and the vector potential $\mathbf{A}(\mathbf{x})$ may be dealt with independently, we show how the normal state single particle Green's

function, $\langle \mathcal{G}_N \rangle$, may be calculated in the absence of an applied external field. We then show how the kernel, $Q_\omega(\mathbf{x}, \mathbf{y})$, defined by Eq. (2.62), may be calculated, in the long-wavelength limit and obtain an explicit expression. We then go on to show how the resultant kernel can be recast into the form of a differential equation. Following the work of de Gennes, we show how the effect of boundaries and interfaces on the kernel may be included through the introduction of suitable boundary conditions.

2.3.2 Explicit Form for the Kernel $Q_\omega(\mathbf{x}, \mathbf{x}')$

We denote by $\mathcal{G}_o$ the one-particle Green's function in the absence of the impurity potential, which may be obtained from the solution of the differential equation

$$\left(i\omega + \frac{\nabla^2}{2m} + \mu \right) \mathcal{G}_o(\mathbf{x}; \mathbf{x}', \omega) = \delta(\mathbf{x} - \mathbf{x}') . \tag{2.64}$$

This may be readily solved to yield

$$\mathcal{G}_o(\mathbf{x} - \mathbf{x}', \omega) = (2\pi)^{-3} \int d^3p \frac{e^{i\mathbf{p}\cdot(\mathbf{x}-\mathbf{x}')}}{i\omega - \xi_{\mathbf{p}}} , \tag{2.65}$$

with

$$\xi_{\mathbf{p}} = \frac{1}{2m}(p^2 - 2m\mu) . \tag{2.66}$$

To obtain the explicit spatial representation of the one-particle Green's function $\mathcal{G}_o$, one can integrate (2.65) over momentum space (Appendix A) to obtain

$$\mathcal{G}_o(\mathbf{x}; \mathbf{x}', \omega) = -\frac{\pi N}{p_F |\mathbf{x} - \mathbf{x}'|} \, e^{-\frac{|\omega|}{v_F}|\mathbf{x}-\mathbf{x}'|} \, e^{i p_F |\mathbf{x}-\mathbf{x}'| \operatorname{sgn}\omega} , \tag{2.67}$$

where N denotes the density of states at the Fermi surface and p_F and $v_F = p_F/m$ denote the Fermi momentum and the Fermi velocity, respectively. In the absence of impurities we may define the kernel $Q^c_\omega(\mathbf{x}, \mathbf{x}')$ as

$$\begin{aligned} Q^c_\omega(\mathbf{x} - \mathbf{x}') &= \mathcal{G}_o(\mathbf{x} - \mathbf{x}', \omega) \mathcal{G}_o(\mathbf{x} - \mathbf{x}', -\omega) \\ &= \left[\frac{\pi N}{p_F |\mathbf{x} - \mathbf{x}'|} \right]^2 e^{-2\frac{|\omega|}{v_F}|\mathbf{x}-\mathbf{x}'|} . \end{aligned} \tag{2.68}$$

The Fourier transform of the kernel $Q^c_\omega(\mathbf{x}-\mathbf{x}')$ is given by

$$\begin{aligned} Q^c_\omega(\mathbf{q}) &= \int d^3x Q^c_\omega(\mathbf{x}) e^{i\mathbf{q}\cdot\mathbf{x}} \\ &= \frac{4\pi}{q}\left[\frac{\pi N}{p_F}\right]^2 \int_0^\infty \frac{\sin(qx)}{x} e^{-2\frac{|\omega|}{v_F}x}\, dx \\ &= \frac{2\pi N}{qv_F}\tan^{-1}\left(\frac{qv_F}{2|\omega|}\right). \end{aligned} \tag{2.69}$$

In a dilute doped superconductor, the one-particle Green's function $\mathcal{G}(\mathbf{x};\mathbf{x}',\omega)$ satisfies

$$\left[i\omega + \frac{\nabla^2}{2m} + \mu - U(\mathbf{x})\right]\mathcal{G}(\mathbf{x};\mathbf{x}',\omega) = \delta(\mathbf{x}-\mathbf{x}'). \tag{2.70}$$

The Green's function that we obtain from Eq. (2.70), and the resultant kernel, will depend on the explicit form of the impurity potential. We will deal with the effect of the scattering of the electrons by impurities through a perturbation expansion which assumes a low concentration of impurities and weak coupling between the electrons and the impurities. Using the result that

$$\mathcal{G}_o[i\omega + \frac{\nabla^2}{2m} + \mu]\mathcal{G} = \mathcal{G}[i\omega + \frac{\nabla^2}{2m} + \mu]\mathcal{G}_o + \nabla\cdot[\mathcal{G}_o\nabla\mathcal{G} - \mathcal{G}\nabla\mathcal{G}_o], \tag{2.71}$$

we may write the solution for $\mathcal{G}$ in an integral form as

$$\mathcal{G}(\mathbf{x},\mathbf{x}',\omega) = \mathcal{G}_o(\mathbf{x}-\mathbf{x}',\omega) + \int d^3y \mathcal{G}_o(\mathbf{x}-\mathbf{y},\omega)U(\mathbf{y})\mathcal{G}(\mathbf{y},\mathbf{x}',\omega), \tag{2.72}$$

where we have assumed that the boundary conditions on $\mathcal{G}$ are such that surface terms may be neglected. For simplicity, we assume that the impurity potential may be approximated by a δ function potential as a short range approximation, i.e.,

$$U(\mathbf{x}) = u\sum_a \delta(\mathbf{x}-\mathbf{x}_a), \tag{2.73}$$

where u denotes the coupling constant between the electrons and the impurities and $\mathbf{x}_a$ denotes the position of the impurity. The iteration of Eq.(2.72) and the average

over the impurities yields

$$\begin{aligned}\langle \mathcal{G}(\mathbf{x},\mathbf{x}',\omega)\rangle &= \mathcal{G}_o(\mathbf{x}-\mathbf{x}',\omega) + \int d^3y \langle \mathcal{G}_o(\mathbf{x}-\mathbf{y},\omega)U(\mathbf{y})\mathcal{G}_o(\mathbf{y}-\mathbf{x}',\omega)\rangle \\ &+ \int d^3y\, d^3z \langle \mathcal{G}_o(\mathbf{x}-\mathbf{y},\omega)U(\mathbf{y})\mathcal{G}_o(\mathbf{y}-\mathbf{z},\omega)U(\mathbf{z})\mathcal{G}_o(\mathbf{z}-\mathbf{x}',\omega)\rangle \\ &+ \cdots . \end{aligned} \tag{2.74}$$

While the above expansion is indeed an exact solution and each of the terms may in principle be calculated, it is impossible to sum over all the terms in this expansion and obtain a solution in closed form. Nevertheless, if we examine the iteration expansion term by term, we can pick out leading terms in each order and obtain an approximate solution in closed form.

Let us consider explicitly the 1st order term in the expansion

$$\begin{aligned} &\int d^3y \langle \mathcal{G}_o(\mathbf{x}-\mathbf{y},\omega)U(\mathbf{y})\mathcal{G}_o(\mathbf{y}-\mathbf{x}',\omega)\rangle \\ &= \int d^3y \langle \mathcal{G}_o(\mathbf{x}-\mathbf{y},\omega)\sum_a u\delta(\mathbf{y}-\mathbf{x}_a)\mathcal{G}_o(\mathbf{y}-\mathbf{x}',\omega)\rangle \\ &= \sum_a u\langle \mathcal{G}_o(\mathbf{x}-\mathbf{x}_a,\omega)\mathcal{G}_o(\mathbf{x}_a-\mathbf{x}',\omega)\rangle \\ &= \sum_a u\frac{1}{V}\int d^3x_a \mathcal{G}_o(\mathbf{x}-\mathbf{x}_a,\omega)\mathcal{G}_o(\mathbf{x}_a-\mathbf{x}',\omega) \\ &= \frac{u}{V}\sum_a (2\pi)^{-3}\int d^3p \mathcal{G}_o(\mathbf{p},\omega)\mathcal{G}_o(\mathbf{p},\omega)e^{i\mathbf{p}\cdot(\mathbf{x}-\mathbf{x}')} \\ &= n_i u(2\pi)^{-3}\int d^3p \mathcal{G}_o(\mathbf{p},\omega)\mathcal{G}_o(\mathbf{p},\omega)e^{i\mathbf{p}\cdot(\mathbf{x}-\mathbf{x}')}, \end{aligned} \tag{2.75}$$

where V denotes the volume of the sample, $n_i = V^{-1}\sum_a$ denotes the concentration of the impurities, and the average over the impurities has been replaced by

$$\langle \cdots \rangle \to \frac{1}{V}\int d^3x_a \cdots . \tag{2.76}$$

The first order term may be represented graphically by

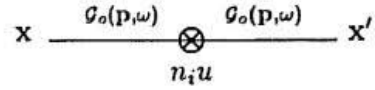

Figure 2.1: Diagrammatic representation of term of order $n_i u$.

where $\otimes$ denotes the impurity and the line denotes the Green's function of a free electron. The average over the impurities for the second order term in Eq. (2.74) should be dealt with carefully since the doubled summation can be divided into two distinct parts, specifically

$$\begin{aligned} U(\mathbf{y})U(\mathbf{z}) &= \sum_{a,b,(a\neq b)} u^2 \delta(\mathbf{y}-\mathbf{x}_a)\delta(\mathbf{z}-\mathbf{x}_b) \\ &+ \sum_a u^2 \delta(\mathbf{y}-\mathbf{x}_a)\delta(\mathbf{z}-\mathbf{x}_a)\,. \end{aligned} \tag{2.77}$$

Substituting this into the second order term in Eq. (2.74) yields

$$\begin{aligned} & \int d^3y\, d^3z\, \langle \mathcal{G}_o(\mathbf{x}-\mathbf{y},\omega)U(\mathbf{y})\mathcal{G}_o(\mathbf{y}-\mathbf{z},\omega)U(\mathbf{z})\mathcal{G}_o(\mathbf{z}-\mathbf{x}',\omega)\rangle \\ = & \sum_{a,b\neq a} u^2 \langle \mathcal{G}_o(\mathbf{x}-\mathbf{x}_a,\omega)\mathcal{G}_o(\mathbf{x}_a-\mathbf{x}_b,\omega)\mathcal{G}_o(\mathbf{x}_b-\mathbf{x}',\omega)\rangle \\ & + \sum_a u^2 \langle \mathcal{G}_o(\mathbf{x}-\mathbf{x}_a,\omega)\mathcal{G}_o(0,\omega)\mathcal{G}_o(\mathbf{x}_a-\mathbf{x}',\omega)\rangle \\ = & \sum_{a,b\neq a} u^2 \frac{1}{V^2} \int d^3x_a\, d^3x_b \mathcal{G}_o(\mathbf{x}-\mathbf{x}_a,\omega)\mathcal{G}_o(\mathbf{x}_a-\mathbf{x}_b,\omega)\mathcal{G}_o(\mathbf{x}_b-\mathbf{x}',\omega) \\ & + \sum_a u^2 \frac{1}{V} \int d^3x_a\, \mathcal{G}_o(\mathbf{x}-\mathbf{x}_a,\omega)\mathcal{G}_o(0,\omega)\mathcal{G}_o(\mathbf{x}_a-\mathbf{x}',\omega) \\ = & (n_i u)^2 (2\pi)^{-3} \int d^3p\, \mathcal{G}_o(\mathbf{p},\omega)\mathcal{G}_o(\mathbf{p},\omega)\mathcal{G}_o(\mathbf{p},\omega)\, e^{i\mathbf{p}\cdot(\mathbf{x}-\mathbf{x}')} \\ & + n_i u^2 \mathcal{G}_o(0,\omega)(2\pi)^{-3} \int d^3p\, \mathcal{G}_o(\mathbf{p},\omega)\mathcal{G}_o(\mathbf{p},\omega)\, e^{i\mathbf{p}\cdot(\mathbf{x}-\mathbf{x}')} \end{aligned} \tag{2.78}$$

The second order term is represented graphically in Fig. 2.2. From this diagrammatic representation it is readily seen that the first order term (2.75) corresponds to the probability amplitude that a particle propagating from $\mathbf{x}$ to $\mathbf{x}'$ will be scattered once

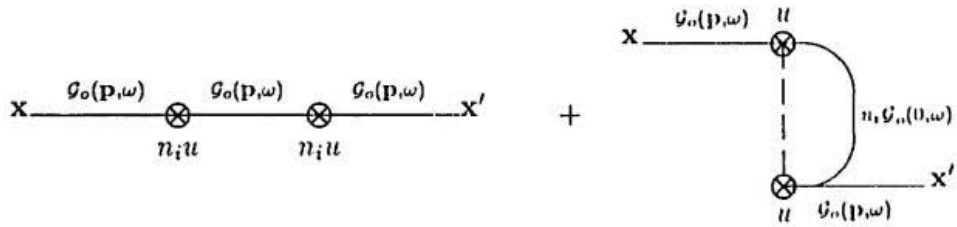

Figure 2.2: Diagrammatic representation of terms of order $(n_i u)^2$ and $n_i u^2$.

by a single impurity. This term contributes to order $n_i u$ to the propagator. Similarly the second order term in Eq. (2.78), corresponds to the probability amplitude that a particle propagating from $\mathbf{x}$ to $\mathbf{x}'$ will be scattered twice by the impurities. The first term of Eq. (2.78) corresponds to the case of two distinct impurities, while the second term of Eq. (2.78) corresponds to the case of multiple scattering of the particle by the same impurity. These terms contribute with order $(n_i u)^2$ and $n_i u^2$, respectively. A diagrammatic representation of the contribution to the third order term is shown in Fig. 2.3. (A diagrammatic representation for the fourth order term is given in Fig. A.1 and A.2 in Appendix A).

The analysis of the diagrammatic expansion suggests that all the terms presented in the iterative expansion of Eq. (2.74) may be classified into groups characterized by a combination of concentration n_i and weak coupling constant u. For example, in Fig. 2.3, one can see that the diagrammatic contribution in (a) will contribute to order $(n_i u)^3$ and is simply a triple product of the first order term while (b), (c) and (e) consist of a product of the first order term and the second order term as analyzed previously and contribute to order $(n_i u)(n_i u^2)$. A new term (d), which contributes to order $(n_i u^3)$, appears in this third order expansion.

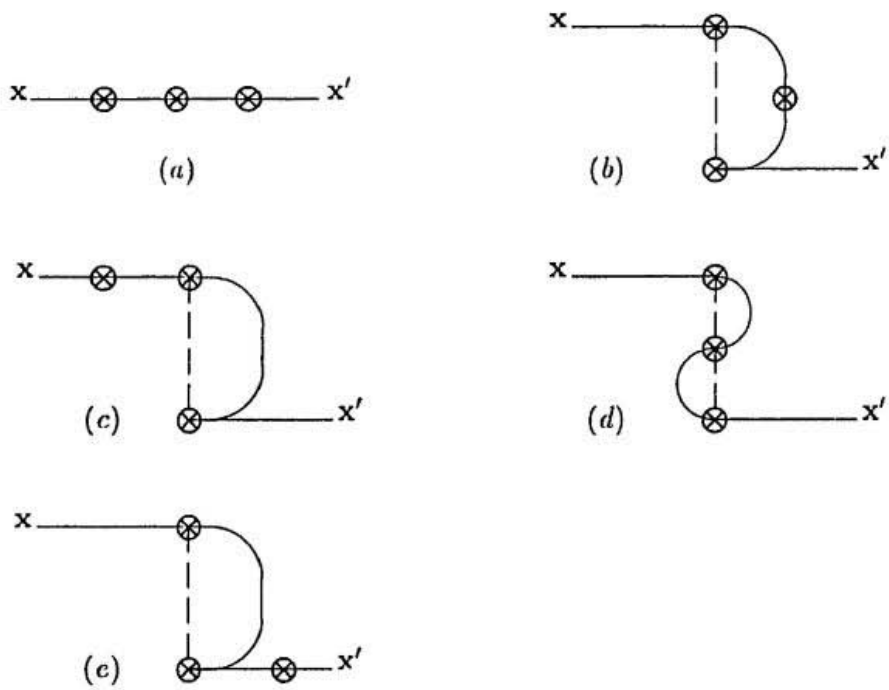

Figure 2.3: Diagrammatic representation of terms of order $(n_i u)^3$, $n_i^2 u^3$ and $n_i u^3$.

A similar analysis may be applied to all the higher order terms in the perturbation series and the various diagrammatic contributions classified according to the coefficient $n_i^p u^q$. Having classified each of the contributions to the perturbation series in terms of the concentration n_i and the coupling constant u, we can identify the leading order contribution in each term in the perturbation series. These are shown diagrammatically in Fig. 2.4. We may immediately write down the solution of the Green's function expressed diagrammatically in Fig. 2.4 as

$$\mathcal{G}(\mathbf{x},\mathbf{x}',\omega) = \mathcal{G}_o(\mathbf{x},\mathbf{x}',\omega) + n_i u (2\pi)^{-3} \int d^3p \mathcal{G}_o(\mathbf{p},\omega) e^{i\mathbf{p}\cdot(\mathbf{x}-\mathbf{x}')} \mathcal{G}(\mathbf{p},\omega). \qquad (2.79)$$

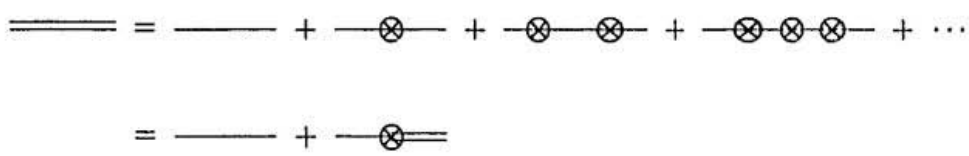

Figure 2.4: Diagrammatic representation of lowest order approximation.

The Dyson equation [62, 63] corresponding to Fig. 2.4 may be written as

$$\begin{aligned} \mathcal{G}^{-1}(\mathbf{p},\omega) &= \mathcal{G}_o^{-1}(\mathbf{p},\omega) - n_i u \\ &= i\omega - \frac{p^2}{2m} + \mu - n_i u \\ &= i\omega - \frac{p^2}{2m} + \mu'. \end{aligned} \tag{2.80}$$

This result suggests that the lowest order process only leads to a renormalization of the Fermi surface (chemical potential), hence, we can absorb the leading order contribution of order $n_i u$ into a renormalized chemical potential μ'. This Fermi surface renormalization implies that all the terms with a factor $(n_i u)^m \quad \forall m \neq 0$ give rise to zero contribution and thus greatly simplifies the analysis of the higher order terms. It may be readily seen, for instance, that only (d) in Fig. 2.3 has a non-zero contribution and similarly (n), (h) and (g) in Fig. A.2 and A.1.

In order to obtain the leading correction we need therefore to consider the corrections characterized by the coefficients $(n_i u^2)^m$. Neglecting the vertex correction terms, for example (g) in Fig. A.1, these terms may be represented diagrammatically as shown in Fig. 2.5. The solution of the Green's function, obtained from this diagrammatic representation, may be written as

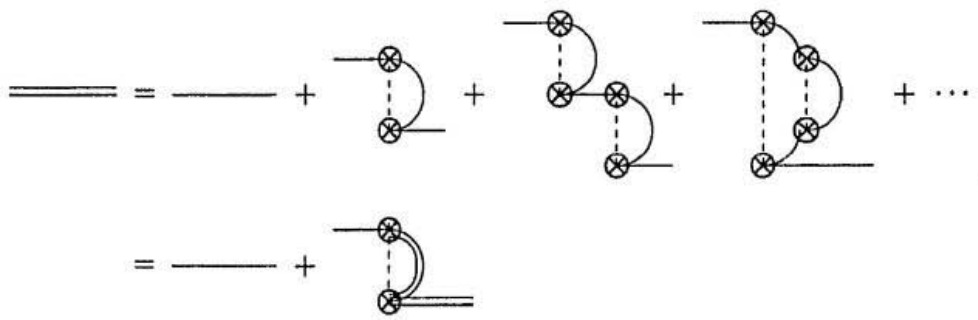

Figure 2.5: Sum of the terms of order $(n_i u^2)^m$

$$\mathcal{G}(\mathbf{x}-\mathbf{x}',\omega) = \mathcal{G}_o(\mathbf{x}-\mathbf{x}',\omega) + n_i u^2 \mathcal{G}(0,\omega)(2\pi)^{-3}\int d^3p \mathcal{G}_o(\mathbf{p},\omega)e^{i\mathbf{p}\cdot(\mathbf{x}-\mathbf{x}')}\mathcal{G}(\mathbf{p},\omega)\,. \tag{2.81}$$

The Dyson equation corresponding to Fig. 2.5 reads

$$\mathcal{G}^{-1}(\mathbf{p},\omega) = \mathcal{G}_o^{-1}(\mathbf{p},\omega) - n_i u^2 \mathcal{G}(0,\omega)\,. \tag{2.82}$$

Assuming the Matsubara Green's function to have the following form

$$\mathcal{G}^{-1}(\mathbf{p},\omega) = i\Gamma - \xi_{\mathbf{p}}\,. \tag{2.83}$$

where $\xi_{\mathbf{p}}$ was defined earlier as $\xi_{\mathbf{p}} = \dfrac{1}{2m}(p^2 - 2m\mu)$. Γ is determined self-consistently from the Dyson equation, Eq. (2.82), as

$$\Gamma = \omega + \frac{1}{2\tau}\mathrm{sgn}\omega, \tag{2.84}$$

with $\tau^{-1} = 2\pi n_i u^2 N$, through the integral

$$\mathcal{G}(\mathbf{x}-\mathbf{x}'=0,\omega) = (2\pi)^{-3}\int d^3p \frac{1}{i\Gamma - \xi_{\mathbf{p}}} = -i\pi N \mathrm{sgn}\Gamma = -i\pi N \mathrm{sgn}\omega\,. \tag{2.85}$$

The spatial representation of the Matsubara function in an infinite domain may be written as

$$\mathcal{G}(\mathbf{x}-\mathbf{x}',\omega) = -\frac{\pi N}{p_F|\mathbf{x}-\mathbf{x}'|}\, e^{-\frac{|\Gamma|}{v_F}|\mathbf{x}-\mathbf{x}'|}\, e^{ip_F|\mathbf{x}-\mathbf{x}'|\mathrm{sgn}\,\Gamma}\,, \tag{2.86}$$

which is the same form as $\mathcal{G}_o$ with ω being replaced by Γ. The kernel for a dilute doped superconductor defined by Eq. (2.62) may be obtained using equation, Eq. (2.72), and averaging over the impurities. We would then find that

$$\begin{aligned}
& Q_\omega(\mathbf{x}-\mathbf{x}') \\
= \;& \langle \mathcal{G}(\mathbf{x}-\mathbf{x}',-\omega)\mathcal{G}(\mathbf{x}-\mathbf{x}',\omega)\rangle \\
= \;& \mathcal{G}_o(\mathbf{x}-\mathbf{x}',-\omega)\mathcal{G}_o(\mathbf{x}-\mathbf{x}',\omega) \\
+ \;& \mathcal{G}_o(\mathbf{x}-\mathbf{x}',-\omega)\int d^3y\, \langle \mathcal{G}_o(\mathbf{x}-\mathbf{y},\omega)U(\mathbf{y})\mathcal{G}(\mathbf{y}-\mathbf{x}',\omega)\rangle \\
+ \;& \mathcal{G}_o(\mathbf{x}-\mathbf{x}',\omega)\int d^3y\, \langle \mathcal{G}_o(\mathbf{x}-\mathbf{y},-\omega)U(\mathbf{y})\mathcal{G}(\mathbf{y}-\mathbf{x}',-\omega)\rangle \\
+ \;& \int d^3y\, \langle \mathcal{G}_o(\mathbf{x}-\mathbf{y},-\omega)U(\mathbf{y})\mathcal{G}(\mathbf{y}-\mathbf{x}',-\omega)\rangle \int d^3z\, \langle \mathcal{G}_o(\mathbf{x}-\mathbf{z},\omega)U(\mathbf{z})\mathcal{G}(\mathbf{z}-\mathbf{x}',\omega)\rangle \\
+ \;& \int d^3y d^3z\, \langle \mathcal{G}_o(\mathbf{x}-\mathbf{y},-\omega)U(\mathbf{y})\mathcal{G}(\mathbf{y}-\mathbf{x}',-\omega)\mathcal{G}_o(\mathbf{x}-\mathbf{z},\omega)U(\mathbf{z})\mathcal{G}(\mathbf{z}-\mathbf{x}',\omega)\rangle \\
- \;& \int d^3y\, \langle \mathcal{G}_o(\mathbf{x}-\mathbf{y},-\omega)U(\mathbf{y})\mathcal{G}(\mathbf{y}-\mathbf{x}',-\omega)\rangle \int d^3z\, \langle \mathcal{G}_o(\mathbf{x}-\mathbf{z},\omega)U(\mathbf{z})\mathcal{G}(\mathbf{z}-\mathbf{x}',\omega)\rangle\,,
\end{aligned} \tag{2.87}$$

where the bracket denotes the average over a random impurity potential.

The first and the second terms in Eq. (2.87) may be combined as

$$\mathcal{G}_o(\mathbf{x}-\mathbf{x}',-\omega)\,\langle \mathcal{G}(\mathbf{x}-\mathbf{x}',\omega)\rangle\,, \tag{2.88}$$

and the third and forth terms in Eq. (2.87) may be written as

$$\int d^3y \langle \mathcal{G}_o(\mathbf{x}-\mathbf{y},-\omega)U(\mathbf{y})\mathcal{G}(\mathbf{y}-\mathbf{x}',-\omega)\rangle\, \langle \mathcal{G}(\mathbf{x}-\mathbf{x}',\omega)\rangle\,. \tag{2.89}$$

Then, terms in Eq. (2.88) and Eq. (2.89) can be expressed as

$$Q^o_\omega(\mathbf{x}-\mathbf{x}') = \langle \mathcal{G}(\mathbf{x}-\mathbf{x}',\omega)\rangle\, \langle \mathcal{G}(\mathbf{x}-\mathbf{x}',\omega)\rangle\,, \tag{2.90}$$

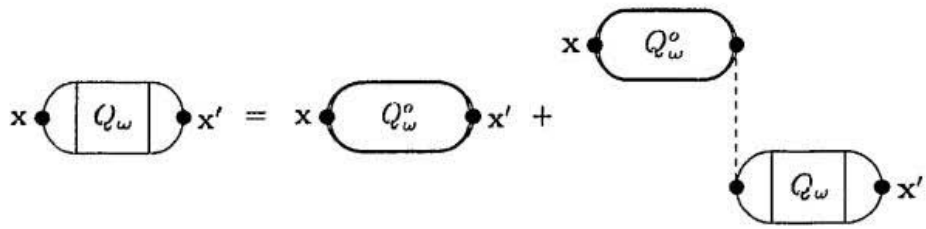

Figure 2.6: Impurity averaging diagrams of vertex in the ladder approximation.

which describes two electrons propagating in the superconductor scattered independently by impurities. Further analysis of the average over impurities for the fifth term in Eq. (2.87) is tedious. However, Werthamer [18] points out that if one only considers the ladder approximation as shown graphically in Fig. 2.6, the fifth and the sixth terms in Eq. (2.87) may be expressed as

$$n_i u^2 \int d^3x_a \, \langle \mathcal{G}(\mathbf{x}-\mathbf{x}_a,-\omega)\rangle \, \langle \mathcal{G}(\mathbf{x}-\mathbf{x}_a,\omega)\rangle \, Q_\omega(\mathbf{x}_a-\mathbf{x}',\omega)\,, \tag{2.91}$$

where the δ function potential has been used.

The integral solution for the kernel is given by

$$\begin{aligned} Q_\omega(\mathbf{x}-\mathbf{x}') &= \langle \mathcal{G}(\mathbf{x}-\mathbf{x}',-\omega)\rangle \, \langle \mathcal{G}(\mathbf{x}-\mathbf{x}',\omega)\rangle \\ &+ n_i u^2 \int d^3x_a \, \langle \mathcal{G}(\mathbf{x}-\mathbf{x}_a,-\omega)\rangle \, \langle \mathcal{G}(\mathbf{x}-\mathbf{x}_a,\omega)\rangle \, Q_\omega(\mathbf{x}_a-\mathbf{x}')\,, \\ &= Q^o_\omega(\mathbf{x}-\mathbf{x}') + n_i u^2 \int d^3x_a Q^o_\omega(\mathbf{x}-\mathbf{x}_a) Q_\omega(\mathbf{x}_a-\mathbf{x}')\,. \end{aligned} \tag{2.92}$$

Using Eq. (2.86), one obtains

$$Q^o_\omega(\mathbf{x}-\mathbf{x}') = \left[\frac{\pi N}{p_F|\mathbf{x}-\mathbf{x}'|}\right]^2 e^{-\frac{2|\Gamma|}{v_F}|\mathbf{x}-\mathbf{x}'|}\,, \tag{2.93}$$

while the Fourier transform of $Q^o_\omega(\mathbf{x}-\mathbf{x}')$ is given by

$$Q^o_\omega(\mathbf{q}) = \frac{2\pi N}{v_F q} \tan^{-1}\left(\frac{v_F q}{2|\Gamma|}\right)\,. \tag{2.94}$$

The Dyson equation for the kernel in the ladder approximation is

$$Q_\omega^{-1}(\mathbf{q}) = [Q_\omega^o(\mathbf{q})]^{-1} - [2\pi N\tau]^{-1}\,, \tag{2.95}$$

and the kernel, in momentum space, is given by

$$Q_\omega(\mathbf{q}) = 2\pi N \left\{ \left[\frac{1}{v_F q} \tan^{-1}\left(\frac{v_F q}{2|\Gamma|} \right) \right]^{-1} - \tau^{-1} \right\}^{-1}\,. \tag{2.96}$$

The result given in Eq. (2.96) for the kernel may be generalized for a more realistic approximation to the impurity potential than that used in obtaining Eq. (2.96). To obtain the equivalent result for the more general form of the impurity potential,

$$U(\mathbf{x}) = \sum_a u(\mathbf{x} - \mathbf{x}_a)\,,$$

one needs only to replace $\tau^{-1} = 2\pi n_i u^2 N$ in Eq. (2.96) by

$$\tau^{-1} = \frac{n_i m p_F}{(2\pi)^2} \int |u(\theta)|^2 d\Omega = n_i v_F \sigma\,, \tag{2.97}$$

where σ denotes the scattering cross-section in the Born approximation.

The preceding derivation assumed that the impurity concentration was low, and therefore, strictly speaking, the result is only valid for the case of a dilute doped superconductor. However, Werthamer [18] has pointed out that the result given in Eq. (2.96) is entirely equivalent to that obtained by de Gennes [26] for the case of a high impurity concentration, when expressed in terms of scattering time τ rather than the concentrations n_i.

2.4 Boundary Conditions and the Proximity Effect

In deriving the expression for the kernel, given by Eq. (2.96), we neglected to consider the role of the boundary conditions, assuming only that the surface terms did

not contribute. In order to consider the effects of geometry on the transition temperature, however, we need to consider the effect of surfaces and interfaces on the kernel, $Q_\omega(\mathbf{x},\mathbf{x}')$.

While in principle it is possible to generalize the preceding arguments to include the boundary conditions on the single electron Green's function, and hence to evaluate the kernel, the generalization to inhomogeneous systems is most easily accomplished following the formulation given by de Gennes [26].

We begin this section by showing how the kernel derived in the preceding sections may be recast in the form of a differential equation. We will then argue, as de Gennes did, that the differential equation describing the kernel is valid even in the presence of surfaces and interfaces. We will then go on to show that the kernel is modified by a free surface through the boundary conditions. An analogous result for a planar interface between two materials is also derived.

Finally, we will show how the kernel may be generalized to include the effect of a homogeneous magnetic field.

2.4.1 Long Wavelength Approximation

If we restrict our considerations to situations for which the spatial variation of the pair amplitude is small, then we need only evaluate the kernel in the long wavelength limit. Expanding the $\tan^{-1}(v_F q/2|\Gamma|)$ in Eq. (2.96) in powers of the momentum leads to

$$\begin{aligned} Q_\omega(\mathbf{q}) &= \frac{\pi N}{|\omega| + q^2 l^2 [6\tau(1+2\tau|\omega|)]^{-1}}, \\ &\approx \frac{\pi N}{|\omega| + q^2 l^2 [6\tau]^{-1}} \qquad (2\tau|\omega| \ll 1), \\ &= \frac{2\pi N}{2|\omega| + Dq^2}, \end{aligned} \tag{2.98}$$

with $D = \frac{1}{3} l v_F$ denoting the diffusion constant.

The spatial representation of the kernel in this long wavelength limit may be given by

$$Q_\omega(\mathbf{x}-\mathbf{x}') = \int e^{-i\mathbf{q}\cdot(\mathbf{x}-\mathbf{x}')}\, Q_\omega(\mathbf{q})\, d^3q \tag{2.99}$$

It is readily shown that $Q_\omega(\mathbf{x}-\mathbf{x}')$ is simply the Green's function for the three dimensional diffusion equation

$$(2|\omega| - D\nabla^2)\, Q_\omega(\mathbf{x}-\mathbf{x}') = 2\pi N\, \delta(\mathbf{x}-\mathbf{x}')\,, \tag{2.100}$$

subject to the boundary conditions

$$\lim_{|\mathbf{x}-\mathbf{x}'|\to\infty} Q_\omega(\mathbf{x},\mathbf{x}') = 0\,. \tag{2.101}$$

Based on a more heuristic argument, de Gennes has shown that $Q_\omega(\mathbf{x},\mathbf{x}')$ satisfies Eq. (2.100). He also argued that the effect of surfaces and interfaces on the kernel may be incorporated by a suitable modification of the boundary condition given by Eq. (2.101).

2.4.2 de Gennes Boundary Conditions for a Free Surface

In order to derive the de Gennes boundary conditions for a free surface, we consider the case of a planar boundary at $x = 0$, with the superconductor occupying the region $x > 0$. In the absence of an applied external field, the order parameter is independent of y and z and thus may be written as

$$\Delta(\mathbf{x}) = \Delta(x)\,. \tag{2.102}$$

The linearized Gor'kov gap equation, Eq. (2.61), then reduces to

$$\Delta(x) \;=\; V\beta^{-1}\sum_\omega \int dx'\, Q_\omega(x,x')\,\Delta(x')\,.$$

The one dimensional kernel, $Q_\omega(x,x')$, satisfies the one dimensional diffusion equation

$$\left[2|\omega| - D\frac{d^2}{dx'^2}\right] Q_\omega(x,x') = 2\pi N\, \delta(x-x')\,. \tag{2.103}$$

The explicit form of the kernel obtained by the integration of the result given by Eq. (2.99) may be readily evaluated as

$$\begin{aligned} Q^s_\omega(x-x') &= \int dy\, dz\, Q_\omega(\mathbf{x}-\mathbf{x}')\,, \\ &= \frac{2\pi N}{(2\pi)^3}\int_{-\infty}^{\infty} d\mathbf{q}\frac{e^{i\mathbf{q}\cdot(\mathbf{x}-\mathbf{x}')}}{2|\omega|+Dq^2}\,dy\,dz\,, \\ &= \frac{2\pi N}{2\pi}\int_{-\infty}^{\infty} dq\frac{e^{iq(x-x')}}{2|\omega|+Dq^2}\,, \\ &= \frac{N}{2|\omega|\xi_\omega}\int_{-\infty}^{\infty} dt\frac{e^{it(x-x')/\xi_\omega}}{1+t^2}\,, \\ &= \frac{2N}{2|\omega|\xi_\omega}\int_{0}^{\infty} dt\frac{\cos[t(x-x')/\xi_\omega]}{1+t^2}\,, \\ &= \frac{\pi N}{2|\omega|\xi_\omega}e^{-|x-x'|/\xi_\omega}\,, \end{aligned} \tag{2.104}$$

where $\xi_\omega = \sqrt{D/2|\omega|}$. However, while this provides a particular solution to Eq. (2.103), it is possible to construct other solutions expressed as the sum of a singular part $Q^s_\omega(x,x')$, and a non-singular part, $\mathcal{R}_\omega(x,x')$, i.e.,

$$Q_\omega(x,x') = Q^s_\omega(x,x') + \mathcal{R}_\omega(x,x')\,, \tag{2.105}$$

where the kernel, Q^s_ω, is given by Eq. (2.104) and $\mathcal{R}_\omega$ is required to satisfy the homogeneous diffusion equation given by

$$\left[2|\omega| - D\frac{d^2}{dx'^2}\right]\mathcal{R}_\omega(x,x') = 0\,, \tag{2.106}$$

together with the reciprocity condition, namely, $\mathcal{R}_\omega(x,x') = \mathcal{R}_\omega(x',x)$. In order to uniquely determine the solution $\mathcal{R}_\omega(x,x')$, it is necessary to impose a boundary condition that reflects the presence of the free surface. To obtain the appropriate boundary condition, we integrate Eq. (2.103) with respect to x' over the domain $[0,\infty]$ to obtain the following expression

$$2|\omega|\int_0^\infty dx'\, Q_\omega(x,x') - D\frac{d}{dx'}\, Q_\omega(x,x')\Big|_0^\infty = 2\pi N\,. \tag{2.107}$$

This condition together with the sum rule [26]

$$|\omega| \int_0^\infty dx' \, Q_\omega(x, x') = \pi N \,, \tag{2.108}$$

and the requirement that

$$\lim_{x' \to \infty} \frac{d}{dx'} Q_\omega(x, x') = 0, \tag{2.109}$$

yields the boundary condition

$$\frac{\partial}{\partial x'} Q_\omega(x, x') = 0 \Big|_{x'=0} \,. \tag{2.110}$$

The homogeneous contribution to the kernel is then given by

$$\mathcal{R}_\omega(x, x') = \frac{\pi N}{2|\omega|\xi_\omega} e^{-|x+x'|/\xi_\omega} \qquad x > 0, x' > 0 \,, \tag{2.111}$$

which yields the following expression for $Q_\omega(x, x')$

$$Q_\omega(x, x') = \frac{\pi N}{2|\omega|\xi_\omega} \left(e^{-|x-x'|/\xi_\omega} + r \, e^{-|x+x'|/\xi_\omega} \right) \qquad x > 0, x' > 0 \,. \tag{2.112}$$

At the free surface denoted by $x = 0$, we have

$$\frac{\partial}{\partial x} Q_\omega(x, x') = \frac{\partial}{\partial x} \left[Q^s_\omega(x, x') + \mathcal{R}_\omega(x, x') \right] = 0 \,, \tag{2.113}$$

which determines $r = 1$. The homogeneous contribution to the kernel may be readily calculated for the more complicated case of two free surfaces. Substituting this kernel into the self-consistent gap equation (2.61), it is easy to show that the boundary condition satisfied by $\Delta(x)$ is

$$\frac{d}{dx} \Delta(x) = \frac{1}{V} \frac{d}{dx} \mathcal{F}(x) = 0 \,, \qquad \text{at the free surface } x = 0 \,, \tag{2.114}$$

2.4.3 de Gennes Continuity Condition for a Planar Interface

A similar boundary condition may be obtained for the kernel $Q_\omega(x, x')$ at a planar interface between two distinct metals [26]. Let us consider a bilayer structure labeled by A and B separated by the plane $x' = 0$ as shown in Fig. 2.7.

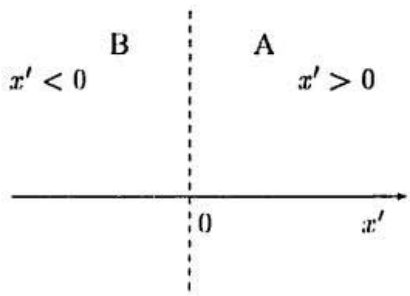

Figure 2.7: Bilayer Geometry.

Using the diffusion equation as derived in the previous section by the Green's function method, we can write down the diffusion equations for the kernels in regions A and B. They are

$$\left[2|\omega| - D_A \frac{d^2}{dx'^2}\right] Q_\omega(x, x') = 2\pi N_A \delta(x - x'), \tag{2.115}$$

and

$$\left[2|\omega| - D_B \frac{d^2}{dx'^2}\right] Q_\omega(x, x') = 2\pi N_B \delta(x - x'), \tag{2.116}$$

respectively. Integrating the two equations with respect to x' over the half space, we obtain

$$\begin{aligned} &2|\omega| \int_{-\infty}^{\infty} dx' Q_\omega(x, x') - \left[D_A \frac{d}{dx'} Q_\omega(x, x')\right]_{x'=0^+}^{x'=\infty} \\ &- \left[D_B \frac{d}{dx'} Q_\omega(x, x')\right]_{x'=-\infty}^{x'=0^-} = 2\pi[\theta(x) N_A + \theta(-x) N_B]. \end{aligned} \tag{2.117}$$

Using this result, together with the sum rule [26],

$$|\omega| \int dx' \, Q_\omega(x, x') = \pi \begin{cases} N_A & x \in A \\ N_B & x \in B \end{cases} \tag{2.118}$$

and the requirement that the contribution at $|x| \to \infty$ vanishes, we obtain the following boundary condition:

$$D_A \frac{d}{dx'} Q_\omega(x,0) = D_B \frac{d}{dx'} Q_\omega(x,0)\,. \tag{2.119}$$

In order to find the second continuity condition, we write the kernels in regions A and B as follows

$$Q_\omega(x,x') = \frac{\pi N_A}{2|\omega|\xi_A}\left[e^{-|x-x'|/\xi_A} + r_A e^{-(x+x')/\xi_A}\right] \qquad x>0, x'>0\,, \tag{2.120}$$

$$Q_\omega(x,x') = \frac{\pi N_B}{2|\omega|\xi_B}\left[e^{-|x-x'|/\xi_B} + r_B e^{(x+x')/\xi_B}\right] \qquad x<0, x'<0\,, \tag{2.121}$$

$$Q_\omega(x,x') = \sigma_A \frac{\pi N_A}{2|\omega|\xi_A} e^{-x/\xi_A + x'/\xi_B} \qquad x>0,\ x'<0\,, \tag{2.122}$$

$$Q_\omega(x,x') = \sigma_B \frac{\pi N_B}{2|\omega|\xi_B} e^{-x'/\xi_A + x/\xi_B} \qquad x<0,\ x'>0\,. \tag{2.123}$$

Using the continuity condition Eq. (2.119) and the reciprocity condition, we obtain

$$\begin{aligned}(1-r_A)N_A &= \sigma_B N_B\,,\\ (1-r_B)N_B &= \sigma_A N_A\,,\\ \frac{\sigma_A N_A}{\xi_A} &= \frac{\sigma_B N_B}{\xi_B}\,,\end{aligned} \tag{2.124}$$

which may be expressed as

$$\begin{aligned}(1-r_A) &= c\,\frac{N_B\xi_B}{N_B\xi_B + N_A\xi_A}\,,\\ (1-r_B) &= c\,\frac{N_A\xi_A}{N_B\xi_B + N_A\xi_A}\,,\\ \sigma_A &= c\,\frac{N_B\xi_A}{N_B\xi_B + N_A\xi_A}\,,\\ \sigma_B &= c\,\frac{N_A\xi_B}{N_B\xi_B + N_A\xi_A}\,,\end{aligned} \tag{2.125}$$

with c to be determined. At $x=0$, the kernel (2.120) and (2.123) are written as

$$Q_\omega(0^+,x') = \frac{\pi N_A}{2|\omega|\xi_A}\left[e^{-x'/\xi_A} + r_A e^{-x'/\xi_A}\right] \qquad x\to 0^+, x'>0\,, \tag{2.126}$$

$$Q_\omega(0^-,x') = \sigma_B \frac{\pi N_B}{2|\omega|\xi_B} e^{-x'/\xi_A} \qquad x\to 0^-,\ x'>0\,. \tag{2.127}$$

The ratio of the two kernels is given by

$$R_1 = \frac{Q_\omega(0^+, x' > 0)}{Q_\omega(0^-, x' > 0)} = \frac{N_A}{N_B}\left[\frac{2}{c} + \frac{2-c}{c}\frac{N_B\xi_B}{N_A\xi_A}\right] . \tag{2.128}$$

Similarly, the ratio between kernels (2.122) and (2.121) at $x = 0$ is expressed as

$$R_2 = \frac{Q_\omega(0^+, x' < 0)}{Q_\omega(0^-, x' < 0)} = \frac{N_A}{N_B}\left[\frac{2}{c} + \frac{2-c}{c}\frac{N_A\xi_A}{N_B\xi_B}\right]^{-1} . \tag{2.129}$$

Therefore, we have

$$Q_\omega(0^+, x' > 0) = R_1 Q_\omega(0^-, x' > 0) , \tag{2.130}$$

$$Q_\omega(0^+, x' < 0) = R_2 Q_\omega(0^-, x' < 0) . \tag{2.131}$$

de Gennes stated that a general boundary condition of the kernel is of the form

$$Q_\omega(0^+, x') = \alpha Q_\omega(0^-, x')\left[1 + \frac{\beta}{\alpha}\frac{1}{Q_\omega(0^-, x')}\frac{d}{dx}Q_\omega(0^-, x')\right] . \tag{2.132}$$

However, the second term in the bracket is proportional to l/ξ_ω and thus it is negligible in the dirty limit. This leads to

$$Q_\omega(0^+, x') = \alpha Q_\omega(0^-, x') \qquad \forall x' . \tag{2.133}$$

By applying de Gennes' argument, we have $R_1 = R_2$, which leads to $c = 2$. de Gennes' second boundary condition of the kernel may be expressed as

$$\frac{Q_\omega(0^+, x')}{Q_\omega(0^-, x')} = \frac{N_A}{N_B} \qquad \text{or} \qquad \frac{Q_\omega(0^+, x')}{N_A} = \frac{Q_\omega(0^-, x')}{N_B} . \tag{2.134}$$

Following de Gennes' work [26], we have obtained the boundary conditions for the spatial variation of the kernel for a bilayer system. While the boundary conditions given by Eqs. (2.114), (2.119) and (2.134) were derived for the particular case of a single planar surface and a single planar interface respectively, they may be cast in a more general three dimensional form as

$$\begin{cases} \mathbf{n}\cdot\nabla Q_\omega(\mathbf{x}, \mathbf{x}') = 0 , & \text{for } \mathbf{x} \text{ at free surface} , \\ D_A\,\mathbf{n}\cdot\nabla Q_\omega(\mathbf{x}^+, \mathbf{x}') = D_B\,\mathbf{n}\cdot\nabla Q_\omega(\mathbf{x}^-, \mathbf{x}') , & \text{for } \mathbf{x} \text{ at interface} , \\ \frac{1}{N_A}Q_\omega(\mathbf{x}^+, \mathbf{x}') = \frac{1}{N_B}Q_\omega(\mathbf{x}^-, \mathbf{x}') , & \text{for } \mathbf{x} \text{ at interface} , \end{cases} \tag{2.135}$$

where **n** denotes the unit vector normal to the surface or interface.

These results allow us to extend the de Gennes formalism to non-planar geometries. The formalism can also be extended to include multiple surfaces and interfaces by requiring that the kernel satisfy the appropriate boundary condition at each of the bounding surfaces and interfaces in the system. This allows us to apply the de Gennes formalism to restricted geometries such as superconducting films, superlattice and multilamellar structures, the principal focus of the present work.

Effect of Magnetic Field

We can also extend the formalism to include the effect of a magnetic field. This is most easily accomplished if we modify the one-particle Green's function, derived for the homogeneous case in Eq. (2.86), to include the effect of the vector potential through the semiclassical phase integral approximation that

$$\begin{aligned} \mathcal{G}_N(\mathbf{x}-\mathbf{x}',\omega) &= e^{-i\frac{e}{c}\int_{\mathbf{x}'}^{\mathbf{x}}\mathbf{A}(\mathbf{x})\cdot d\mathbf{l}}\,\mathcal{G}(\mathbf{x}-\mathbf{x}',\omega)\,, \\ &\approx e^{-i\frac{e}{c}\mathbf{A}(\mathbf{x})\cdot(\mathbf{x}-\mathbf{x}')}\,\mathcal{G}(\mathbf{x}-\mathbf{x}',\omega)\,, \end{aligned} \tag{2.136}$$

the resultant kernel may then be expressed as

$$\begin{aligned} Q^{A}_{\omega}(\mathbf{x},\mathbf{x}') &= e^{\frac{-2ie}{\hbar c}\mathbf{A}(\mathbf{x})\cdot(\mathbf{x}-\mathbf{x}')}\,Q_{\omega}(\mathbf{x}-\mathbf{x}')\,, \\ &= e^{i\frac{2\pi}{\phi_o}\mathbf{A}(\mathbf{x})\cdot(\mathbf{x}-\mathbf{x}')}\,Q_{\omega}(\mathbf{x}-\mathbf{x}')\,. \end{aligned} \tag{2.137}$$

with $\phi_o = \frac{hc}{2|e|}$. The diffusion equation for the kernel given by Eq. (2.103) is then modified to give a generalized gauge invariant form

$$\left[2|\omega| + \hat{L}(\mathbf{\Pi})\right] Q_{\omega}(\mathbf{x},\mathbf{y}) = 2\pi N\,\delta(\mathbf{x}-\mathbf{y})\,, \tag{2.138}$$

where the operator $\mathbf{\Pi}$ is defined as

$$\mathbf{\Pi} = \left[\nabla - i\frac{2\pi}{\phi_o}\mathbf{A}\right]\,, \tag{2.139}$$

and $\hat{L}$ is given by

$$\hat{L}(\mathbf{\Pi}) = -hD\left[\nabla - i\frac{2\pi}{\phi_o}\mathbf{A}\right]^2 . \tag{2.140}$$

By analogy with the zero field case, the effect of surfaces and interfaces may be incorporated by means of appropriate boundary conditions, similar to those given in Eqs. (2.135). However, in order to preserve the invariance of the theory under a gauge transformation, the boundary conditions must be modified to include the effect of the vector potential. The boundary conditions are therefore given by

$$\begin{cases} \mathbf{n}\cdot\mathbf{\Pi}\, Q_\omega(\mathbf{x},\mathbf{y}) = 0\,, & \text{for } \mathbf{x} \text{ at free surface}, \\ D_A\,\mathbf{n}\cdot\mathbf{\Pi}\, Q_\omega(\mathbf{x}^+,\mathbf{y}) = D_B\,\mathbf{n}\cdot\mathbf{\Pi}\, Q_\omega(\mathbf{x}^-,\mathbf{y})\,, & \text{for } \mathbf{x} \text{ at interface}, \\ \frac{1}{N_A} Q_\omega(\mathbf{x}^+,\mathbf{y}) = \frac{1}{N_B} Q_\omega(\mathbf{x}^-,\mathbf{y})\,, & \text{for } \mathbf{x} \text{ at interface}. \end{cases} \tag{2.141}$$

The boundary conditions imposed on the pair amplitude $\mathcal{F}$ may be readily obtained by using Gor'kov equation, Eq. (2.57), together with Eq. (2.141),

$$\begin{cases} \mathbf{n}\cdot\mathbf{\Pi}\,\mathcal{F}(\mathbf{x}) = 0\,, & \text{for } \mathbf{x} \text{ at free surface}, \\ D_A\,\mathbf{n}\cdot\mathbf{\Pi}\,\mathcal{F}(\mathbf{x}^+) = D_B\,\mathbf{n}\cdot\mathbf{\Pi}\,\mathcal{F}(\mathbf{x}^-), & \text{for } \mathbf{x} \text{ at interface}, \\ \frac{1}{N_A}\mathcal{F}(\mathbf{x}^+) = \frac{1}{N_B}\mathcal{F}(\mathbf{x}^-)\,, & \text{for } \mathbf{x} \text{ at interface}. \end{cases} \tag{2.142}$$

2.5 Application of the de Gennes Formalism

In the preceding sections we have shown how the solution of the linearized Gor'kov equation may be expressed in terms of the kernel, $Q_\omega(\mathbf{x},\mathbf{x}')$. Following the arguments of Werthamer [18], we have shown how the kernel may be expressed in terms of a diffusion equation as proposed by de Gennes [26], when the spatial variation of the order parameter is small. We then went on to show how the effects of surfaces and interfaces might be included in the kernel through the application of appropriate boundary conditions. The resultant formalism was readily extended to include

the effect of a finite magnetic field by the gauge invariant replacement

$$i\nabla \rightarrow i\mathbf{\Pi} = i(\nabla - i\frac{2\pi}{\phi_o}\mathbf{A})\,. \tag{2.143}$$

In this section, we apply the de Gennes formalism to two explicit examples. In the first we consider a homogeneous magnetic field in an infinite sample. This relatively simple application illustrates the simplest non-trivial application of the de Gennes theory and allows us to recover some results for the upper critical field that will be useful in our subsequent discussion. The second example we wish to consider is the less trivial case of a system consisting of M alternating layers of metals A and B, at least one of which is superconducting. We assume that the thickness of the layers does not vary along the length of sample and we denote the thickness of the A-type layers by d_A and the thickness of the B-type layers by d_B. This geometry includes the superconducting film ($A = B$) and the superlattice ($M \rightarrow \infty$) as specific cases.

2.5.1 Homogeneous Superconductor

For a homogeneous superconductor, the linearized Gor'kov equation for the pair amplitude is given by

$$\mathcal{F}(\mathbf{x}) = k_B T \sum_{\omega} \int d^3y\; Q_\omega(\mathbf{x},\mathbf{y})\, V\, \mathcal{F}(\mathbf{y})\,, \tag{2.144}$$

where the kernel satisfies the boundary condition specified by Eq. (2.101). Let us consider the following eigenvalue equation

$$[\epsilon_j - \hat{L}(\mathbf{\Pi})]\,\phi_j(\mathbf{x}) = 0\,, \tag{2.145}$$

subject to the boundary condition

$$\lim_{|\mathbf{x}|\rightarrow\infty} \phi_j(\mathbf{x}) = 0\,. \tag{2.146}$$

The orthogonality and closure properties of the eigenfunctions are

$$\int dx^3 \phi_{j'}(\mathbf{x}) \frac{1}{N} \phi_j^*(\mathbf{x}) = \delta_{jj'}\,, \tag{2.147}$$

$$\sum_j \phi_j(\mathbf{x}) \phi_j^*(\mathbf{y}) = N\delta(\mathbf{x}-\mathbf{y})\,. \tag{2.148}$$

The kernel, $Q_\omega(\mathbf{x},\mathbf{y})$, can now be written as

$$Q_\omega(\mathbf{x},\mathbf{y}) = 2\pi \sum_j \frac{\phi_j(\mathbf{x})\,\phi_j^*(\mathbf{y})}{2|\omega| + \epsilon_j}\,, \tag{2.149}$$

and the summation of the kernel over the Matsubara frequency can be expressed as

$$k_B T \sum_\omega Q_\omega(\mathbf{x},\mathbf{y}) = \sum_j \phi_j(\mathbf{x})\,\phi_j^*(\mathbf{y})\,S(\epsilon_j)\,, \tag{2.150}$$

where $S(\epsilon_j)$ is defined as

$$S(\epsilon_j) = 2\pi k_B T \sum_\omega \frac{1}{2|\omega| + \epsilon_j}\,. \tag{2.151}$$

It is readily seen that $S(\epsilon_j)$ would diverge if the summation over the Matsubara frequencies went to infinity. However, this divergence does not occur because of the presence of the BCS cutoff, $|\omega| < \omega_c$, that yields the result

$$S(0) = 2\pi k_B T \sum_\omega \frac{1}{2|\omega|} = \ln\left(\frac{1.134\hbar\omega_D}{k_B T}\right)\,. \tag{2.152}$$

We then write the frequency sum in the form proposed by de Gennes [26]

$$\begin{aligned} S^{\mathrm{dG}}(\epsilon_j) &= [S(\epsilon_j) - S(0)] + S(0) \\ &= \ln\left(\frac{1.134\hbar\omega_D}{k_B T}\right) - \chi\left(\frac{\epsilon_j}{2\pi k_B T}\right)\,, \end{aligned} \tag{2.153}$$

where

$$\chi(z) = \psi\left(\frac{1}{2} + \frac{1}{2}z\right) - \psi\left(\frac{1}{2}\right) \tag{2.154}$$

and $\psi(z)$ is the digamma function. However, Lodder and Koperdraad [52] have argued that this cutoff may produce unphysical results if $\epsilon_j \gtrsim \hbar\omega_D$. Instead they proposed the following for $S(\epsilon_j)$

$$S^{\mathrm{LK}}(\epsilon_j) = \psi\left(\frac{\hbar\omega_D}{2\pi k_B T} + \frac{\epsilon_j}{4\pi k_B T} + 1\right) - \psi\left(\frac{\epsilon_j}{4\pi k_B T} + \frac{1}{2}\right)\,, \tag{2.155}$$

together with a modified BCS transition temperature formula [52]

$$\frac{1}{NV} = \psi\left(\frac{\hbar\omega_D}{2\pi k_B T_c} + 1\right) - \psi\left(\frac{1}{2}\right). \tag{2.156}$$

$S^{dG}(\epsilon_j)$ and $S^{LK}(\epsilon_j)$ are consistent for $\epsilon \ll \omega_D$.

Using the complete set of the eigenfunctions, $\{\phi_j(\mathbf{x})\}$, we write the order parameter, the left side of Eq. (2.144), as

$$\begin{aligned}\mathcal{F}(\mathbf{x}) &= \int d^3y\, \delta(\mathbf{x}-\mathbf{y})\, \mathcal{F}(\mathbf{y}) \\ &= \int d^3y \sum_j \phi_j(\mathbf{x})\, \phi_j^*(\mathbf{y})\, \frac{\mathcal{F}(\mathbf{y})}{N},\end{aligned} \tag{2.157}$$

while the right side of Eq. (2.144) is expressed as

$$k_B T \sum_\omega \int d^3y Q_\omega(\mathbf{x},\mathbf{y})\, V\, \mathcal{F}(\mathbf{y}) = \int d^3y \sum_j \phi_j(\mathbf{x})\, \phi_j^*(\mathbf{y})\, S(\epsilon_j) V\, \mathcal{F}(\mathbf{y}), \tag{2.158}$$

Substituting Eqs. (2.157) and (2.158) into Eq. (2.144), we obtain

$$\int d^3y \sum_j \phi_j(\mathbf{x})\, \phi_j^*(\mathbf{y}) \left[\frac{1}{NV} - S(\epsilon_j)\right] V\, \mathcal{F}(\mathbf{y}) = 0, \tag{2.159}$$

which for a homogeneous superconductor reduces to

$$\left[\frac{1}{NV} - S(\epsilon_j)\right] = 0, \tag{2.160}$$

with $\mathcal{F}(\mathbf{y}) \propto \phi_j(\mathbf{y})$ since N and V are constants. Using the conventional cutoff introduced by de Gennes, Eq. (2.153), we obtain the familiar Werthamer relation [28]

$$\chi\left(\frac{\epsilon_j}{2\pi k_B T}\right) + \ln\left(\frac{T}{T_c}\right) = 0, \tag{2.161}$$

where the BCS relation

$$\frac{1}{NV} = \ln\left(\frac{1.134\hbar\omega_D}{T_c}\right), \tag{2.162}$$

was used.

The problem of finding the highest transition temperature for a homogeneous superconductor in the presence of applied field is reduced to finding the minimum eigenvalue ϵ_j by solving the eigenvalue equation, Eq. (2.145), subject to the boundary condition, Eq. (2.146). We choose the London gauge

$$\mathbf{A} = H(0, x, 0)\,, \tag{2.163}$$

and write the ansatz for the pair amplitude

$$\mathcal{F}(\mathbf{x}) = e^{ipz}\, e^{iky}\, f_j(x)\,. \tag{2.164}$$

The eigenvalue problem, Eq. (2.145) and Eq. (2.146), reduces to a quantum mechanical harmonic oscillator problem

$$hD\left[-\frac{d^2}{dx^2} + \frac{2\pi H}{\phi_o}(x-k)^2\right] f_j(x) = \epsilon_j\, f_j(x)\,, \tag{2.165}$$

with

$$\lim_{x\to\infty} f_j(x) \to 0\,, \tag{2.166}$$

and $p = 0$ was taken since we are interested in the lowest eigenvalue. The lowest eigenvalue ϵ is readily found to be

$$\epsilon = hD\frac{2\pi H}{\phi_o}\,, \tag{2.167}$$

and the highest transition temperature is determined from the expression

$$\chi\left[\frac{hD}{2\pi k_B T}\,\frac{2\pi H}{\phi_o}\right] + \ln\left(\frac{T}{T_c}\right) = 0\,, \tag{2.168}$$

which describes the co-existence curve at the upper critical field, $H = H_{c2}$, as a function of temperature, T. A second order phase transition occurs when this curve is crossed.

Of particular interest are the two limits, $T \to T_c$ and $T \to 0$. We have in those two cases

$$\frac{\pi^2}{4}\,\frac{hD}{2\pi k_B T}\,\frac{2\pi H(T_c)}{\phi_o} = \frac{T_c - T}{T}\,, \qquad T \to T_c\,, \tag{2.169}$$

and

$$2\frac{h\,D}{2\pi k_B T_c}\frac{2\pi H(0)}{\phi_o} = e^{-\gamma}, \qquad T \to 0, \tag{2.170}$$

where the Taylor expansion and the asymptotic expansion of the digamma function, $\psi(z)$, were used, and $\gamma = 0.5772$ is the Euler constant. It is important to note that Eq. (2.169) provides a means of determining the diffusion constant, D, from the slope of the upper critical field at the transition temperature, T_c:

$$\frac{h\,D}{\phi_o k_B} = \frac{4}{\pi^2}\left|\frac{dH}{dT}\right|^{-1}_{T_c}. \tag{2.171}$$

The upper critical field at zero temperature is related to the transition temperature at zero field through Eq. (2.170), and is given by

$$H(0) = \frac{1}{2}e^{-\gamma}\frac{\pi^2}{4}\,T_c\left|\frac{dH}{dT}\right|_{T_c} = 0.6927\,T_c\left|\frac{dH}{dT}\right|_{T_c}. \tag{2.172}$$

It is seen that, within the framework of de Gennes' theory, the upper critical field at zero temperature for a homogeneous superconductor is proportional to the transition temperature at zero field, T_c, with a non-trivial proportionality constant, $0.6927\left|\frac{dH}{dT}\right|_{T_c}$, a measure of the "dirtiness" of the superconducting material.

2.5.2 Multilayered Systems

In oder to apply the de Gennes theory to a multilayer system, we begin with the linearized Gor'kov equation in a multilayer system, given by

$$\mathcal{F}(\mathbf{x}) = k_B T \sum_{\omega} \int d^3y\, Q_\omega(\mathbf{x},\mathbf{y})\, V(\mathbf{y})\, \mathcal{F}(\mathbf{y}). \tag{2.173}$$

We assume that the de Gennes' diffusion equation, Eq. (2.138), and the continuity condition, Eq. (2.141) derived for a bilayer system, can be generalized to a multi-interface system. Without loss of generality, we consider a two component multilayer system, with the components denoted by A and B, respectively and introduce the

notation

$$V(\mathbf{x}) = \begin{cases} V_A\,, & \mathbf{x} \in A\,, \\ V_B\,, & \mathbf{x} \in B\,, \end{cases} \tag{2.174}$$

$$N(\mathbf{x}) = \begin{cases} N_A\,, & \mathbf{x} \in A\,, \\ N_B\,, & \mathbf{x} \in B\,, \end{cases} \tag{2.175}$$

$$D(\mathbf{x}) = \begin{cases} D_A\,, & \mathbf{x} \in A\,, \\ D_B\,, & \mathbf{x} \in B\,, \end{cases} \tag{2.176}$$

$$T(\mathbf{x}) = \begin{cases} T_A\,, & \mathbf{x} \in A\,, \\ T_B\,, & \mathbf{x} \in B\,. \end{cases} \tag{2.177}$$

We rewrite the gauge invariant diffusion equation for the kernel, Eq. (2.138), as

$$[2|\omega| + \hat{L}(\mathbf{\Pi})]Q_\omega(\mathbf{x},\mathbf{y}) = 2\pi N(\mathbf{x})\,\delta(\mathbf{x}-\mathbf{y})\,, \tag{2.178}$$

with

$$\hat{L}(\mathbf{\Pi}) = -hD(\mathbf{x})\,\mathbf{\Pi}^2 = \begin{cases} -hD_A\,\mathbf{\Pi}^2\,, & \mathbf{x} \in A\,, \\ -hD_B\,\mathbf{\Pi}^2\,, & \mathbf{x} \in B\,. \end{cases} \tag{2.179}$$

By analogy with the eigenfunction method used for the homogeneous superconductor case, we consider the eigenvalue equation

$$[\epsilon_j - \hat{L}(\mathbf{\Pi})]\,\phi_j(\mathbf{x}) = 0\,, \tag{2.180}$$

together with the boundary condition at the free surfaces

$$\mathbf{n}\cdot\mathbf{\Pi}\,\phi_j(\mathbf{x}) = 0\,, \tag{2.181}$$

and continuity conditions at the interfaces denoted by $\mathbf{x}_0$,

$$\frac{1}{N_A}\,\phi_j(\mathbf{x})\Big|_{\mathbf{x}\in A\to\mathbf{x}_0} = \frac{1}{N_B}\,\phi_j(\mathbf{x})\Big|_{\mathbf{x}\in B\to\mathbf{x}_0}\,, \tag{2.182}$$

$$D_A\,\mathbf{n}\cdot\mathbf{\Pi}\,\phi_j(\mathbf{x})|_{\mathbf{x}\in A\to\mathbf{x}_0} = D_B\,\mathbf{n}\cdot\mathbf{\Pi}\,\phi_j(\mathbf{x})|_{\mathbf{x}\in B\to\mathbf{x}_0}\,. \tag{2.183}$$

The orthogonality and closure properties of the eigenfunctions are given by

$$\int d^3x \phi_{j'}(\mathbf{x}) \frac{1}{N(\mathbf{x})} \phi_j^*(\mathbf{x}) = \delta_{jj'} , \tag{2.184}$$

$$\sum_j \phi_j(\mathbf{x}) \phi_j^*(\mathbf{y}) = N(\mathbf{x}) \delta(\mathbf{x} - \mathbf{y}) . \tag{2.185}$$

Following the algebraic manipulation shown previously, we can write the linearized Gor'kov equation as

$$\int d^3y \sum_j \phi_j(\mathbf{x}) \, \phi_j^*(\mathbf{y}) \left[\frac{1}{N(\mathbf{y}) V(\mathbf{y})} - S(\epsilon_j) \right] V(\mathbf{y}) \mathcal{F}(\mathbf{y}) = 0 . \tag{2.186}$$

The problem is to find the highest temperature which yields a solution to the above equation. In the following section, we discuss two approaches. The first, the so-called Werthamer approximation, is valid for systems involving large length scales. The second, while somewhat more complicated, is nevertheless valid over a much wider range of length scales.

2.5.3 Werthamer Approximation

The well-known Werthamer approximation can be explicitly shown by using Eq. (2.186). If one assumes that the closure property of the eigenfunctions, Eq. (2.185), is still valid in the integrand of Eq. (2.186). One can introduce the BCS relation

$$\frac{1}{N(\mathbf{x}) V(\mathbf{x})} = \ln \left(\frac{T(\mathbf{x})}{1.134 \hbar \omega_D} \right) , \tag{2.187}$$

and find that

$$\int d^3y \left[\ln \left(\frac{T}{T(\mathbf{y})} \right) + \chi \left(\frac{\hat{L}(\mathbf{\Pi})}{2\pi k_B T} \right) \right] \delta(\mathbf{x} - \mathbf{y}) \, N(\mathbf{y}) V(\mathbf{y}) \mathcal{F}(\mathbf{y}) = 0 . \tag{2.188}$$

This leads to the Werthamer differential equation

$$\begin{aligned} 0 &= \left[\ln \left(\frac{T}{T(\mathbf{x})} \right) + \chi \left(\frac{\hat{L}(\mathbf{\Pi})}{2\pi k_B T} \right) \right] N(\mathbf{x}) V(\mathbf{x}) \mathcal{F}(\mathbf{x}) \\ &= \left[\ln \left(\frac{T}{T(\mathbf{x})} \right) + \chi \left(\frac{\hat{L}(\mathbf{\Pi})}{2\pi k_B T} \right) \right] N(\mathbf{x}) \Delta(\mathbf{x}) , \end{aligned} \tag{2.189}$$

except for a modulated density of states, $N(\mathbf{x})$, which was treated as a constant in Werthamer's original work [28].

It is readily seen that the application of the closure property of the eigenfunctions to the integral equation, Eq. (2.186), is not justified, since the modulated BCS coupling constant, $V(\mathbf{y})$, does not satisfy the same continuity condition at the interfaces as do the eigenfunctions, $\phi_j(\mathbf{y})$. In particular, at the interface ($\mathbf{x} = \mathbf{x}_0$), the integral

$$\int d^3y\, \delta(\mathbf{x}_0 - \mathbf{y})\, V(\mathbf{y}) = V(\mathbf{x}_0^+) \quad \text{or} \quad V(\mathbf{x}_0^-), \tag{2.190}$$

is not well defined.

Under the Werthamer approximation, the transition temperature at zero applied field for a thin bilayer system, (e.g. Nb/Cu with $V_{\rm Cu} = 0$ for Cu and $d_{\rm Cu}, d_{\rm Nb} \to 0$), is given by [28]

$$\frac{T}{T_{\rm Nb}} \approx \frac{1}{1 + \frac{\pi^2}{4}\frac{d_{\rm Cu}}{d_{\rm Nb}}}. \tag{2.191}$$

This expression gives rise to a higher transition temperature than that given by Cooper [27] and de Gennes [26]

$$\frac{T}{T_{\rm Nb}} = \left(\frac{T_{\rm Nb}}{1.14\theta_D}\right)^{\frac{d_{\rm Cu}}{d_{\rm Nb}}}. \tag{2.192}$$

It is generally established that Werthamer's result, Eq. (2.191), is inappropriate in the thin film limit [25, 43] since T is higher than that found in experiments [44], and thus Eq. (2.192) is applicable. However, for thick films, Eq. (2.191) qualitatively fits the experimental data and Eq. (2.192) usually underestimates the transition temperature.

2.5.4 General Formalism

In order to avoid the difficulty met in Werthamer's approximation, we notice that the pair amplitude satisfies the same boundary conditions specified in Eq. (2.142)

as $\{\phi_j(\mathbf{x})\}$ specified in Eqs. (2.181), (2.182) and (2.183), so we expand the pair amplitude as

$$\mathcal{F}(\mathbf{y}) = \sum_i c_i \, \phi_i(\mathbf{y}) \,, \tag{2.193}$$

and substitute into Eq. (2.186). We obtain

$$\sum_{i,j} \phi_j(\mathbf{x}) \int d^3y \, \phi_j^*(\mathbf{y}) \left[\ln\left(\frac{T}{T(\mathbf{y})}\right) + \chi\left(\frac{\epsilon_j}{2\pi k_B T}\right) \right] V(\mathbf{y}) \, \phi_i(\mathbf{y}) \, c_i = 0 \,. \tag{2.194}$$

Multiplying Eq. (2.194) by $\phi_m(\mathbf{x})/N(\mathbf{x})$ and integrating with respect to $\mathbf{x}$, we obtain

$$\sum_{i,m} \int d^3y \, \phi_m^*(\mathbf{y}) \left[\ln\left(\frac{T}{T(\mathbf{y})}\right) + \chi\left(\frac{\epsilon_m}{2\pi k_B T}\right) \right] V(\mathbf{y}) \, \phi_i(\mathbf{y}) \, c_i = 0 \,. \tag{2.195}$$

We introduce two matrices,

$$\hat{A}_{mi}(T) = \int d^3y \, \phi_m^*(\mathbf{y}) \ln\left(\frac{T}{T(\mathbf{y})}\right) V(\mathbf{y}) \, \phi_i(\mathbf{y}) \,, \tag{2.196}$$

$$\hat{B}_{mi}(T) = \chi\left(\frac{\epsilon_m}{2\pi k_B T}\right) \int d^3y \, \phi_m^*(\mathbf{y}) V(\mathbf{y}) \, \phi_i(\mathbf{y}) \,. \tag{2.197}$$

The existence of a non-trivial solution of Eq. (2.195) then leads to a secular equation

$$\det \left| \hat{A}(T) - \hat{B}(T) \right| = 0 \,. \tag{2.198}$$

The highest temperature obtained in solving this secular equation is the transition temperature. Of particular interest are two classes of materials specified by

$$\begin{cases} T_A = T_B, \quad V_A = V_B, \quad N_A = N_B, \quad D_A \neq D_B, & \text{for a superlattice,} \\ T_A = T_B, \quad V_A = V_B, \quad N_A = N_B, \quad D_A = D_B, & \text{for a single film,} \end{cases} \tag{2.199}$$

for which the secular equation, Eq. (2.198), reduces to the Werthamer equation, Eq. (2.189), and therefore, the Werthamer formalism becomes exact. The application of DW formalism to these geometries in the presence of an applied field reduces to solving an eigenvalue equation

$$-\hbar D \left(\nabla - i\frac{2\pi}{\phi_o}\mathbf{A}\right)^2 \mathcal{F}(\mathbf{x}) = \epsilon_j \, \mathcal{F}(\mathbf{x}) \,, \tag{2.200}$$

together with the boundary conditions, Eq. (2.142).

The research work presented in this thesis consists of theoretical studies of the transition temperature in the presence of applied field for these two classes of materials.

It can be readily shown that secular equation, Eq. (2.198), reduces to the form proposed by Takahashi and Tachiki [25, 36, 42, 52],

$$\det\left|\delta_{jj'} - \sum_{\omega} \frac{2\pi k_B T}{2|\omega| + \epsilon_j} V_{jj'}\right| = \det\left|\delta_{jj'} - S(\epsilon_j)\, V_{jj'}\right| = 0\,, \tag{2.201}$$

without introducing de Gennes' cutoff. Auvil and Ketterson [43] and Lodder and Koperdraad [52] were able to show numerically that the transition temperature for a bilayer in both thick and thin film limits, e.g. Nb/Cu or Nb/Al, can be recovered by using Takahashi-Tachiki's secular equation, Eq. (2.201), if the cutoff is treated carefully and $S(\epsilon_j)$ is evaluated using Eq. (2.155).

Chapter 3

Surface Superconductivity in a Homogeneous Superconductor

3.1 Introduction

It is well established both theoretically and experimentally that the temperature dependence of the upper critical field can be significantly modified by the presence of surfaces. The best known result in this context is the expression for the parallel critical field, first obtained by Landau and Ginzburg [64], for a superconducting thin film

$$H_{\parallel} = \sqrt{24}\,\frac{\lambda(T)}{d}\,H_c(T)\,, \tag{3.1}$$

where d denotes the thickness of thin film, $\lambda(T)$ is the penetration length and $H_c(T)$ is the thermodynamic critical field. This yields the following temperature dependence

$$H_{\parallel} \approx \frac{2}{\pi}\sqrt{\frac{12k_B\phi_o^2}{\hbar D d^2 2\pi}}\sqrt{T_c - T}\,, \qquad T \to T_c\,, \tag{3.2}$$

in terms of the extended GL theory in dirty limit [10, 11]. This result has been confirmed by numerous experimental studies and differs significantly from the corresponding result for a homogeneous system in Ginzburg-Landau theory, in which case

$$H_{c2} = \sqrt{2}\,\kappa\,H_c(T) = \frac{4}{\pi^2}\frac{\phi_o k_B}{\hbar D}(T_c - T)\,, \qquad T \to T_c\,. \tag{3.3}$$

The upper critical field in systems of intermediate thickness was studied in the early sixties by Saint-James and de Gennes [65] within the framework of Ginzburg-Landau theory. They discovered that while the temperature dependence of the upper

critical field exhibited a crossover from a two-dimensional regime, $\lim_{T\to T_c} H_{\|} \propto \sqrt{T_c - T}$, to a three dimensional regime, $\lim_{T\to T_c} H_{\|} \propto (T_c - T)$, with increasing thickness, the resultant proportionality coefficient is 1.69 times larger than that of a homogeneous superconductor, $H_{\|} = 1.69\, H_{c2}$. This result implied that the presence of a free surface could induce the superconductivity to persist to a higher applied field than it otherwise would. This phenomena is referred to as surface superconductivity, since the order parameter is localized close to the surface within a distance of $x_0 = \sqrt{0.59010}\,\xi_H$ ($\xi_H = \sqrt{\phi_o/2\pi H}$), and forms a superconducting sheath. The theoretical results of Saint-James and de Gennes have been confirmed experimentally and the phenomenon of surface superconductivity is well established.

In addition to the work of Saint-James and de Gennes, Tinkham [20] examined the angular dependence of the upper critical field for a thin film, $H(\theta)$. He obtained the following result

$$\frac{H(\theta)}{H_{\perp}} \sin\theta + \frac{H^2(\theta)}{H_{\|}^2} \cos^2\theta = 1\,, \tag{3.4}$$

with $H_{\perp} = H(\frac{\pi}{2})$. While Tinkham's result is, strictly speaking, valid only in the thin film limit, expressed in the above form, it is often used as an interpolation formula for films of arbitrary thickness by substituting the experimentally determined values for $H_{\|}$ and $H_{\perp}$ into the above formula. This interpolation formula is even used in the interpretation of the angular dependence of upper critical field in superlattice geometries.

The extension of Tinkham's result to the angular dependence of the upper critical field for films of arbitrary thickness may be expected to lead to some understanding as to how the superconducting sheath, appearing in the parallel field case, is modified in the case of a finite angle. The first such studies were presented by Saint-James [21]. Using Ginzburg-Landau theory, Saint-James derived an expression for the

logarithmic derivative, Φ, in the limit $\theta \to 0$, defined by

$$\Phi = \lim_{\theta \to 0} \frac{1}{H} \frac{\partial H}{\partial \theta}\bigg|_T , \tag{3.5}$$

as a function of the reduced field, $h = \frac{1}{4}\frac{d^2}{\xi_H^2}$ with d denoting the thickness of a film and ξ_H denoting the magnetic coherence length, by means of a perturbation expansion in terms of the angle θ of the applied field relative to the surface. One particularly interesting aspect of the result obtained by Saint-James was that the dependence of the logarithmic derivative Φ, on the reduced field h, exhibited a cusp at $h = h_c = 1.62$. The value of the logarithmic derivative at $h = h_c$ is $\Phi = -0.5341$.

While experimental studies appeared to confirm the result obtained by Saint-James, Thompson [24] later pointed out that Saint-James' result was in fact in error. Specifically Thompson was able to show that all the even terms in the perturbation series used by Saint-James contributed to the logarithmic derivative, Φ, and, by considering only the second order term in the perturbation series Saint-James had obtained only an approximate result. Thompson was able to sum the leading terms in each order of the perturbation series and obtain an exact expression. While the result obtained by Thompson was qualitatively similar to that given by Saint-James, inasmuch as it reduced to Tinkham's result in the thin film limit and it exhibited a cusp at $h = h_c = 1.62$, there are important quantitative differences between the two results. Most notably, the value of the logarithmic derivative, Φ, goes to zero at the cusp in Thompson's analysis. Thompson [24] also analyzed earlier work, carried out by Yamafuji et al. [55], on the full angular dependence of the upper critical field for a semi-infinite geometry. In this case, Thompson pointed out that the boundary condition used by Yamafuji et al. [55] was inappropriate.

Despite the fact that previous studies, notably that of Saint-James [21] and Yamafuji et al. [55], on this topic have a restricted domain of validity and the fact that their work was mathematically problematical, both claim good agreement with

certain experimental studies. In the case of the results presented by Saint-James [22, 23] we suggest, on the basis of results obtained from our analysis and presented in this chapter, that the experimental results considered by Saint-James are not sufficiently precise to distinguish between the various theoretical results and that more detailed and systematic experimental studies are required.

While new results and a critical re-examination of previous work on the upper critical fields in superconducting films are of themselves interesting, the results are also relevant to similar studies on superconducting superlattices, a topic of considerable current interest both theoretically and experimentally. Indeed it was the analysis of the angular dependence of the upper critical field in superlattice structures [38] that motivated the present calculation for a single film, since we have already noted that results obtained for thin films are often used in the interpretation of data from superlattice structures. The formalism used in the present study and the subtleties encountered also manifest themselves in the case of the superlattice geometries.

In this chapter, we will calculate the upper critical field for a superconducting film for all orientations $0 \leq \theta \leq \pi/2$ and a range of thicknesses, including both finite thickness and the semi-infinite geometry.

In Section 3.2, we will formulate the eigenvalue problem based on the de Gennes-Werthamer dirty limit theory. It will be shown that the application of de Gennes-Werthamer dirty limit theory to a superconducting film can be accomplished by two steps. One first needs to solve the partial differential equation for the order parameter, incorporating the given geometry and boundary conditions given by Eqs. (3.6) and (3.7), in order to obtain the eigenvalue, E_g. Then one maps the eigenvalue to the temperature dependent upper critical field using the Werthamer equation, Eq. (3.8), to obtain the transition temperature.

In Section 3.3, we will show how we can recover the thin film limit, Eq. (3.2),

using the DW formalism by means of a simple mean field argument. We will then introduce the concept of the nucleation center and show how it plays a crucial role in determining the upper critical field and the nature of the order parameter when the reduced field $h > h_c$ (i.e., for moderately thick films). In particular, we will show how this leads to the enhancement of the upper critical field in the case of thick films ($h \gg h_c$) and the fact, alluded to earlier, that the order parameter is confined to a thin sheath ($x_0 \sim \xi_H$) close to the surface.

In Section 3.4, we will review in somewhat more detail previous work [20, 21, 24, 54, 55] on the angular dependence of the upper critical field in superconducting films. The purpose of this review is to examine the validity of earlier work and to draw attention to the inconsistenc es that exist among the various theoretical results.

In Section 3.5, we present an eigenfunction expansion technique to solve the eigenvalue problem posed by the DW formalism for the case of a tilted magnetic field. Using this technique we are able to calculate the eigenvalue as a function of θ over the range $0 < \theta \leq \frac{\pi}{2}$ for various values of slab thicknesses. In particular, we discuss the non-analytic nature of the eigenvalue problem in the limit $\theta \to 0$.

In Section 3.6, we use the eigenvalue calculated in Section 3.5 to study the full angular dependence of the upper critical field, $H(\theta)$, at fixed temperature using the Werthamer equation, Eq. (3.8). The range of thickness of the slab studied includes thin, moderate and thick films. A semi-infinite geometry is included as the limiting case of a thick film. A new dimensional crossover, which may be referred to as a transition from a surface effect (single surface dominant) to a size effect (double surface dominant), is predicted by the theoretical calculation.

In Section 3.7, we show the consistency between our numerical results for the logarithmic derivative, $\lim_{\theta \to 0} \frac{1}{H} \frac{\partial H(\theta)}{\partial \theta}\Big|_T$, and Thompson's theoretical result. One

interesting and important aspect associated with the calculation of the angular dependence of the upper critical field relates to the fact that, while the result of the upper critical field in the limit $\theta \rightarrow 0$ agrees with the result obtained for the parallel field case, the limit is far from trivial. This arises as a consequence of the fact that the underlying eigenvalue problem for the tilted field differs qualitatively from the corresponding eigenvalue problem in the parallel field calculation. This is more than a simple technicality, as it means that particular care is needed in the determination of $\Phi = \frac{1}{H}\frac{\partial H}{\partial \theta}\Big|_T$ in the limit $\theta \rightarrow 0$. This is particularly so in the case of the analyses presented by Saint-James [21] and Thompson [24] who evaluated the slope by means of a perturbation with respect to the parallel field case. We will show that our results for $\Phi = \frac{1}{H}\frac{\partial H}{\partial \theta}\Big|_T$ are, within the numerical precision of our calculations, consistent with those obtained by Thompson [24]. The experimental implications of measuring this quantity are discussed in detail. In Section 3.8, we present a number of conclusions drawn from the present work.

3.2 Eigenvalue Problem in the de Gennes-Werthamer Theory

In this section we wish to consider the evaluation of the upper critical field of a superconducting film of arbitrary thickness mounted on an insulating substrate at an orientation θ relative to the direction of the applied field, by means of the DW theory. The specific geometry is shown in Fig. 3.1.

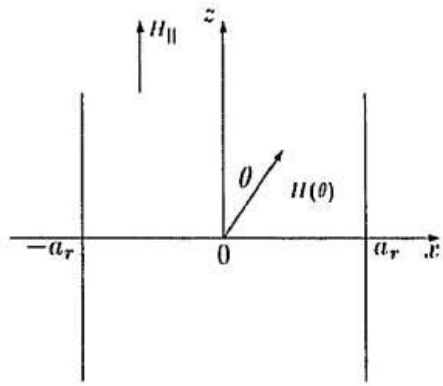

Figure 3.1: Slab Geometry.

Since the superconducting properties of the film are uniform across the thickness, we see from our earlier discussion that the problem, defined by Eq. (2.200), reduces to the determination of the minimum eigenvalue, which we denote by E_g, defined by

$$-\hbar D (\nabla - i\frac{2\pi}{\phi_o}\mathbf{A})^2 \mathcal{F}(\mathbf{x}) = E_g \mathcal{F}(\mathbf{x}), \tag{3.6}$$

together with the boundary condition

$$(\frac{\partial}{\partial x} - i\frac{2\pi}{\phi_o}\mathbf{A}_x)\mathcal{F}(\mathbf{x})\Big|_{x=\pm a_r} = 0. \tag{3.7}$$

The transition temperature for a given applied magnetic field H, orientation θ and thickness $2a_r$ may then be obtained from the Werthamer equation, Eq. (2.200),

$$\chi(\frac{E_g}{2\pi k_B T}) + \ln\left(\frac{T}{T_c}\right) = 0. \tag{3.8}$$

For the geometry shown in Fig. 3.1, we choose the London gauge,

$$\mathbf{A}(\mathbf{x}) = H(0, x\cos\theta - z\sin\theta, 0)\,, \tag{3.9}$$

where θ is the angle between the direction of the applied field and the z axis and H lies in the $x-z$ plane.

The operator, $-(\nabla - i\frac{2\pi}{\phi_o}\mathbf{A})^2$, in Eq. (3.6), for the chosen gauge is expressed as

$$-(\nabla - i\frac{2\pi}{\phi_o}\mathbf{A})^2 = -\frac{\partial^2}{\partial x^2} - \frac{\partial^2}{\partial z^2} - [\frac{\partial}{\partial y} - i\frac{2\pi}{\phi_0}H(x\cos\theta - z\sin\theta)]^2\,. \tag{3.10}$$

We define a magnetic coherence length ξ_H as

$$\xi_H = \sqrt{\frac{\phi_o}{2\pi H}}\,, \tag{3.11}$$

and introduce the dimensionless variables

$$x \to \frac{x}{\xi_H}\,, \qquad z \to \frac{z}{\xi_H}\,, \qquad y \to \frac{y}{\xi_H}\,. \tag{3.12}$$

We may write the operator, $-(\nabla - i\frac{2\pi}{\phi_o}\mathbf{A})^2$, in terms of the dimensionless variables as

$$-(\nabla - i\frac{2\pi}{\phi_o}\mathbf{A})^2 = \xi_H^{-2}\left\{-\frac{\partial^2}{\partial x^2} - \frac{\partial^2}{\partial z^2} - [\frac{\partial}{\partial y} - i(x\cos\theta - z\sin\theta)]^2\right\}\,, \tag{3.13}$$

and we will hereafter use

$$\hat{\mathcal{L}} = \left\{-\frac{\partial^2}{\partial x^2} - \frac{\partial^2}{\partial z^2} - [\frac{\partial}{\partial y} - i(x\cos\theta - z\sin\theta)]^2\right\}\,. \tag{3.14}$$

We therefore wish to determine the minimum eigenvalue $\varepsilon = E_g\xi_H^2/\hbar D$ that satisfies the differential equation

$$\hat{\mathcal{L}}\,\mathcal{F}(x,y,z) = \varepsilon\,\mathcal{F}(x,y,z) \tag{3.15}$$

together with the boundary condition

$$\frac{\partial}{\partial x}\mathcal{F}(x,y,z)\Big|_{x=\pm a_r/\xi_H} = 0\,. \tag{3.16}$$

In the following sections, we will first solve Eq. (3.15) for the parallel field case, $\theta = 0$. We will show the role played by the nucleation center in the determination of the lowest eigenvalue due to the boundary conditions imposed by the surface effect [19]. We then study the case of arbitrary angle ($\theta \neq 0$) for which the surface effect is completely destroyed due to the perpendicular component of the applied field which penetrates the entire slab. The persistence of the surface effect in the parallel field case and the destruction of the surface effect when the applied field tilted at an angle relative to the surface leads to a non-analytical behavior of the lowest eigenvalues determined by the eigenvalue equation, Eq. (3.15), in the limit $\theta \to 0$.

3.3 Parallel Upper Critical Magnetic Field

In this section, we show how the lowest eigenvalue determined from the Weber equation and corresponding boundary condition may be obtained by solving a non-linear first order differential equation, the Ricatti equation, through a proper transformation of both the equation and boundary condition. Numerical solutions to the eigenvalue problem are presented and discussed. Using the Ricatti function, we then obtain an approximate expression for the lowest eigenvalue as a function of the reduced applied field, h, over the range $h \leq h_c$, by a mean field approximation.

The temperature dependence of the upper critical field for $T \lesssim T_c$ is given to show the dimensional transition as the thickness of the slab varies from finite to infinite. We show how the results of Ginzburg and Landau, and Saint-James and de Gennes may be recovered in the thin film and thick film limits respectively.

3.3.1 Weber Equation and Ricatti Equation

For the $\theta = 0$ case, the eigenvalue equation, Eq. (3.15), reduces to

$$\left[-\frac{\partial^2}{\partial x^2} - \frac{\partial^2}{\partial z^2} - (\frac{\partial}{\partial y} - ix)^2\right] \mathcal{F}(x,y,z) = \varepsilon\, \mathcal{F}(x,y,z)\,. \tag{3.17}$$

Substituting the following ansatz for the order parameter

$$\mathcal{F}(x,y,z) = f_\Lambda(x)\, e^{iky}\, e^{ipz}\,, \tag{3.18}$$

into Eq. (3.17), the eigenvalue equation further reduces to the Weber equation

$$\left[-\frac{d^2}{dx^2} + (x-k)^2\right] f_\Lambda(x) \;=\; \lambda\, f_\Lambda(x)\,, \tag{3.19}$$

where the Weber function, $f_\Lambda(x)$, is subject to the boundary condition

$$\frac{d}{dx} f_\Lambda(x)\bigg|_{x=\pm a} = 0\,, \qquad a = \frac{a_r}{\xi_H}\,. \tag{3.20}$$

The eigenvalue, ε, defined in Eq. (3.17), is then given by

$$\varepsilon = \lambda + p^2 . \tag{3.21}$$

It is readily seen that $p = 0$ is necessary to obtain the minimum eigenvalue.

Since the solution corresponding to the minimum eigenvalue has no nodes, we may introduce an auxiliary function, $R_\lambda(x)$, defined as

$$R_\lambda(x) = \frac{1}{f_\lambda(x)} \frac{d}{dx} f_\lambda(x) . \tag{3.22}$$

Using the Weber equation, Eq. (3.19), one can show that this auxiliary function satisfies the Ricatti equation

$$\frac{d}{dx} R_\lambda(x) = -R_\lambda^2(x) + (x-k)^2 - \lambda , \tag{3.23}$$

subject to the boundary condition

$$R_\lambda(x)|_{x=\pm a} = 0 . \tag{3.24}$$

The minimum eigenvalue problem stated by Eqs. (3.23) and (3.24) in terms of the function, $R_\lambda(x)$, is entirely equivalent to the one stated by Eqs. (3.19) and (3.20) in terms of Weber function, $f_\lambda(x)$. However, because it is a first order differential equation, Eq. (3.23) is particularly well-suited to numerical calculation. In addition to providing a basis for numerical calculation, Eq. (3.23) may also be used to obtain approximate results.

We have solved Eq. (3.23) numerically, together with the boundary condition, (3.24). The eigenvalue spectrum for the reduced applied fields in the range, $0.1 \leq h \leq 5$ is presented in Fig. 3.2. It is seen that for $h < h_c = 1.62$ the minimum eigenvalue, denoted by λ^*, is found at $k^* = 0$. The corresponding eigenfunction, $f_\lambda(x)$, is a symmetric function. This indicates that the spatial distribution of the

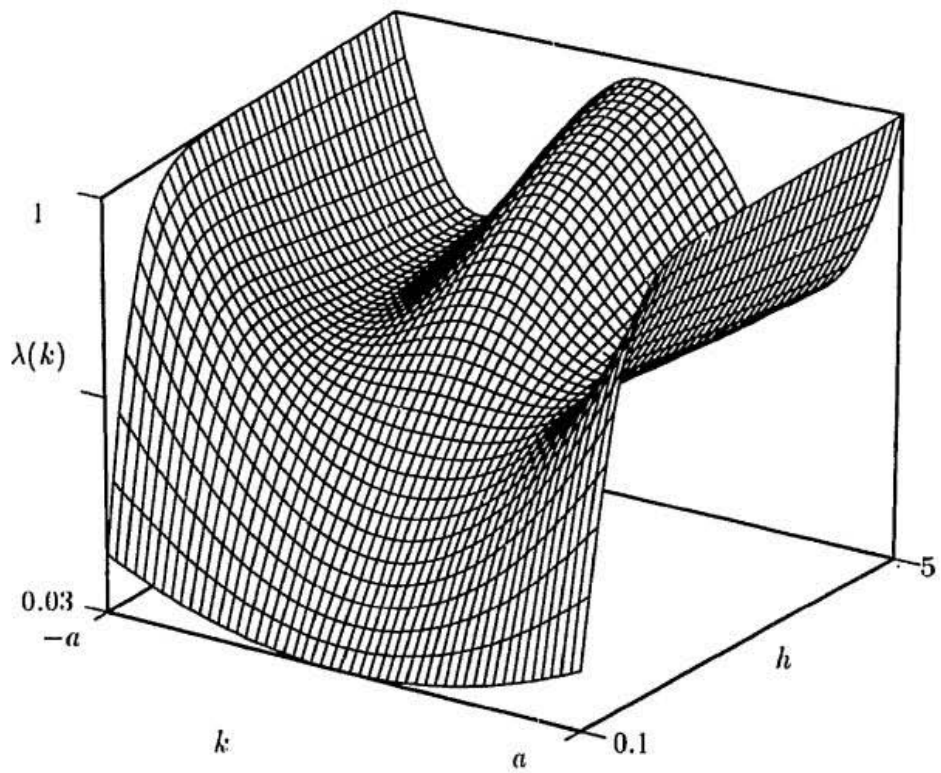

Figure 3.2: Surface plot of the eigenvalue λ as a function of k and h for the slab geometry in parallel applied field case.

order parameter in the film is dominated by the size effect, since the character of the order parameter is strongly influenced by both of the free surfaces. For $h > h_c$, however, we see that the eigenvalue λ has double minima at $k = \pm k^*$ respectively, which shows a two-fold degeneracy of the eigenstate [65] corresponding to the appearance of a vortex solution as proposed by Saint-James [66]. The minimum eigenvalue, λ^*, as a function of h is presented in Fig. 3.3 (curve (1)). The temperature dependence of the upper critical field in the thick film limiting case may be obtained by the following analysis.

For $h \gg h_c$, we approach the limiting form

$$k^* = a - \sqrt{0.59010}\,, \tag{3.25}$$

in which the corresponding eigenfunctions are strongly localized around $x \sim \pm k^*$ with a spatial extent of order $\sim \xi_H$. The corresponding eigenvalue is given by

$$\lambda^* = 0.59010\,. \tag{3.26}$$

This corresponds to the phenomenon of surface superconductivity first discussed by Saint-James and de Gennes [65]. Substituting the asymptotic form of the eigenvalue into the Werthamer equation, Eq. (3.8), we obtain

$$\chi\left(\frac{0.5901 h\, D}{2\pi k_B T}\frac{2\pi H}{\phi_o}\right) + \ln\left(\frac{T}{T_c}\right) = 0\,. \tag{3.27}$$

Taking the limit that $T \to T_c$ and $H \to 0$, we obtain the result given by Eq. (3.3)

$$\lim_{T\to T_c} H(T) = 1.69\,\frac{4}{\pi^2}\frac{\phi_o k_B}{h\, D}(T_c - T)\,, \tag{3.28}$$

where we have used the expansion of $\lim_{z\to 0}\chi(z) \to \frac{\pi^2}{4}z$. Comparing this with the corresponding result for the upper critical field of an infinite homogeneous superconductor given by Eq. (2.169), we see that

$$\frac{H_{\parallel}(T)}{H_{c2}(T)} = 1.69\,. \tag{3.29}$$

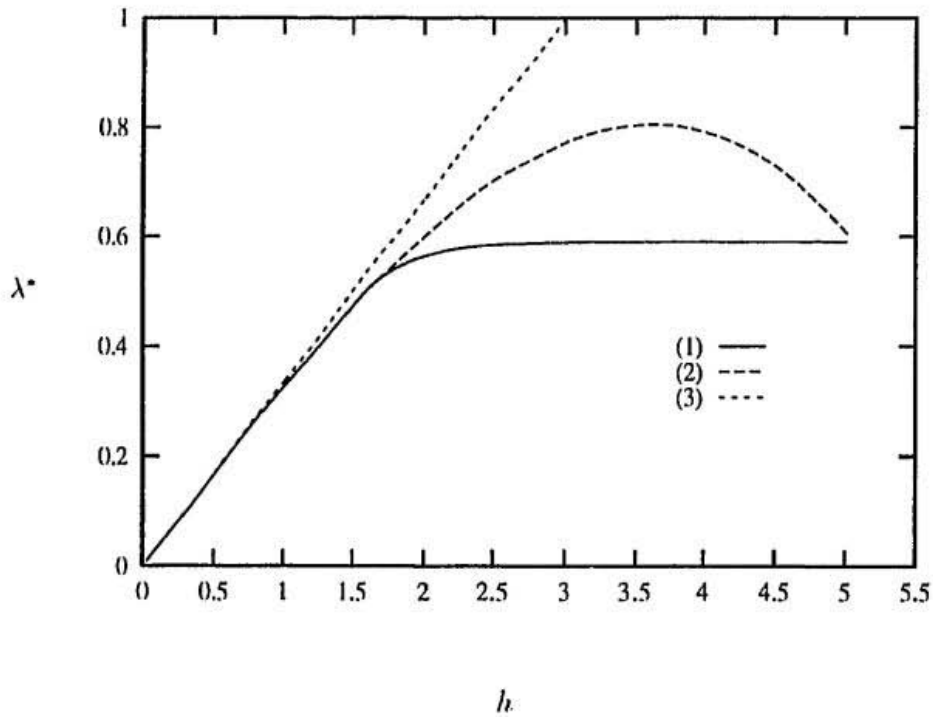

Figure 3.3: Plot of the minimum of the eigenvalue λ^* found at k^* as function of h for the slab geometry. The solid line is the result of numerical calculation. The other two curves are obtained using the mean field approximation (2) and linearization (3), respectively.

The parallel upper critical field for a semi infinite superconductor is typically referred to as H_{c3}. Thus we see that the appearance of the double minima in the spectrum of $\lambda(k)$ for $h > h_c$ signals the onset of surface superconductivity.

3.3.2 Mean Field Approximation in the Thin Film Limit

In order to treat the thin film limit, we consider the dispersion relation obtained by integrating Eq. (3.23)

$$\lambda = \frac{1}{3}a^2 + k^2 - \frac{1}{2a}\int_{-a}^{a} dx\, R_\lambda^2(x)\,, \tag{3.30}$$

which shows the dependence of the eigenvalue, λ, on both the reduced thickness, $2a = 2\sqrt{h}$, and the phase parameter k. In order to obtain an analytical expression of the minimum eigenvalue over a certain range of h, we suggest the following mean field approximation and then verify its validity by comparing with the numerical result. For the symmetric solution, $k^* = 0$, The Ricatti equation, Eq. (3.23), may be approximated as

$$\frac{d}{dx}R_\lambda(x) = -\overline{R_\lambda^2(a)} + x^2 - \lambda^*\,, \tag{3.31}$$

where the average is defined as

$$\overline{R_\lambda^2(a)} = \frac{1}{2a}\int_{-a}^{a} R_\lambda^2(x)\,dx\,. \tag{3.32}$$

The solution is immediately found to be

$$R_\lambda(x) = \frac{1}{3}x^3 - \left[\lambda^* + \overline{R_\lambda^2(a)}\right] x\,, \tag{3.33}$$

with

$$\lambda^* = \frac{1}{3}a^2 - \overline{R_\lambda^2(a)}\,. \tag{3.34}$$

The average value, $\overline{R_\lambda^2(a)}$, is then obtained self-consistently through the integral

$$\begin{aligned}\overline{R_\lambda^2(a)} &= \frac{1}{2a}\int_{-a}^{a}\left[\frac{1}{3}x^3 - \frac{1}{3}a^2\,x\right]^2 dx\,,\\ &= \frac{8}{945}a^6 = \frac{8}{945}h^3\,.\end{aligned}$$

The minimum eigenvalue in this mean field approximation can be expressed as

$$\lambda^* = \frac{1}{3}a^2(1 - \frac{8}{315}a^4) = \frac{1}{3}h(1 - \frac{8}{315}h^2)\,. \tag{3.35}$$

In the thin film approximation, $\frac{8}{315}h^2 \ll 1$, we obtain

$$\lambda^* = \frac{1}{3}a^2 = \frac{1}{3}h\,. \tag{3.36}$$

Maki [67] obtained this result in the thin film limit of $2a_r \ll \xi_H$ by treating the order parameter as a constant. In fact, this result may be obtained from the approximation of $R_\lambda^2(x) = 0$ in Eq. (3.30), which is a much looser condition than $2a_r \ll \xi_H$. The curves of λ^* as a function of h for both the mean field approximation and the thin film approximation are given in Fig. 3.3, curves (2) and (3), respectively. Compared with the numerical solution, it is seen that the validity of the thin film approximation is $h \lesssim 0.5$ or $2a_r \lesssim \sqrt{2}\xi_H$ instead of $2a_r \ll \xi_H$, and the mean field approximation provides a good description of the minimum eigenvalue, λ^*, for $h \leq h_c$.

The temperature dependence of the parallel upper critical field for a given film with thickness $2a_r$ can be obtained by substituting the minimum eigenvalue, λ^*, into the Werthamer equation, Eq. (3.8),

$$\chi\left[\frac{\xi_0^2}{a_r^2}\frac{h\,\lambda^*(h)}{t}\right] + \ln(t) = 0\,, \tag{3.37}$$

where $t = \frac{T}{T_c}$ and we introduce

$$\xi_0^2 = \frac{h\,D}{2\pi\,k_B T_c}\,. \tag{3.38}$$

Near the bulk transition temperature $T \approx T_c$ ($h \to 0$), we obtain

$$\frac{\pi^2}{4}\frac{\xi_0^2}{a_r^2} h\,\lambda^*(h) = \frac{T_c - T}{T_c}\,, \tag{3.39}$$

where $\lim_{z\to 0}\,\chi(z) \to z\pi^2/4$ was used. The temperature dependence of the upper critical field in thin film limit is recovered by substituting $\lambda^* = \frac{1}{3}h$ into Eq. (3.39), which yields

$$\frac{1}{3}\frac{\pi^2}{4}\frac{\xi_0^2}{a_r^2} h^2 = \frac{T_c - T}{T_c}\,, \tag{3.40}$$

and thus

$$H_{\|} \approx \frac{2\phi_o}{\pi^2}\sqrt{\frac{3}{\xi_0^2 d^2}}\sqrt{\frac{(T_c - T)}{T_c}}\,, \qquad (d = 2a_r)\,. \tag{3.41}$$

3.3.3 Dimensional Crossover for Films of Intermediate Thickness

Using the calculated values of the lowest eigenvalues shown in Fig. 3.3, we can compute the temperature dependence of the upper critical field for any value of thickness a_r. The results for several values of a_r are shown in Fig. 3.4 (a). The upper critical field is normalized with respect to $H_{c2}(0)$, which is defined by

$$H_{c2}(0) = \xi_0^{-2}\frac{\phi_o}{4\pi}\,e^{-\gamma}\,. \tag{3.42}$$

These results clearly show the crossover from the two-dimensional behavior as $T \to T_c$ to the three-dimensional behavior as the upper critical field curve obtained for the films with finite thickness merge into the upper critical field curve denoted by $2a_r/\xi_0 \to \infty$. Defining the temperature at which the crossover occurs as the value of $h = 1.62$ at which the minimum eigenvalue λ^* becomes degenerate, we can readily calculate the dependence of the crossover temperature on the thickness a_r. The graph is given in Fig. 3.4(b). Again the thickness is expressed in terms of the length scale ξ_0.

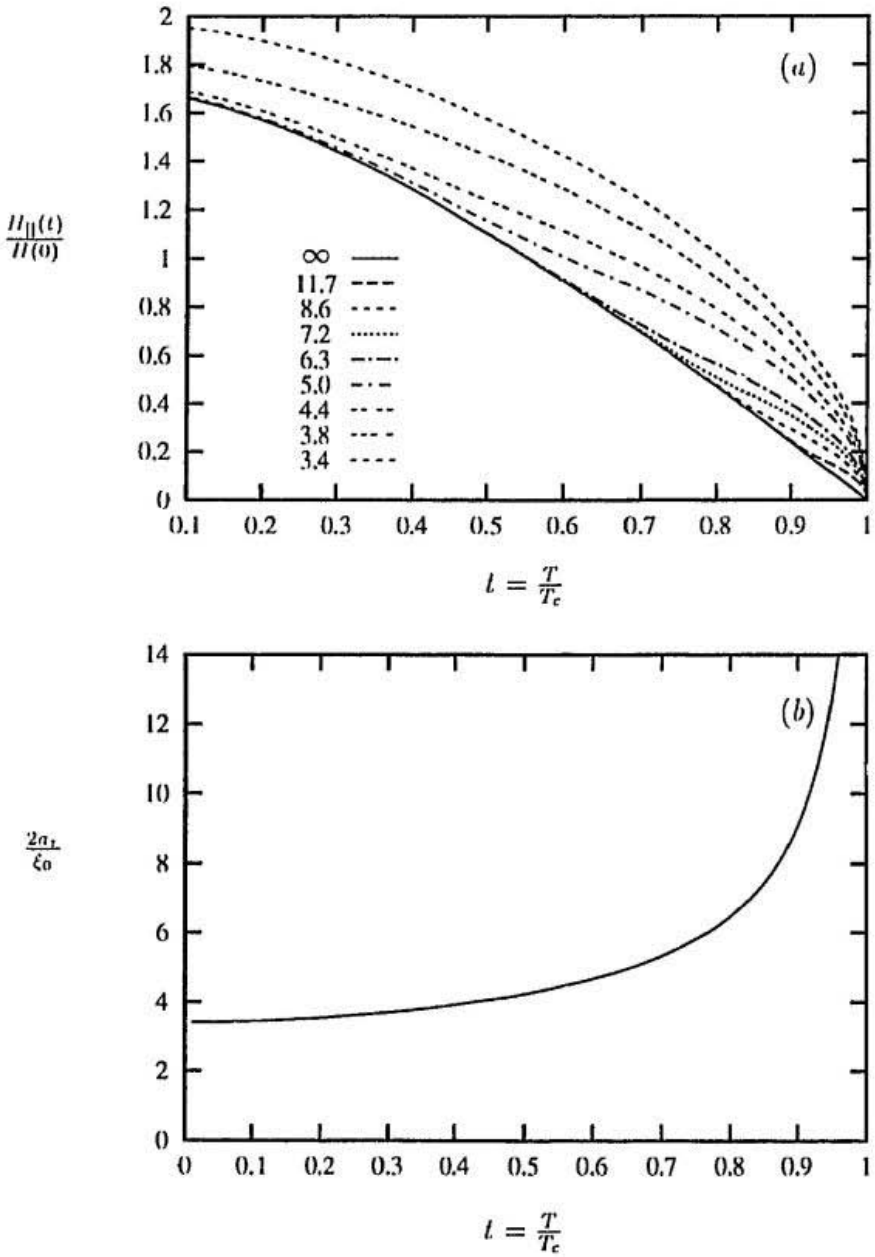

Figure 3.4: Fig. (a) shows the temperature dependence of the parallel upper critical field corresponding to various reduced thicknesses of $2a_r/\xi_0$ $(3.4 - \infty)$. Fig. (b) shows the critical thickness at which the dimensional crossover occurs.

3.4 Angular Dependence of the Upper Critical Field

The earliest work on the angular dependence of the upper critical field was carried out by Tinkham [20] based on the linearized Ginzburg-Landau (GL) theory using a variational method. We can recover the result obtained by Tinkham within the DW theory in a relatively straightforward manner. Substituting the ansatz

$$\mathcal{F}(x,y,z) = e^{iky\cos\theta}\,\mathcal{F}(x,z)\,, \tag{3.43}$$

into Eq. (3.15), the eigenvalue problem reduces to

$$\left\{-\frac{\partial^2}{\partial x^2} - \frac{\partial^2}{\partial z^2} + [(x-k)\cos\theta - z\sin\theta)]^2\right\}\mathcal{F}(x,z) = \varepsilon\,\mathcal{F}(x,z)\,, \tag{3.44}$$

$$\frac{\partial}{\partial x}\mathcal{F}(x,z)\bigg|_{x=\pm a} = 0\,, \quad \lim_{z\to\pm\infty}\mathcal{F}(x,z) \to 0\,. \tag{3.45}$$

Tinkham's [68] approximation is based on the premise that for a very thin film, the boundary conditions given by Eq. (3.45) implies that the eigenfunction $\mathcal{F}(x,z)$ will depend only weakly on the coordinate x and, the nucleation center $k^* = 0$ can be chosen to be the same as in the parallel field case [67]. Integrating Eq. (3.44) with respect to x over the range $(-a \le x \le a)$ yields the following eigenvalue problem

$$\left[-\frac{d^2}{dz^2} + \langle(x\cos\theta - z\sin\theta)^2\rangle\right] g(z) = \varepsilon\, g(z)\,, \tag{3.46}$$

where we have defined

$$g(z) = \frac{1}{2a}\int_{-a}^{a}\mathcal{F}(x,z)\,dx\,, \tag{3.47}$$

and

$$\langle(\cdots)\rangle = \int_{-a}^{a}(\cdots)\mathcal{F}(x,z)\,dx\left(\int_{-a}^{a}\mathcal{F}(x,z)\,dx\right)^{-1}. \tag{3.48}$$

Assuming $\mathcal{F}$ depends only weakly on x, we may approximate

$$\langle(x\cos\theta - z\sin\theta)^2\rangle \approx z^2\sin^2\theta + \frac{1}{3}a^2\cos^2\theta\,, \tag{3.49}$$

and the eigenvalue equation reduces to

$$\left[-\frac{d^2}{dz^2} + z^2 \sin^2\theta\right] g(z) = \left(\varepsilon - \frac{1}{3}h\cos^2\theta\right) g(z)\,, \tag{3.50}$$

with $a = \sqrt{h}$. This may be solved to yield a minimum eigenvalue

$$\varepsilon = \sin\theta + \frac{1}{3}h\cos^2\theta\,. \tag{3.51}$$

The minimum eigenvalue, E_g defined by Eq. (3.6), is thus written as

$$\frac{E_g}{hD} = h(\theta)\,\varepsilon = h(\theta)\sin\theta + \frac{1}{3}h^2(\theta)\cos^2\theta\,. \tag{3.52}$$

At fixed temperature, T, differentiating the Werthamer equation, Eq. (2.161),

$$\Upsilon\left(\frac{E_g[h(\theta),\theta]}{2\pi k_B T}\right) + \ln\left(\frac{T}{T_c}\right) = 0\,, \tag{3.53}$$

with respect to θ leads to $\frac{d}{d\theta}E_g[h(\theta),\theta] = 0$ for all the orientations ($0 < \theta < \frac{\pi}{2}$). One finds that

$$\frac{E_g}{hD} = \begin{cases} \frac{1}{3}h_{\parallel}^2\,, & \theta = 0\,, \\ h_{\perp}\,, & \theta = \frac{\pi}{2}\,. \end{cases} \tag{3.54}$$

Tinkham's formula, Eq. (3.4), for the angular dependence of the upper critical field is thus given by

$$\begin{aligned} 1 &= \frac{h(\theta)}{h_{\perp}}\sin\theta + \frac{h^2(\theta)}{h_{\parallel}^2}\cos^2\theta \\ &= \frac{H(\theta)}{H_{\perp}}\sin\theta + \frac{H^2(\theta)}{H_{\parallel}^2}\cos^2\theta\,. \end{aligned} \tag{3.55}$$

While experiments by Harper and Tinkham [69] show excellent agreement with Tinkham's formula for thin films, as they should, however, for moderately thick films the data falls consistently above or below the theoretical curve, depending on the film thickness and temperature. Our own numerical results (will be shown in Section 3.6) indicate that Tinkham's formula gives a good approximation to the

angular dependence of the upper critical field for $a_r < \xi_H/\sqrt{2}$. Yamafuji et al. [54] claim to have generalized Tinkham's formula to include films of moderate thickness. They give the following formula for $H(\theta)$ for a film of moderate thickness:

$$\frac{H^2(\theta)}{H_{\parallel}^2}\cos^2(\theta)\left[1-3(1+\sqrt{2})\frac{H_{\perp}^2}{H_{\parallel}^2}\frac{H(\theta)}{H_{\perp}}\sin(\theta)\right]+\frac{H(\theta)}{H_{\perp}}\sin(\theta)=1\,. \qquad (3.56)$$

Yamafuji et al. showed the agreement of this formula with a set of experimental data, which lies above Tinkham's curve. However, given the fact that the experimental data [69] may also lie below Tinkham's curve for thick films, it is difficult to draw any conclusion from Yamafuji's formula, Eq. (3.56). In a later paper, Yamafuji et al. [55] suggested a somewhat different formula for extremely thick films by means of a variational method,

$$\frac{H^2(\theta)}{H_{\parallel}^2}\cos^2(\theta)\left[1+\tan(\theta)(1-\sin(\theta))\right]+\frac{H(\theta)}{H_{\perp}}\sin(\theta)=1\,, \qquad (3.57)$$

and again, Yamafuji et al. were able to find a set of experimental data which agreed with their expression. However, as Thompson [24] pointed out, a boundary condition valid in the parallel field case, $\frac{\partial^2}{\partial^2 x}\mathcal{F}\Big|_{x=0}=0$, instead of $\frac{\partial}{\partial x}\mathcal{F}\Big|_{x=0}=0$, was used in Yamafuji's work.

The earliest calculation of the angular dependence of the upper critical field for films of arbitrary thickness was given by Saint-James [21] using the GL formalism. However, due to the perturbation nature of the calculation, Saint-James was able to obtain the slope of the logarithmic derivative $\frac{1}{H}\frac{\partial H}{\partial\theta}$ only in the limit $\theta\to 0$.

To recover Saint-James' result within the DW framework, we write the eigenvalue problem as

$$\left\{-\frac{\partial^2}{\partial x^2}-\frac{\partial^2}{\partial z^2}+[(x-k)\cos\theta-z\sin\theta)]^2\right\}\mathcal{F}(x,z)=\varepsilon\,\mathcal{F}(x,z)\,, \qquad (3.58)$$

$$\frac{\partial}{\partial x}\mathcal{F}(x,z)\Big|_{x=\pm a}=0\,,\quad \lim_{z\to\pm\infty}\mathcal{F}(x,z)\to 0\,, \qquad (3.59)$$

where the ansatz defined in Eq. (3.43) was used.

Defining

$$\hat{\mathcal{L}}_x = -\frac{d^2}{dx^2} + (x-k)^2 \cos^2\theta\,, \tag{3.60}$$

$$\hat{\mathcal{L}}_z = -\frac{d^2}{dz^2} + z^2 \cos^2\theta\,, \tag{3.61}$$

$$\hat{V} = -2\,(x-k)\,z\,\sin\theta\cos\theta\,, \tag{3.62}$$

Saint-James noted that the term $\hat{V}$ tends to zero in the limit $\theta \to 0$ and, he argued, it should be possible to obtain an expression for the angular dependence of the eigenvalue in the limit $\theta \to 0$ using perturbation theory. The unperturbed eigenvalue, ε_0, may be obtained by solving the following equations

$$\hat{\mathcal{L}}_x\, f_j(x) = \lambda_j f_j(x)\,, \qquad \frac{d}{dx} f_j(x)\Big|_{x=\pm a} = 0\,, \tag{3.63}$$

$$\hat{\mathcal{L}}_z\, g_m(z) = \eta_m\, g_m(z)\,, \qquad \lim_{z\to\pm\infty} g_m(z) = 0\,, \tag{3.64}$$

with

$$\begin{aligned}\varepsilon_0 = \lambda_j + \eta_m &= (2\nu_j + 1)\cos\theta + (2m+1)\sin\theta\,, \qquad j, m = 0, 1, 2, \cdots\,, \\ &\approx (2\nu_j + 1) + (2m+1)\theta\,.\end{aligned} \tag{3.65}$$

Including the second order perturbation correction, the eigenvalue is expressed as

$$\begin{aligned}\varepsilon(\theta) &= \varepsilon_0 - 2\sin\theta\cos\theta \left[\sum_{j\neq 0} \frac{|\langle\lambda_0|(x-k)|\lambda_j\rangle|^2}{\lambda_j - \lambda_0}\right]_{\theta\to 0} \\ &\approx \varepsilon_0 - 2\theta \left[\sum_{j\neq 0} \frac{|\langle\lambda_0|(x-k)|\lambda_j\rangle|^2}{\lambda_j - \lambda_0}\right]_{\theta\to 0} \\ &= \lambda_0 - S\,\theta\end{aligned} \tag{3.66}$$

where

$$S = 1 - 2\sum_{j\neq 0} \frac{|\langle\lambda_0|(x-k)|\lambda_j\rangle|^2}{\lambda_j - \lambda_0}\,, \tag{3.67}$$

and the notation

$$|\lambda_j\rangle \rightarrow f_j(x), \quad |n\rangle \rightarrow g_n(z), \tag{3.68}$$

and the relations

$$\langle n|z\sqrt{2\sin\theta}|n\rangle = 0, \quad \langle 0|z\sqrt{2\sin\theta}|1\rangle = 1, \tag{3.69}$$

were used.

Saint-James [66] was then able to relate the summation of the matrix elements over the excited states to the curvature of the eigenvalue spectrum, $\lambda(k)$ at $k = k^*$, calculated in the parallel case, through

$$\left.\frac{\partial^2\lambda_0(k)}{\partial k^2}\right|_{k=k^*} = 2\left[1 - 4\sum_{j\neq 0}\frac{|\langle\lambda_0|(x-k^*)|\lambda_j\rangle|^2}{\lambda_j - \lambda_0}\right], \tag{3.70}$$

which leads to

$$S = \frac{1}{4}\left[2 + \frac{\partial^2\lambda_0(k)}{\partial k^2}\right]_{k=k^*}. \tag{3.71}$$

Saint-James obtained the expression for the logarithmic derivative of the upper critical field in the limit $\theta \rightarrow 0$ for fixed T as

$$\lim_{\theta\rightarrow 0}\frac{1}{H(\theta)}\left.\frac{\partial H(\theta)}{\partial\theta}\right|_T = -\frac{1}{4}\left[2 + \frac{\partial^2\lambda_0(k^*)}{\partial k^2}\right]\left(\frac{\partial(h\lambda_0^*)}{\partial h}\right)^{-1}. \tag{3.72}$$

Originally, Saint-James' result had been thought to be an exact solution, since all the higher order terms in the perturbation are characterized by a factor of θ^p ($p > 1$). However, Thompson [24, 56] later pointed out that Saint-James' calculation of the perturbation correction up to the second order was in error and that there should be contributions proportional to θ from higher order terms. The problem stems from the fact that the eigenvalues for the excited states with the same value of j are degenerate in the limit $\theta \rightarrow 0$. As a consequence of this, it can be shown that all the even-ordered terms in the perturbation series contribute to $\varepsilon(\theta)$ to order θ.

Thompson [24] concluded that, summing over all the leading term contributions, the correct expression for the slope should be of the form

$$S = \left[1 - 4\sum_{j\neq 0}\frac{|\langle\lambda_0|(x-k^*)|\lambda_j\rangle|^2}{\lambda_j-\lambda_0}\right]^{\frac{1}{2}} = \sqrt{\frac{1}{2}\frac{\partial^2\lambda_0(k^*)}{\partial k^2}}\,. \tag{3.73}$$

The corrected logarithmic derivative of the upper critical field in the limit $\theta \longrightarrow 0$ at temperature, T, is given by

$$\lim_{\theta\to 0}\frac{1}{H(\theta)}\frac{\partial H(\theta)}{\partial\theta}\bigg|_T = -\sqrt{\frac{1}{2}\frac{\partial^2\lambda_0(k^*)}{\partial k^2}}\left(\frac{\partial(h\lambda_0^*)}{\partial h}\right)^{-1}\,. \tag{3.74}$$

Despite the fact that early experiments [22, 23] appeared to confirm the result given by Eq. (3.72), the result is obviously in error. To understand this we simply apply Eq. (3.72), to a homogeneous superconductor, with the boundary conditions given by

$$\lim_{x\to\pm\infty}\mathcal{F}(x,y) = 0\,. \tag{3.75}$$

In this case the eigenvalue $\lambda^* = 1$ is entirely independent of the wave number k and hence we obtain the result

$$\frac{\partial^2\lambda(k^*)}{\partial k^2} = 0\,. \tag{3.76}$$

From Eq. (3.72), this implies that, in the case of a homogeneous bulk sample, the upper critical field would exhibit an angular dependence with

$$\lim_{\theta\to 0}\frac{1}{H}\frac{\partial H}{\partial\theta}\bigg|_T = -\frac{1}{2}\,, \tag{3.77}$$

a result that is obviously incorrect.

On the other hand, Thompson's result, Eq. (3.74), gives

$$\lim_{\theta\to 0}\frac{1}{H}\frac{\partial H}{\partial\theta}\bigg|_T = 0\,. \tag{3.78}$$

for a homogeneous sample.

In the case of thin films, the results obtained from Eq. (3.72) and (3.74) are closely approximated by the corresponding results obtained from the Tinkham formula given by Eq. (3.55). For $a_r \gtrsim \xi_{II}$, however, the results obtained differ significantly. In particular the theory of Saint-James predicts the existence of a cusp when the logarithmic derivative of the upper critical field is plotted as a function of the reduced magnetic field $h = a_r^2/\xi_{II}^2$. The value of the reduced field h at which the cusp appears corresponds to the value for which the nucleation center acquires a non zero value. Thus, while Thompson's result exhibits a cusp as the nucleation center acquires a non-zero value, the derivative is zero, in obvious contradiction to the value of -0.5341 obtained previously by Saint-James. Harper and Tinkham [69] measured $\lim_{\theta\to 0} \frac{1}{H}\frac{\partial H}{\partial \theta}\Big|_T$ for a Pb film and showed that the experimental data were systematically larger than Saint-James result around the cusp point, however, all the data are finite and no zero slope was found. As far as we are aware there have been no experimental studies which resolve the discrepancy between the two results, and the result obtained by Thompson appears to have gone largely unnoticed in the literature. A comparison of the values obtained for the $\lim_{\theta\to 0} \frac{1}{H}\frac{\partial H}{\partial \theta}\Big|_T$ given by the different authors is presented in Fig. 3.5.

While Thompson has correctly identified an inconsistency in Saint-James' analysis, it is nevertheless not entirely clear that the result presented by Thompson is correct. To understand this we note that Thompson's result depends on the nucleation center, k^*, found in the parallel field case. While the corresponding eigenvalue equation for the parallel field case, Eq. (3.17), may be obtained by setting $\theta = 0$ in Eq. (3.44), it can be readily shown that the resultant eigenvalue spectra, ε, differs qualitatively. This is best demonstrated if we consider the fact that, in the case of a parallel field, the eigenvalue spectrum that one obtains from Eq. (3.17) exhibits

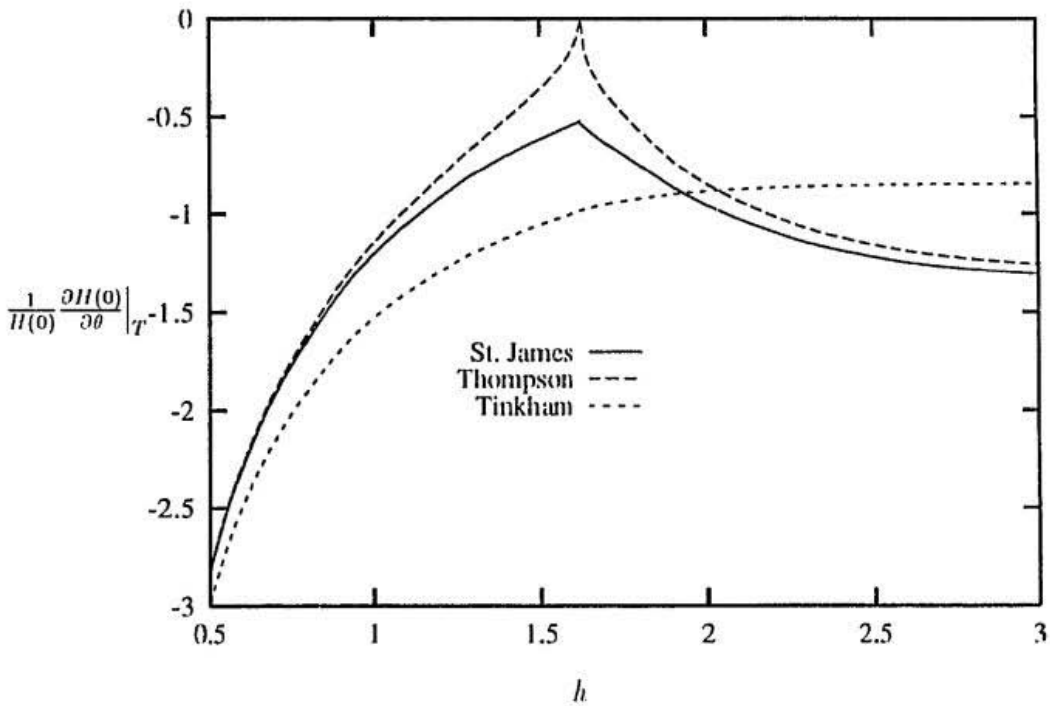

Figure 3.5: Plot of the logarithmic derivative $\lim_{\theta\to 0} \frac{1}{H(\theta)} \frac{\partial H(\theta)}{\partial \theta}\Big|_T$ as a function of the dimensionless magnetic field $0.5 \leq h \leq 3.0$ for the theories of Tinkham, Saint-James and Thompson.

a non-trivial dependence on the value of the wave number k. In contrast, for finite θ one can simply remove the variable k from the eigenvalue equation, Eq. (3.44), through the transformation

$$z \rightarrow z' = z + k \cot \theta \, . \tag{3.79}$$

Since this transformation leaves the boundary conditions unchanged, this implies that the resultant eigenvalue spectrum is entirely independent of k. Given the previous discussion of the parallel field case, and in particular, the critical role played by the wave number k in defining the nucleation center, this represents an important distinction between the parallel field case and the case of finite θ.

These considerations show that the calculation of the upper critical field for finite θ cannot be regarded as a simple generalization of the parallel field case. Moreover, this distinction between the eigenvalue spectra at finite θ and in the parallel field case leads to the question of how the results of the parallel field case are recovered in the limit $\theta \rightarrow 0$. It is reasonable to suppose, and we will show explicitly, that the minimum eigenvalue $\varepsilon(\theta)$ approaches $\varepsilon_{\|}^{*}$, the value obtained in the parallel field case, in the limit $\theta \rightarrow 0$. However, this is by no means self-evident. Moreover, even if the limiting eigenvalue $\lim_{\theta \rightarrow 0} \varepsilon^{*}(\theta)$ agrees with the corresponding eigenvalue obtained for the parallel field case, it is obvious that the eigenvalue spectrum, defined by Eq. (3.44) together with the boundary conditions Eq. (3.45), will exhibit non-analytic behavior in the limit $\theta \rightarrow 0$.

This non-analytic behavior is examined in more detail in Appendix B. In this appendix, we show how the limit may be taken analytically by introducing an additional term, αz^2, in the eigenvalue equation, Eq. (3.44). The limit $\alpha \rightarrow 0$ is then investigated and the non-analytical character of the limit $\theta \rightarrow 0$ examined. However, we will show this non-analytical behavior of the eigenvalue spectrum ε in the cases of finite θ and $\theta = 0$ explicitly by performing a numerical calculation in next

section.

3.5 Eigenvalue Problem for the Tilted Field

We have shown how previous work on this topic has been restricted to either thin films [20] or to the limiting case of $\theta \to 0$ [21, 24]. In this section we will present numerical calculations for the angular range $0 < \theta < \pi/2$ for the entire range of thicknesses.

In order to obtain the eigenvalue from the partial differential equation, Eq. (3.58), we expand the order parameter in terms of a complete set of eigenfunctions as

$$\mathcal{F}(x,z) = \sum_{m,j} A_{mj}\, f_j(x)\, g_m(z) \tag{3.80}$$

where the eigenfunction $f_j(x)$ satisfies the Weber equation, Eq. (3.19),

$$\hat{\mathcal{L}}_x\, f_j(x) = \left[-\frac{d^2}{dx^2} + x^2\cos^2\theta\right] f_j(x) = \lambda_j\, f_j(x)\,, \tag{3.81}$$

subject to

$$\frac{d}{dx}\, f_j(x)\bigg|_{x=\pm a} = 0\,, \tag{3.82}$$

and the eigenfunction $g_m(z)$ satisfies

$$\hat{\mathcal{L}}_z\, g_m(z) = \left[-\frac{d^2}{dz^2} + z^2\sin^2\theta\right] g_m(z) = \eta_m\, g_m(z)\,, \tag{3.83}$$

subject to

$$\lim_{z\to\pm\infty} g_m(z) = 0\,. \tag{3.84}$$

The orthogonality of the eigenfunctions is expressed as

$$\int_{-a}^{a} dx\, f_{\lambda_j}(x)\, f_{\lambda_{j'}}(x) \;=\; \delta_{jj'}\,, \tag{3.85}$$

$$\int_{-\infty}^{\infty} dz\, g_m(z)\, g_{m'}(z) \;=\; \delta_{mm'}\,. \tag{3.86}$$

Substituting the expansion of the order parameter into the eigenvalue equation, Eq. (3.58), yields

$$\begin{aligned}\varepsilon\,\mathcal{F}(x,z) &= \sum_{m,j} A_{mj}\left\{-\frac{\partial^2}{\partial x^2}-\frac{\partial^2}{\partial z^2}+[k-x\,\cos\theta+z\,\sin\theta]^2\right\} f_j(x)\,g_m(z)\\ &= \varepsilon\sum_{m,j} A_{mj}\,f_j(x)\,g_m(z)\,, \qquad (3.87)\end{aligned}$$

where, for convenience, we have absorbed the $\cos\theta$ dependence in k.

Multiplying Eq. (3.87) with $f_i(x)\,g_n(z)$ and integrating with respect to x and z, the eigenvalue, ε, may be expressed as

$$\begin{aligned}\varepsilon &= \sum_{m,n,i,j} A^*_{mj}\,A_{ni}\int dx\,dz\,f_j(x)\,g_m(z)\hat{\mathcal{L}}(x,z)\,f_i(x)\,g_n(z)\left[\sum_{m,j}|A_{mj}|^2\right]^{-1}\\ &= \sum_{m,n,i,j} A^*_{mj}\,A_{ni}\,\langle j,m\left|\hat{\mathcal{L}}(k)\right|i,n\rangle\left[\sum_{m,j}|A_{mj}|^2\right]^{-1}\,, \qquad (3.88)\end{aligned}$$

where we have introduced the notation $|j,m\rangle = f_j(x)\,g_m(z)$. The derivation of the matrix representation of the differential operator, $\hat{\mathcal{L}}$, is given in Appendix B. There it is shown that

$$\begin{aligned}\langle j,m|\hat{\mathcal{L}}(k)|i,n\rangle &= \int_{-a}^{a}dx\int_{-\infty}^{\infty}dz\;f_j(x)\,g_m(z)\;\hat{\mathcal{L}}\,f_i(x)\,g_n(z)\\ &= \left[\lambda_j+\eta_m+k^2\right]\delta_{ij}\,\delta_{mn}-\sqrt{\sin\theta\,\cos\theta}\,\mathcal{X}_{ij}\,\mathcal{Z}_{mn}\\ &+\; k\left[\mathcal{X}_{ij}\,\delta_{mn}\,\sqrt{2\cos\theta}-\mathcal{Z}_{mn}\,\delta_{ij}\,\sqrt{2\sin\theta}\right]\,, \qquad (3.89)\end{aligned}$$

where the matrix elements $\mathcal{X}_{ij}$ and $\mathcal{Z}_{mn}$ are given by

$$\mathcal{X}_{ij} = C_i^+C_j^-\int_{-a\sqrt{2\cos\theta}}^{a\sqrt{2\cos\theta}} e^{-\frac{1}{2}t^2}\,M\left[\frac{1-\nu_j}{2},\frac{3}{2},\frac{t^2}{2}\right]M\left[\frac{-\nu_i}{2},\frac{1}{2},\frac{t^2}{2}\right]t^2dt, \qquad (3.90)$$

$$\mathcal{Z}_{mn} = \left[\sqrt{n+1}\,\delta_{m,n+1}+\sqrt{n}\,\delta_{m,n-1}\right]\,, \qquad (3.91)$$

$$C_i^{+-2} = \int_{-a\sqrt{2\cos\theta}}^{a\sqrt{2\cos\theta}} e^{-\frac{1}{2}t^2}\,M^2\left[\frac{-\nu_i}{2},\frac{1}{2},\frac{t^2}{2}\right]dt\,, \qquad (3.92)$$

$$C_j^{-2} = \int_{-a\sqrt{2\cos\theta}}^{a\sqrt{2\cos\theta}} e^{-\frac{1}{2}t^2}\,M^2\left[\frac{1-\nu_j}{2},\frac{3}{2},\frac{t^2}{2}\right]t^2dt\,, \qquad (3.93)$$

where $M[a,b,z]$ is the Kummer function [70] and $\lambda_j = (2\nu_j+1)\cos\theta$.

In order to obtain the minimum eigenvalue, we require

$$\frac{\delta}{\delta A^*_{mj}} \varepsilon(k) = 0 , \tag{3.94}$$

which yields the secular equation

$$\det \left| \langle j, m | \hat{\mathcal{L}}(k) | i, n \rangle - \varepsilon(k) \right| = 0 , \tag{3.95}$$

where we write ε as $\varepsilon(k)$ to explicitly indicate the k dependence of the eigenvalue. This secular equation provides a basis for the computation of the minimum eigenvalue for given magnetic field H, angle θ and sample thickness. However, we note that the magnetic field and the physical thickness of the sample, denoted by a_r, do not enter the calculation of the eigenvalue independently. The eigenvalue is determined by a dimensionless quantity defined by

$$a^2 = h = \frac{2\pi H}{\phi_o} a_r^2 . \tag{3.96}$$

In Fig. 3.6(a) and (b), we show the minimum eigenvalue obtained for two values of the effective thickness as a function of the reduced wave number k for $\theta = 1°$ and $2°$. The corresponding result for the parallel field case is also shown. Note that, for the case of finite θ, the minimum eigenvalue is, within the numerical precision of the calculation, entirely independent of the wave number k. It is also worth noting that in order to obtain sufficient accuracy it was necessary to include in excess of 1,000 terms in the expansion for $\mathcal{F}(x, z)$. As a comparison, a curve calculated by including 100 terms in the expansion for $\mathcal{F}(x, z)$ is plotted in Fig. 3.6(a) and (b).

In Fig. 3.7 we show a plot of the minimum eigenvalue as a function of angle θ for the values of reduced thickness shown in Fig. 3.6. The minimum eigenvalue for the corresponding parallel field case is also included and we see that, despite the qualitative differences between the curves of $\varepsilon(k)$ for the the parallel field case and the finite θ case, the minimum eigenvalue nevertheless appears to map continuously to the value found in parallel field case as a function of θ.

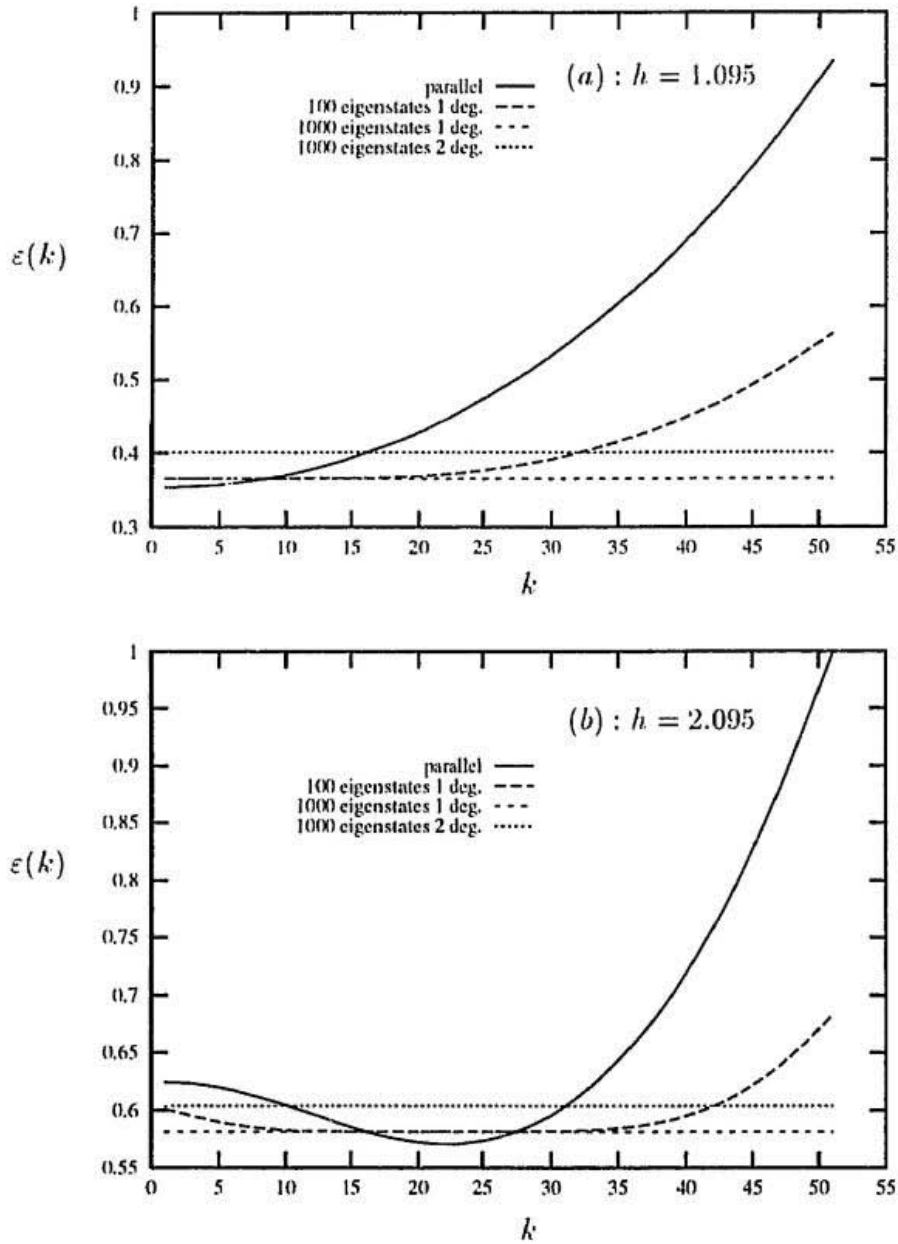

Figure 3.6: Plots showing the k-independence of $\varepsilon(k)$ for $\theta \neq 0$ and k-dependence for $\theta = 0$, respectively. Two values of reduced field $h = 1.095$ in (a) and $h = 2.095$ in (b) are chosen. Curve (parallel) shows the k-dependence of $\varepsilon(k)$ in parallel field case. Curve (100 eigenstates 1°) shows the artificial k-dependence for $\theta = 1°$ by including 100 eigenstates in numerical calculation. The other two curves show the k-independence of $\varepsilon(k)$ by including 1,000 eigenstates in numerical calculation for $\theta = 1°$ and $2°$, respectively.

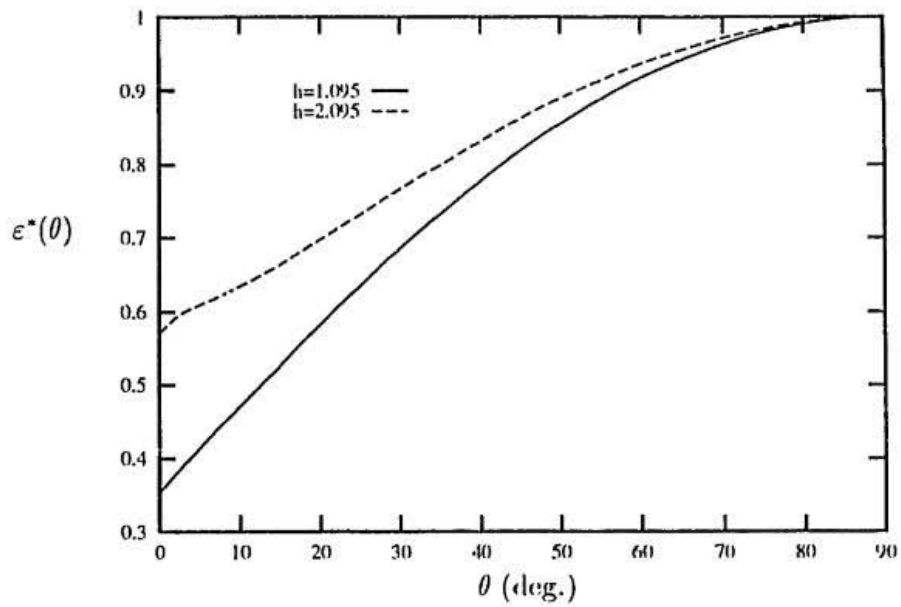

Figure 3.7: Angular dependence of the eigenvalue for $h = 1.095$ and $h = 2.095$. The eigenvalue $\varepsilon(0)$ is obtained from the calculation for the parallel field case.

3.6 Angular Dependence of the Upper Critical Field $H(\theta)$

Given the eigenvalue, ε, calculated in last section, we obtain the upper critical field from the Werthamer equation, Eq. (3.8),

$$\chi\left[\frac{\xi_0^2}{a_r^2}\frac{h(\theta)\,\varepsilon[h(\theta),\theta]}{t}\right]+\ln(t)=0\,, \tag{3.97}$$

where $t=T/T_c$ denotes the reduced temperature ($0\le t\le 1$) and T_c is the transition temperature of the superconductor at zero magnetic field. It is readily seen that the full angular dependence of the reduced critical magnetic field $h(\theta)$ at fixed temperature t is determined by the condition

$$h(\theta)\,\varepsilon[h(\theta),\theta]=const. \tag{3.98}$$

and this constant may be calculated from the eigenvalue found at $\theta=0$

$$h(\theta)\,\varepsilon[h(\theta),\theta]=h(0)\,\varepsilon[h(0),\theta=0]\,. \tag{3.99}$$

A self-consistent equation determining the reduced angular dependent upper critical field is given by

$$\frac{h(\theta)}{h(0)}=\frac{H(\theta)}{H(0)}=\frac{\varepsilon[h(0),\theta=0]}{\varepsilon\left[\theta,h(0)\frac{H(\theta)}{H(0)}\right]}\,, \tag{3.100}$$

where $h(0)$ may be given by the experimental data $H_{\|}=H(0)$ and thickness a_r of the sample and the eigenvalue $\varepsilon[0,h(0)]$ is determined by

$$\varepsilon[h(0),0]=\frac{H_\perp}{H_{\|}}\,. \tag{3.101}$$

The numerical results of $H(\theta)/H(0)$ corresponding to several values of the reduced parallel field, $h(0)=h_{\|}$, are presented in Figs. 3.8 and 3.9. For $h_{\|}=0.49h_c$ we see from Fig. 3.8(a) that the angular dependence of the critical field is well approximated by Tinkham's expression, Eq. (3.55). However for $h=1.05h_c$ we see that the angular dependence of the upper critical field, shown in Fig. 3.8(b), deviates significantly

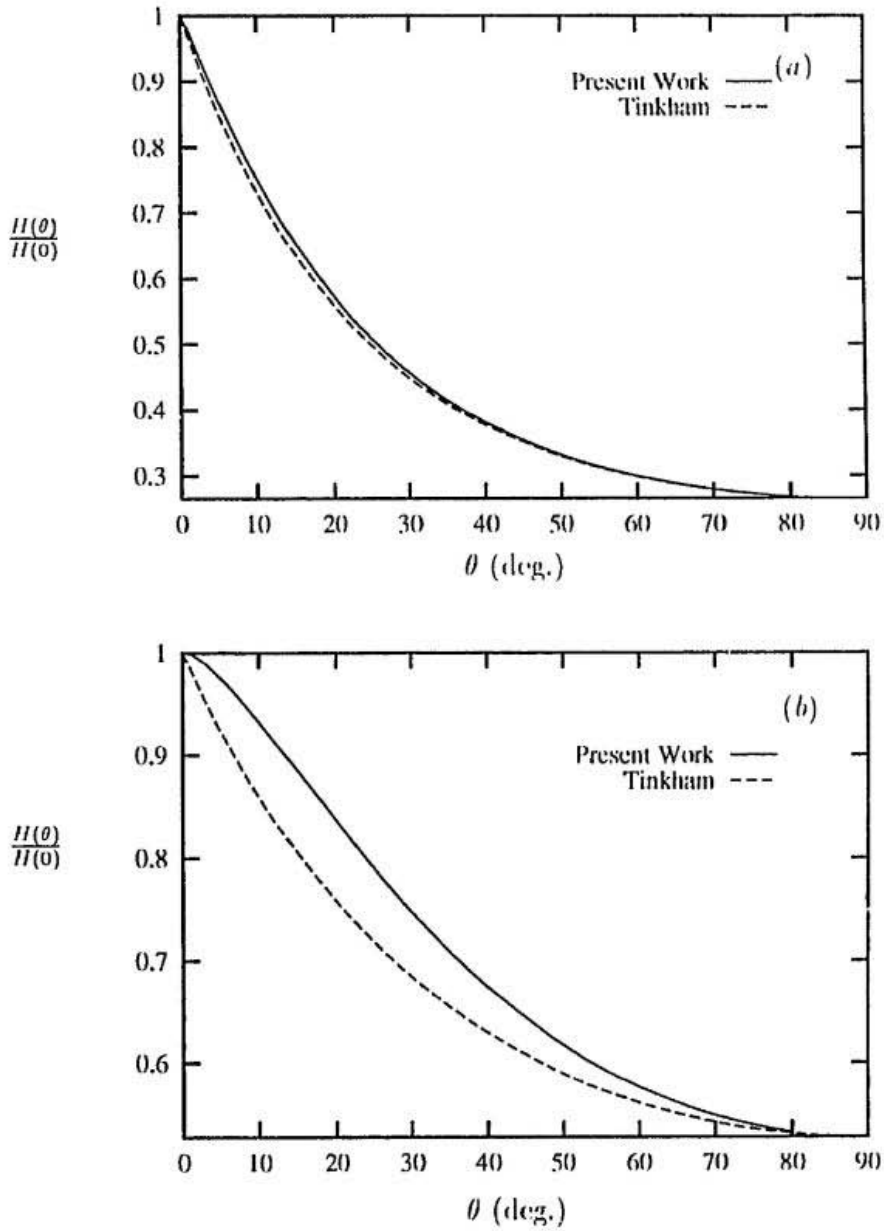

Figure 3.8: Plot of $H(\theta)/H(0)$ vs. θ for $h = 0.8$ in (a) and $h = 1.7$ in (b). The solid line shows the result from the self-consistent equation. The dashed line is computed using Tinkham's formula. Fig. (a) shows the thin film behavior of $H(\theta)$. Fig. (b) shows the deviation of $H(\theta)$ from Tinkham's theory for a larger thickness.

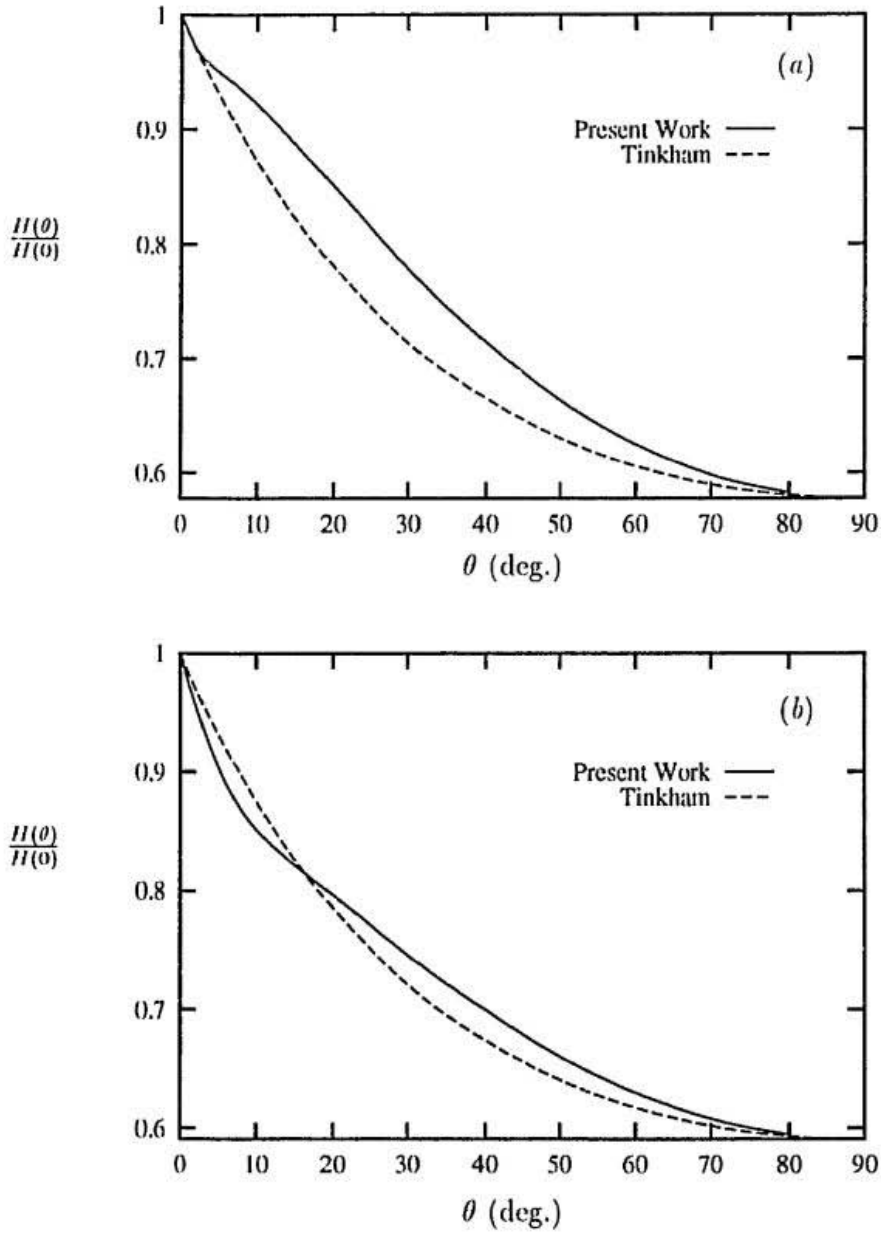

Figure 3.9: Plot of $H(\theta)/H(0)$ vs. θ for $h = 2.2$ in (a) and $h = 3.5$ in (b). In Fig. (a), for a thicker film, a knee appearing at a small angle ($\theta \sim 5°$) shows a transition from semi-infinite to finite-thickness behavior. Fig. (b) shows that for $h = 3.5$, the numerical results differ significantly from those of Tinkham for all θ.

from Tinkham's curve, particularly close to $\theta = 0$, where the slope is close to zero. Increasing the effective field beyond h_c to a value of $1.36h_c$, we see in Fig. 3.9(a), that of $H(\theta)$ again acquires a finite slope for $\theta = 0$ which is close to the corresponding value given by the Tinkham formula. However the disagreement between the Tinkham's formula and the results of the present work become more pronounced with increasing θ. As $h_{\parallel}$ is increased yet further to a value of $2.16h_c$, shown in Fig. 3.9(b), the slope at $\theta = 0$ falls below the value given by the Tinkham's formula. However the slope of the curve obtained from the present work increases and the curves cross at a value of around 16° and the calculated value then lies above the value obtained by Tinkham's formula. In order to understand this dimensional crossover predicted by our theoretical calculation in the thick film case, we perform a separate calculation for the semi-infinite geometry as a limit of a thick film.

3.6.1 $H(\theta)$ for the Semi-Infinite Geometry

The semi-infinite geometry is shown in Fig. 3.10.

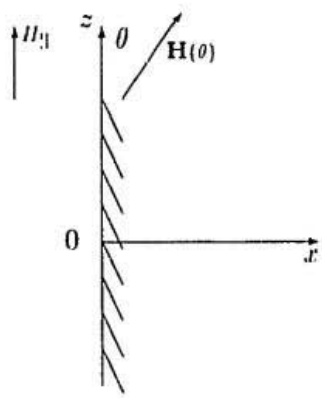

Figure 3.10: Semi-Infinite Bulk Superconductor.

The form of the secular equation, Eq. (3.95), used in this calculation remains unchanged. However, the matrix element X_{ij} is recalculated corresponding to the

change of the boundary condition. An appropriate set of eigenfunctions corresponding to the modified boundary conditions imposed on the order parameter may be chosen by solving the Weber equation

$$\left[-\frac{d^2}{dx^2} + x^2\cos^2\theta\right] f_j(x) = \lambda_j f_j(x)\,, \tag{3.102}$$

subject to the boundary conditions

$$\left.\frac{df_j(x)}{dx}\right|_{x=0} = 0\,, \qquad f_j(x)|_{x\to\infty} = 0\,. \tag{3.103}$$

It is immediately seen that the following complete set of the normalized eigenfunctions

$$f_j(x) = C_{2l}\, e^{-\frac{1}{2}(x\sqrt{\cos\theta})^2}\, H_{2l}\left(x\sqrt{\cos\theta}\right) \tag{3.104}$$

where H_{2l} denotes the even order Hermite polynomial, and

$$\lambda_j = [2(2l)+1]\cos\theta\,; \qquad l = 0, 1, 2, \cdots \tag{3.105}$$

satisfy both the Weber equation and the boundary conditions. The normalization constant is determined by

$$C_{2l}^{-2} = \int_0^\infty e^{-x^2\cos\theta}\, H_{2l}^2\left(x\sqrt{\cos\theta}\right)\, dx\,. \tag{3.106}$$

The eigenvalue λ_j of the set of basis functions describing the x dependence of the order parameter is a function of θ and independent of the magnitude of the applied magnetic field H. Labeling λ_j by $2l$ so that $f_j(x) = f_{2l}(x)$, it is straightforward to calculate the matrix element $X_{ll'}$

$$X_{ll'} = \int_0^\infty f_{2l}(x)\, x\, f_{2l'}(x)\, dx\,. \tag{3.107}$$

A numerical calculation of the minimum eigenvalue $\varepsilon(\theta)$, similar to the calculation for the finite sample, generates the full angular dependence of the upper critical field $H(\theta)$ given by

$$\frac{H(\theta)}{H(0)} = \frac{h(\theta)}{h(0)} = \frac{\varepsilon(\theta=0)}{\varepsilon(\theta)} = \frac{0.59010}{\varepsilon(\theta)}\,, \tag{3.108}$$

where $\varepsilon(0) = 0.59010$ is the eigenvalue obtained in Section 3.3.1, and first given by Saint-James [66] in considering the surface superconductivity for a semi-infinite bulk superconductor.

We can qualitatively understand the curve shown in Fig. 3.9(b) if we compare it with the corresponding curve obtained for the semi-infinite case $a_r/\xi_{II} \to \infty$. In Fig. 3.11 the dependence of $H(\theta)/H_{\|}$ on θ, obtained from the present calculation, for both the semi infinite case and the case $h_{\|} = 2.16h_c$ are presented. We note that the value of $H(\theta)/H_{\|}$ is close to the corresponding value for the semi-infinite case for small values of θ but deviates significantly for higher values of θ. This suggests that we can attribute the abrupt increase in the slope that appears in the curve for $h = 2.16h_c$ at around 10° as arising from crossover from a dominant single surface effect to a size effect (double-surface effect).

In Fig. 3.11, we also show the dependence of $H(\theta)/H_{\|}$ on θ obtained from the calculation by Yamafuji et al. for the semi-infinite case. While the two results agree for small values of θ, the curves differ significantly for larger values of θ.

A summary of the results obtained by the present calculation is given in Fig. 3.12. The results are normalized with respect to $H_{\perp}$ to show the systematic variation with respect to the reduced field.

In comparing the results for the full angular dependence of the upper critical field, we note that while the result obtained by Yamafuji et al. for moderately thick films [54], falls above the curve obtained from Tinkham's interpolation formula, the result obtained for the semi-infinite geometry [55] falls below. Yamafuji has argued that his results are consistent with certain experimental studies [71], and indeed the later results of Harper and Tinkham [69] show measurements of H vs. θ, which fall either consistently above or below the theoretical curve given by Eq. (3.55), depending on the film thickness. It is nevertheless difficult to see how the experimental data can

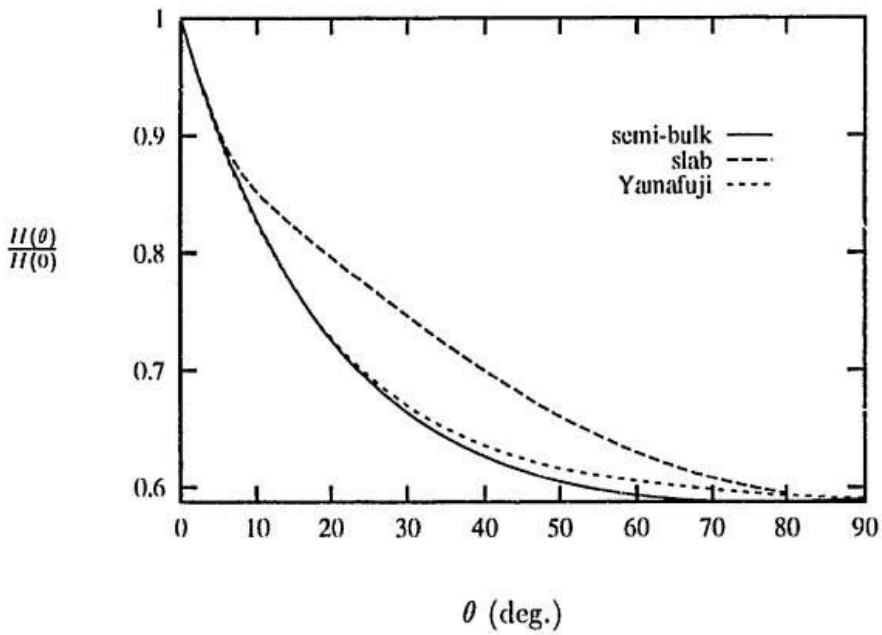

Figure 3.11: $H(\theta)/H(0)$ for a thick film is compared with that for the semi-infinite geometry. Yamafuji's curve is also presented as a comparison. The knee at $\theta = 10°$ in the thick film curve clearly indicates a dimensional crossover from single surface effect to double surface effect.

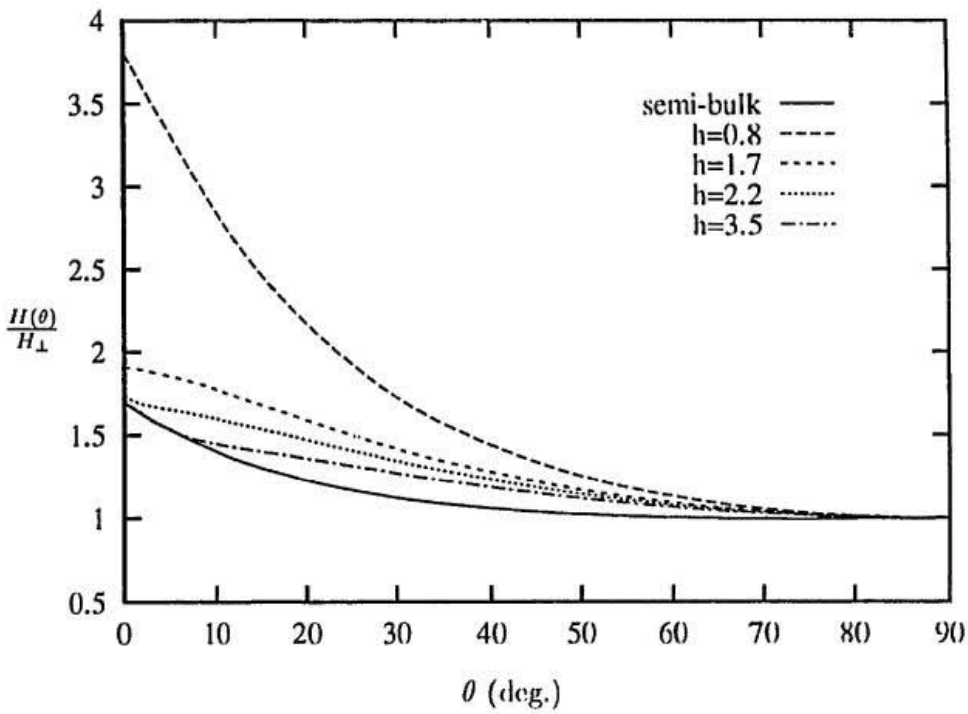

Figure 3.12: $H(\theta)/H_\perp$ calculated for various values of the reduced field $h = 0.49h_c$, $1.05h_c$, (c) $1.36h_c$ and (d) $2.16h_c$, together with the result obtained for the semi-infinite geometry.

be systematically accounted for by the results obtained Yamafuji [54, 55]. Moreover, given that the boundary condition used in the variational procedure by Yamafuji et al. [55] is inadequate, we must conclude that the degree of agreement between Eq. (3.57) and the experimental results is fortuitous.

While the results contained in the present work exhibit many of the features observed in the experimental studies, a quantitative comparison is difficult due in part to the lack of precise systematic studies of the angular dependence of the upper critical field of superconducting films. Part of the motivation in presenting the results of these calculations is to point out the discrepancies that exist in the existing experimental and theoretical work and to illustrate the need for further investigation in this area.

3.7 $H(\theta)$ in the Limit $\theta \to 0$

We have investigated the full angular dependence of the upper critical field for several sample thicknesses ranging from thin film, $h(0) = 0.8$, to thick film, $h(0) = 3.5$, as well as for the sample with infinite length scale. It is found, from the results and discussions presented in previous sections, that the small-angle behavior of $H(\theta)$ undergoes an intriguing dimensional crossover between a single surface effect and a size effect as the sample thickness is increased. Therefore, in this section, we will study the small-angle dependence of $H(\theta)$ in more detail in the range $0.5 \leq h(0) \leq 2.2$ and compare our numerical results with the theoretical work of previous authors.

Using the secular equation, Eq. (3.95), it is possible to estimate the derivative $\lim_{\theta \to 0} \frac{\partial \varepsilon}{\partial \theta}$, and hence calculate the logarithmic derivative of the upper critical field as a function of angle at fixed temperature by means of the equation

$$\frac{1}{H} \frac{\partial H(\theta)}{\partial \theta}\bigg|_T = -\frac{\partial \varepsilon^*}{\partial \theta} \left[\lambda^* + h \frac{\partial \lambda^*}{\partial h} \right]^{-1} . \tag{3.109}$$

In order to evaluate the expression for $\frac{1}{H}\frac{\partial H(\theta)}{\partial \theta}\Big|_T$ given in Eq. (3.109) the minimum eigenvalue $\varepsilon^*(\theta)$ was calculated for $\theta = 0.2°$ to $1°$ in intervals of $0.2°$, for a fixed value of the reduced field h. These data, together with the corresponding result obtained from the parallel field case, were combined and fitted with an interpolating function in the range $0°$ to $1°$ using cubic spline fit. The derivative $\lim_{\theta\to 0}\partial\varepsilon^*/\partial\theta$ was then extracted from the interpolating function. Estimating the derivative in this way assumes that the result of the parallel field calculation maps continuously to the result obtained for finite θ and requires that the eigenvalues be calculated with sufficient precision. Both these conditions appear to be satisfied in the present calculation.

However, over a narrow range of the reduced field, $1.59 < h < 1.76$, the value of the slope estimated by using cubic spline fit from our numerically calculated eigenvalues deviates slightly from Thompson's result as shown in Fig. 3.13. This may be attributed to the fact that the calculated angular dependence of the eigenvalue cannot be adequately represented by its value at a discrete set of points, in the domain $0° \to 1°$ for this particular range of reduced field. From this graph it is seen that, except for the range $1.59 < h < 1.76$, the numerically calculated slope agrees very closely with the result obtained by means of Thompson's formula given by Eq. (3.74). While this means that we are unable to confirm the Thompson's expression within this region, it suggests that the limit $\lim_{\theta\to 0}\partial H/\partial\theta|_T$ may not be a particularly useful means of characterizing the upper critical field for $\theta \approx 0$, and difficult to determine experimentally in this range of reduced field. In the thick film limit, the semi-infinite geometry, the value of logarithmic derivative of the upper critical field in the limit $\theta \to 0$ obtained from various theories are presented in Table 3.1.

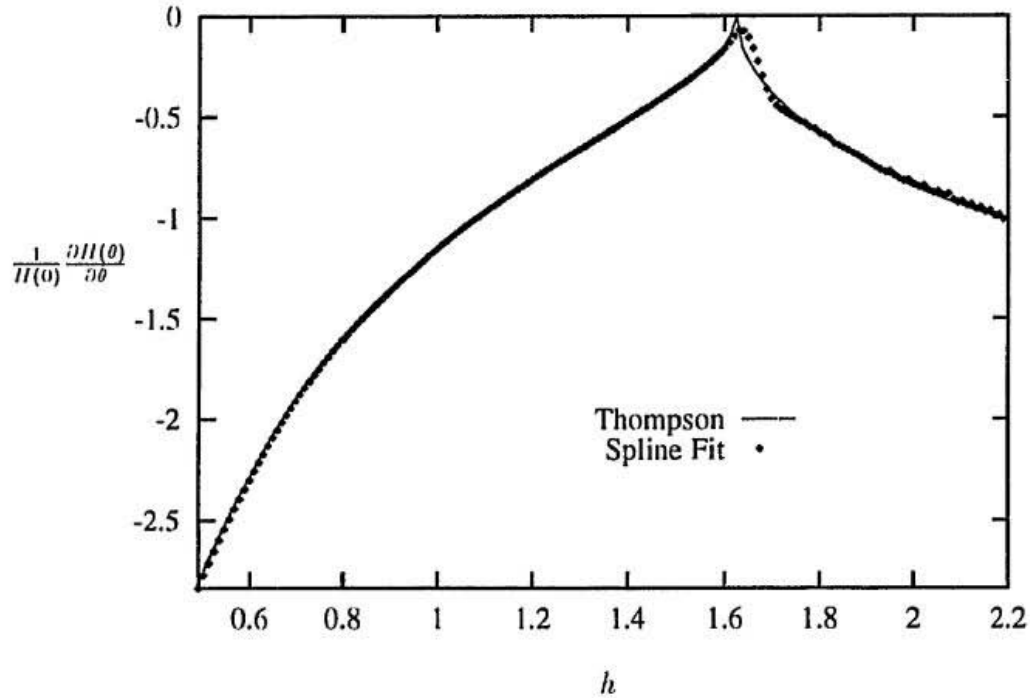

Figure 3.13: A plot showing the calculated value of the limiting slope $\lim_{\theta\to 0}\frac{1}{H}\frac{\partial H}{\partial \theta}\Big|_T$ as a function of the reduced field h, together with the result given by Eq. (3.74). The calculated values of the limiting slope are obtained from a cubic spline interpolation of the minimum energy eigenvalue ε^* in the range $0° < \theta < 1°$.

Author	References	$\lim_{\theta\to 0} \frac{1}{H} \frac{\partial H}{\partial \theta}\Big\vert_T$
Tinkham	[69]	-0.8450
Saint-James	[21]	-1.3455
Yamafuji	[55]	-1.3473
Thompson	[24]	-1.3000
Present work		-1.2963

Table 3.1: Values of logarithmic derivative of the upper critical field in the limit $\theta \to 0$ for a semi-infinite geometry.

In the preceding discussion we have drawn attention to the fact that there exist, within the existing literature, several distinct and mutually exclusive theoretical predictions for both the slope $\lim_{\theta\to 0} \frac{1}{H} \frac{\partial H}{\partial \theta}\Big\vert_T$ and the full angular dependence of the upper critical field of a planar superconducting film. We have shown to what extent the results of the present calculation are consistent with previous work and where there exist differences. The question then arises as to what measurements would allow one to distinguish between the various theoretical results and what conclusions one can draw from existing experimental data.

If we first consider the limiting slope $\lim_{\theta\to 0} \frac{1}{H} \frac{\partial H}{\partial \theta}\Big\vert_T$, then it is important to note that the results given by Eqs. (3.72) and (3.74), and discussed in the previous sections, reduce to the Tinkham's result, Eq. (3.55), in the thin film limit $a \ll \xi_{H_\parallel}$. In the other limit $a \gg \xi_{H_\parallel}$ the results given by Eqs. (3.72) and (3.74) do differ somewhat from the value given by Tinkham's interpolation formula, however the difference between the results given by Eqs. (3.72) and (3.74) are small and might not provide a practical means of distinguishing experimentally between the alternate expressions. The difference between the alternate expressions given by Eqs. (3.72) and (3.74) is most marked for films of intermediate thickness. Moreover it is in this domain that the most notable distinction between the expression obtained from

Tinkham's interpolation formula, Eq. (3.55), and Eqs. (3.72) and (3.74) occurs, specifically the presence of the cusp shown in Fig. (3.13) for $h_{||} = h^* = 1.62$. It is therefore significant that, while both the expression given by Thompson, Eq. (3.74), and that of Saint-James, Eq. (3.72), predict the existence of a cusp at $h = h^*$, Thompson predicts that the value of the slope at the cusp is zero while Saint-James [21] results yield a value of -0.5341.

While several experimental studies [23, 69, 71, 72] concerning the angular dependence of the upper critical field of a superconducting film have been published, their interpretation in the light of the preceding discussion is somewhat problematical. In particular, early experimental work [23, 71, 72] appears to be in good quantitative agreement with the expression given by Eq. (3.72). However later, more detailed, experimental studies by Harper and Tinkham [69] appear to indicate that, while the logarithmic derivative of the upper critical field in the limit $\theta \to 0$ is finite at the cusp, its value is nevertheless lower than that predicted by Eq. (3.72).

A possible explanation for these discrepancies not only between theory and experiment, but also between different experiments, may be attributed to the fact that, over a range of values of the reduced field, in the vicinity of the cusp, the limiting slope $\lim_{\theta\to 0} \partial H/\partial\theta|_T$ serves to characterize the angular dependence of the upper critical field only in a very narrow domain close to $\theta = 0$. This implies that, in this region at least, the precise experimental determination of the slope $\partial H/\partial\theta$ will be limited by the angular resolution of the measurements. This may be demonstrated explicitly if we define an effective slope as

$$\frac{1}{H}\overline{\left.\frac{\partial H}{\partial\theta}\right|_T} = \frac{H(\Delta\theta) - H(0)}{H(0)\Delta\theta} . \tag{3.110}$$

The effective slope is plotted for various values of $\Delta\theta$ in Fig. 3.14. We note that, while the effective slope exhibits a well defined maximum as distinct from a cusp, the value of the logarithmic derivative at the maximum does not go to zero, but

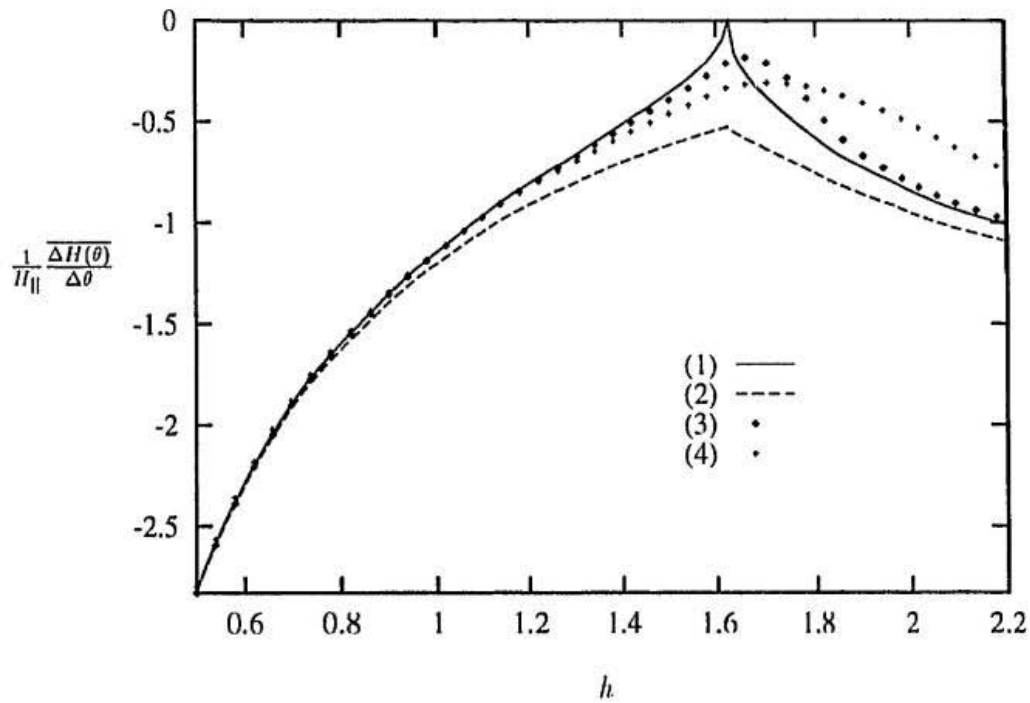

Figure 3.14: A plot of the effective slope defined by Eq. (3.110) for (3) $\Delta\theta = 1^{\circ}$ and (4) $\Delta\theta = 5^{\circ}$ in comparison with Thompson's result (1) from Eq. (3.74) and Saint-James' result (2) from Eq. (3.72).

instead exhibits a finite value whose magnitude increases as $\Delta\theta$ increases. This possible explanation of the discrepancy between experiment and theory is consistent with the fact that the angular resolution in Harper and Tinkham's experiments [69] is greater than that in the earlier work of Burger et al. [71] and that consequently the value of the slope at the cusp is smaller.

3.8 Conclusions

We have presented a calculation of the full angular dependence of the upper critical field using the de Gennes-Werthamer formalism, that is valid for both thin and thick films and includes the case of the semi-infinite geometry. It is also valid for all angles $0 < \theta < \pi/2$. The resultant curves for several values of the reduced field h are shown in Fig. 3.12.

It is shown that while the underlying eigenvalue problem differs qualitatively from that posed by the parallel field calculation, we nevertheless recover the upper critical field for the parallel field case in the limit $\theta \to 0$. The numerical results for the slope $\lim_{\theta\to 0} \frac{1}{H} \frac{\partial H}{\partial \theta}\Big|_T$ are consistent with the expression obtained by Thompson [24]. This predicts that the dependence of the slope $\lim_{\theta\to 0} \frac{1}{H} \frac{\partial H}{\partial \theta}\Big|_T$ on the reduced thickness h will exhibit a cusp at $h = h^* = 1.62$ with $\lim_{\theta\to 0} \frac{1}{H} \frac{\partial H}{\partial \theta}\Big|_T = 0$. This result contradicts the earlier work of Saint-James [21] .

While existing experimental studies indicate the presence of the cusp predicted by Thompson [24] and Saint-James [21], the observed slope remains finite [69], in contradiction with the result obtained by Thompson [24]. In the present work it is shown that for $h \approx h^*$ the precise experimental determination of the slope, $\frac{1}{H} \frac{\partial H}{\partial \theta}\Big|_T$, at $\theta = 0$ will be limited by the angular resolution of the measurements. It is suggested that this may account for the apparent discrepancy, and more careful and systematic experimental studies are required in order to distinguish between the

various theoretical predictions. In particular, it is important to establish whether the maximum value of the derivative $\lim_{\theta \to 0} \frac{1}{H} \left.\frac{\partial H}{\partial \theta}\right|_T$ is zero as predicted.

A comparison with previous theoretical work is given and it is shown that the results obtained for the full angular dependence are in good agreement with those of Tinkham for thin films and, for small angles, are in good qualitative agreement with Yamafuji et al. in the case of the semi-infinite geometry.

Finally we note that much of this work was motivated by our interest in the corresponding problem in the superlattice geometry. While the superlattice geometry represents a more technically difficult problem with a much wider range of phenomena than the case of the superconducting film, many of the problems that manifest themselves in the superlattice find a similar counterpart in the superconducting film. In particular it has been shown [56] that the result given by Eq. (3.74) for a superconducting film may be readily generalized to the superlattice geometry. A proper understanding of the problem posed by the superconducting film must be regarded as an essential precursor to a proper understanding of the corresponding problem in the superlattice geometry. This is particularly so given the nature of the inconsistencies that we have alluded to that exist within the current literature regarding the angular dependence of the upper critical field in a superconducting film.

Chapter 4

Upper Critical Field of a Superconducting Superlattice

There exists considerable theoretical and experimental interest in synthetically modulated materials consisting of alternating layers of metals, at least one of which is a superconductor. A number of such systems have been fabricated and studied. These include superlattice structures consisting of superconducting/normal metal layers [25, 73] and superconducting/ferromagnetic layers [45, 47, 74], as well as superlattices composed of alternating layers of superconducting materials with different bulk properties [37, 38, 39, 40, 75]. This new class of superconducting materials exhibits a wide range of intriguing phenomenon that provides a critical test of the current theoretical models of the proximity coupling in superconductivity. Of particular interest are effects that arise as a consequence of the coherence between the order parameter in the separate layers. Such effects can manifest themselves quite dramatically in the temperature dependence of the upper critical field.

Of the various proximity coupled superlattice structures that have been studied, the effect of an applied magnetic field is perhaps the most prominent in those in which the composite metals share the same bulk transition temperature, but which have different electron diffusion constants. In such systems, differences in the superconducting properties only become apparent in the presence of an applied magnetic field. At least two superlattice structures, Nb/NbTi and Nb/NbZr [37, 38, 39, 40, 75], are known to belong to this class of structures. Such systems have the additional advantage of being easier to understand theoretically. As we discussed in Section 2.5, the de Gennes theory reduces to the much simpler de

Gennes-Werthamer theory, if we can assume the composite metals share the same BCS coupling constant, density of states and Debye temperature.

Despite the simplicity of such systems, the temperature dependence of the upper critical field is known to exhibit a number of interesting features that arise as a consequence of the proximity effect. The most obvious is the rapid upturn in the parallel upper critical field curve that is observed close to T_c as the magnetic coherence length approaches the modulation length of the superlattice. This is generally referred to as the dimensional crossover from two to three dimensions, an effect first predicted and discussed for Josephson-coupled superlattices by Lawrence and Doniach [76]. More recently Takahashi and Tachiki [53] predicted that, for certain parameters, the upper critical field curve for such a system would exhibit a discontinuous slope. The origin of the discontinuity in the slope of the upper critical field lies in the effect of the superlattice geometry on the nucleation of the superconductivity. For sufficiently low values of H it is found that the superconductivity nucleate in a clean (N) layer. However for a certain range of parameters the nucleation switches to a dirty (S) layer when the field H exceeds a certain value H^*. It is this translation of the nucleation center that gives rise to the discontinuity in slope.

It should also be noted that experimental studies on other structures in which the bulk transition temperatures of the composite materials differ significantly (Nb/NbTa [32]) or which include a non superconducting component (V/Cu [77]) exhibit a similar feature at low temperature, indicating that the phenomenon predicted by Takahashi and Tachiki [53] may manifest itself in a wide variety of superlattice structures.

The phenomenon of surface superconductivity, discussed earlier in the context of homogeneous superconductors [19], also manifests itself in these layered systems. In such systems the location of the nucleation center is determined through the subtle

combination of the attractive nature of the free surface and the modulation induced by the multilamellar structure of the superlattice. This gives rise to a qualitatively different temperature dependence of H_{c3} than obtained in the case of the homogeneous superconductor discussed in the previous chapter. The de Gennes-Werthamer theory of the proximity effect predicts two distinct effects here. The first is that the upper critical field H_{c3} can be considerably larger than is the value calculated for a homogeneous superconductor and can exhibit a non-trivial temperature dependence. The second is that the upper critical field exhibits a sensitive dependence on the nature of the initial layer. Both these effects have been observed experimentally and provide a crucial test of the de Gennes-Werthamer theory of the proximity effect.

The layout of this chapter is as follows: In Section 4.1, the dimensional crossover induced by the modulation of a superlattice, predicted by Takahashi and Tachiki [53] will be studied in detail. Our theoretical calculation will be performed using a ratio of diffusion constants $D_{\rm Nb}/D_{\rm NbZr} = 0.2586$ and the layer thickness $d = d_{\rm Nb} = d_{\rm NbZr} = 250$ Å corresponding to an Nb/NbZr superlattice prepared by Kuwasawa et al. [38]. In this superlattice, we will show that the origin of the discontinuity in the temperature dependence of the upper critical field originates from a discontinuous translation of the nucleation center of the pair amplitude. For sufficiently low values of the applied field, the nucleation center of the pair amplitude at the transition temperature is located in the center of a clean N (Nb) layer. As the applied field H is increased beyond a certain value H^* the nucleation center shifts discontinuously to the center of a dirty S (NbZr) layer at temperature T^*. We then will show the one-to-one correspondence of the discontinuous translation of the nucleation center and the discontinuous slope in the temperature dependence of the upper critical field, $\frac{\partial H}{\partial T}\Big|_{H=H^*,T=T^*}$, through the application of the Werthamer equation, Eq. (3.8). The theoretical results obtained show good quantitative agreement with the experimental

data.

In Section 4.2, we will investigate the interplay of the surface effect [19] and the Takahashi-Tachiki effect [53] in a multilayer system, which will be modeled as a superlattice with one free surface, starting with either the N or the S component. It will be shown [50] that the location of the nucleation center and the resultant temperature dependence of the upper critical field in a layered structure are strongly affected by the presence of a free surface. This has significant implications for the interpretation of existing experimental data and suggests further work in this area. Similar conclusions have been arrived at independently by Aarts et al. on the basis of experimental studies [41, 78]. Their studies confirmed the principal results contained in our work, namely that the nature of the initial layer (i.e. N or S) significantly modifies the temperature dependence of the upper critical field.

In Section 4.3, detailed results from an investigation of the dependence of the surface effect on the various parameters will be presented. Our calculation for a superlattice with one free surface will cover a wide range of the ratio of the diffusion constants, $0.05 < D_S/D_N < 1$, while the layer thicknesses will be assumed to be equal. We will present a scaling law describing the relation between the modulation length of the sample and the critical value H^*, at which the slope of the upper critical field curve as a function of temperature is discontinuous.

A further quantitative examination of the effects of the insulating substrate on the temperature dependence of the upper critical field, for Nb/NbZr superlattices will be presented in Section 4.4. In particular we will show how differences between previous measurements [38, 39, 40] of the upper critical field on Nb/NbZr superlattice structures can be reconciled if surface effects are included. We also show how the experimental results of Maj and Aarts [41], which examine the effect on the upper critical field of varying the thickness of the initial layer can be accounted for

by the de Gennes-Werthamer theory of the proximity coupling. The analysis will show that the pair-breaking effect of the electron spin paramagnetism contributes significantly to the evaluation of the upper critical field at low temperatures.

4.1 Upper Critical Field for Infinite Superlattice

In this section, we wish to consider the superconducting transition temperature in an infinite superlattice in the presence of a homogeneous magnetic field applied parallel to the planes. The geometry is shown schematically in Fig. 4.1.

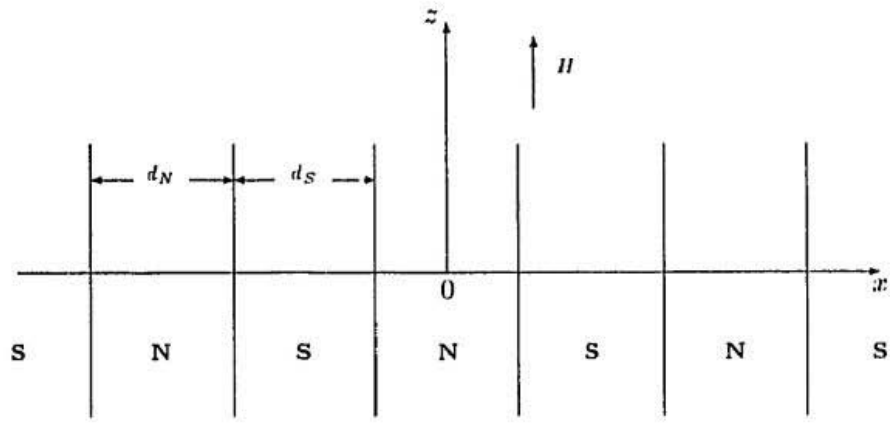

Figure 4.1: Parallel upper critical field applied to a superlattice. $T_{cS} = T_{cN}$ and $D_S \neq D_N$. $d = d_N = d_S$ denote the thicknesses for N and S layers, respectively.

We further assume that the superconducting materials, which we label N and S, share a common BCS coupling constant, density of states at the Fermi surface and Debye temperature. We assume, however, that the electron diffusion constant D is different in the two materials, with

$$D_S < D_N . \tag{4.1}$$

We denote the thickness of the S N layers by d_S and d_N, respectively.

As discussed previously in Section 2.5.4, the calculation of the transition temperature in a multilayer system reduces to the determination of the minimum eigenvalue given by Eq. (2.180),

$$h\,D_S\left(i\nabla-\frac{2\pi}{\phi_o}\mathbf{A}\right)^2\mathcal{F} \;=\; E_g\mathcal{F}, \qquad \mathbf{x}\in S, \tag{4.2}$$

$$h\,D_N\left(i\nabla-\frac{2\pi}{\phi_o}\mathbf{A}\right)^2\mathcal{F} \;=\; E_g\mathcal{F}, \qquad \mathbf{x}\in N, \tag{4.3}$$

subject to the continuity conditions

$$\begin{aligned} D_N\mathbf{n}\cdot\left(i\nabla-\frac{2\pi}{\phi_o}\mathbf{A}\right)\mathcal{F}(\mathbf{x}\in N) &= D_S\mathbf{n}\cdot\left(i\nabla-\frac{2\pi}{\phi_o}\mathbf{A}\right)\mathcal{F}(\mathbf{x}\in S), \\ \mathcal{F}(\mathbf{x}\in N) &= \mathcal{F}(\mathbf{x}\in S), \end{aligned} \tag{4.4}$$

at each of the interfaces.

We introduce dimensionless ratios

$$\rho=\frac{D_S}{D_N}, \tag{4.5}$$

and

$$\varepsilon_g=\frac{E_g}{hD_N}. \tag{4.6}$$

Eqs. (4.2), (4.3) and (4.4) then become

$$\rho\left(i\nabla-\frac{2\pi}{\phi_o}\mathbf{A}\right)^2\mathcal{F} \;=\; \varepsilon_g\mathcal{F}, \qquad \mathbf{x}\in S, \tag{4.7}$$

$$\left(i\nabla-\frac{2\pi}{\phi_o}\mathbf{A}\right)^2\mathcal{F} \;=\; \varepsilon_g\mathcal{F}, \qquad \mathbf{x}\in N, \tag{4.8}$$

with

$$\begin{aligned} \mathbf{n}\cdot\left(i\nabla-\frac{2\pi}{\phi_o}\mathbf{A}\right)\mathcal{F}(\mathbf{x}\in N) &= \rho\mathbf{n}\cdot\left(i\nabla-\frac{2\pi}{\phi_o}\mathbf{A}\right)\mathcal{F}(\mathbf{x}\in S), \\ \mathcal{F}(\mathbf{x}\in N) &= \mathcal{F}(\mathbf{x}\in S), \end{aligned} \tag{4.9}$$

at each of the interfaces.

The reduced transition temperature, $t = \frac{T}{T_c}$ is then given by the Werthamer relation

$$\chi\left(\xi_N^2 \frac{\varepsilon_g}{t}\right) + \ln(t) = 0\,, \tag{4.10}$$

where $\xi_N^2 = \frac{\hbar D_N}{2\pi k_B T_c}$. Choosing the London gauge, we have for the vector potential

$$\mathbf{A}(\mathbf{x}) = H(0, x, 0)\,. \tag{4.11}$$

We then introduce the dimensionless variables

$$x \to \frac{x}{\xi_H}\,, \qquad z \to \frac{z}{\xi_H}\,, \qquad y \to \frac{y}{\xi_H}\,, \tag{4.12}$$

where ξ_H is the magnetic coherence length defined by Eq. (3.11). We can write the order parameter in terms of these dimensionless coordinates as

$$\mathcal{F}(\mathbf{x}) = e^{ipz}\, e^{iky}\, f_{\lambda(k)}(x)\,, \quad \text{for} \quad x \in N, S\,, \tag{4.13}$$

where $f_{\lambda(k)}(x)$ satisfies the following differential equation (Weber Equation):

$$\rho\left[-\frac{d^2}{dx^2} + (x-k)^2\right] f_{\lambda(k)}(x) = \lambda(k)\, f_{\lambda(k)}(x)\,, \quad x \in S\,, \tag{4.14}$$

$$\left[-\frac{d^2}{dx^2} + (x-k)^2\right] f_{\lambda(k)}(x) = \lambda(k)\, f_{\lambda(k)}(x)\,, \quad x \in N\,, \tag{4.15}$$

with

$$\varepsilon_g = \xi_H^{-2}\left[\lambda(k) + p^2\right]\,. \tag{4.16}$$

From which it is clear that $p = 0$ is necessary to obtain the minimum eigenvalue.

The continuity condition at the interfaces given in Eq. (4.9) reduces to

$$\rho\,\frac{d}{dx} f_{\lambda(k)}(x_i) = \frac{d}{dx} f_{\lambda(k)}(x_i)\,, \quad f_{\lambda(k)}(x_i) = f_{\lambda(k)}(x_i)\,, \tag{4.17}$$

with x_i denoting the coordinate of i^{th} interface of the superlattice. The periodic nature of the superlattice geometry means that the eigenvalue spectrum is highly degenerate with

$$\lambda(k) = \lambda(k + \wedge/\xi_H)\,, \tag{4.18}$$

where $\wedge = (d_S + d_N)$ denotes the modulation length of the lattice in reduced units and

$$f_{\lambda(k+\wedge/\xi_H)}(x) = f_{\lambda(k)}(x - \wedge/\xi_H)\,. \tag{4.19}$$

Eqs. (4.14) and (4.15) together with the continuity condition specified by Eq. (4.17) provide a basis for the numerical calculation of the eigenvalue spectrum, $\lambda(k)$, for a wide class of superlattices specified by $0 < \rho \leq 1$. Since the eigenvalue spectra corresponding to different values of ρ show qualitatively similar structure, we present our numerical results only for $\rho = 0.2586$ and $d_S = d_N = 250$ Å, which corresponds to the Nb/NbZr multilayer system prepared by Kuwasawa et al. [38]. The purpose of choosing this superlattice model is to provide a quantitative comparison of the theoretical calculation with the experimental data.

A surface plot of the eigenvalue λ as a function of k and $a = \wedge/(2\xi_H) = d/\xi_H$ is shown in Fig. 4.2 for the wave number k crossing four NS cells. From this surface plot of the eigenvalue we find that for H sufficiently small (i.e. modulation length $\wedge \ll$ magnetic coherence length ξ_H), the detailed structure of the superlattice does not manifest itself in the functional dependence of the minimum eigenvalue λ^* on the parameter k. Instead what is observed is a flat line with a constant eigenvalue which can be evaluated in the limit $H \to 0$, (see Appendix C) as,

$$\lim_{H\to 0} \lambda^* = \sqrt{\rho} \tag{4.20}$$

This behavior is characteristic of an infinite homogeneous superconductor, with an effective electron diffusion constant $\sqrt{D_S D_N}$. However, as the applied field H is increased, the modulated structure of the superlattice is seen to manifest itself in the k dependence of λ. What we observe is a curve with multiple minima located at the centers of the N layers, reflecting the periodic nature of the superlattice. The fact that the nucleation center k^* switches over from the clean (N) layer to the dirty

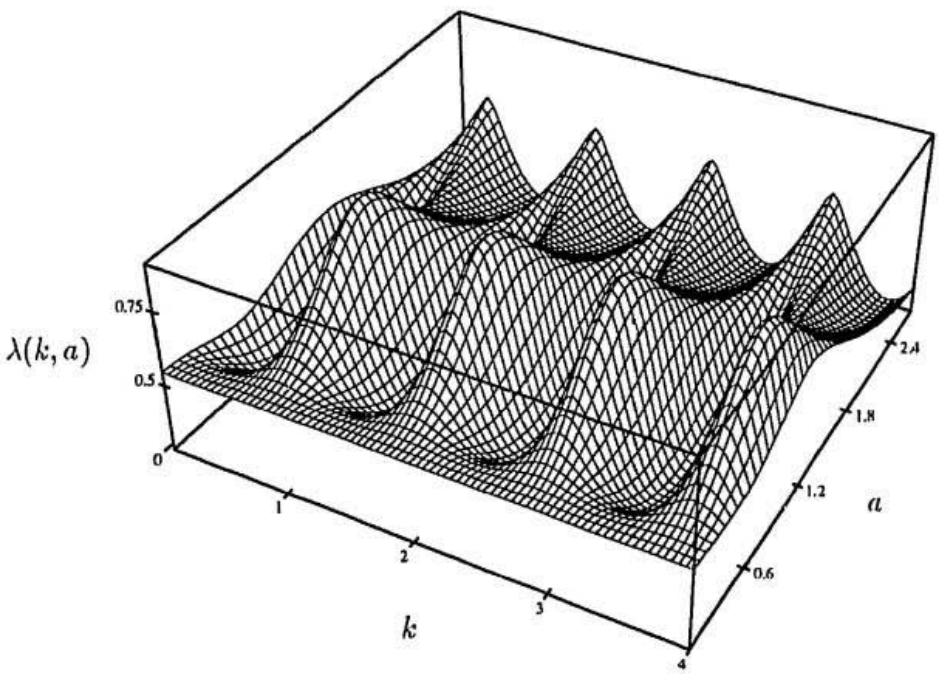

Figure 4.2: Surface plot of the eigenvalue spectrum, $\lambda(k,a)$, as a function of k and a for a superlattice geometry in parallel field case ($\rho = 0.2586$).

(S) layer with increasing magnetic field gives rise to a discontinuous slope in the dependence of $\lambda^*(a)$ on the reduced layer thickness a, as may be seen in Fig. 4.3(a). Substituting the minimum eigenvalue into the Werthamer equation, Eq. (4.10),

$$\chi\left(\frac{\xi_N^2}{\xi_{II}^2}\frac{\lambda^*}{t}\right) + \ln(t) = 0 \tag{4.21}$$

with t denoting the reduced temperature $\frac{T}{T_c}$, we obtain the temperature dependent upper critical field shown in Fig. 4.3(b). This figure clearly shows a discontinuity in the slope of the upper critical field $H_{||}$ corresponding to the discontinuity in slope of the minimum eigenvalue. This is the basis for the novel dimensional crossover behavior predicted by Takahashi and Tachiki [53] and subsequently confirmed experimentally [37, 38]. Nevertheless, we note that the determination of the temperature dependence of the upper critical field in a superlattice using the Werthamer equation, Eq. (4.10), depends explicitly upon the length scale $d = d_N = d_S$, while the minimum eigenvalue, λ^*, depends only on the reduced thickness $a = d/\xi_{II}$ for a given value of ρ. Therefore, to observe the dimensional crossover in the curve $H_{||}(t)$ for $t > 0$ for a given material (e. g. Nb/NbZr), one has to choose an appropriate layer thickness. For the samples prepared by Kuwasawa et al. [38], we can estimate the smallest layer thickness in terms of the asymptotic expansion of the χ function in the limit $T \to 0$ as

$$d_c \geq \xi_N \sqrt{2\, e^{\gamma} \lambda^* a^{*2}}\,, \tag{4.22}$$

where

$$\xi_N = \sqrt{\frac{\hbar D_N}{2\pi k_B T_c}} = \sqrt{\frac{4\phi_o}{2\pi^3 T_c}\left|\frac{dH}{dT}\right|^{-1}} = 0.514 \times 10^2\ \text{Å}\,, \tag{4.23}$$

with $T_c = 9.2$ K and $\left|\frac{dH}{dT}\right| = 0.550$ T/K, $\gamma = 0.5772$ is the Euler constant, $a^* = 2.015$ and $\lambda^* = 0.4757$. The resultant thickness is $d_c \approx 135$ Å. For a superlattice with layer thickness less than d_c, the dimensional crossover in the upper critical field is

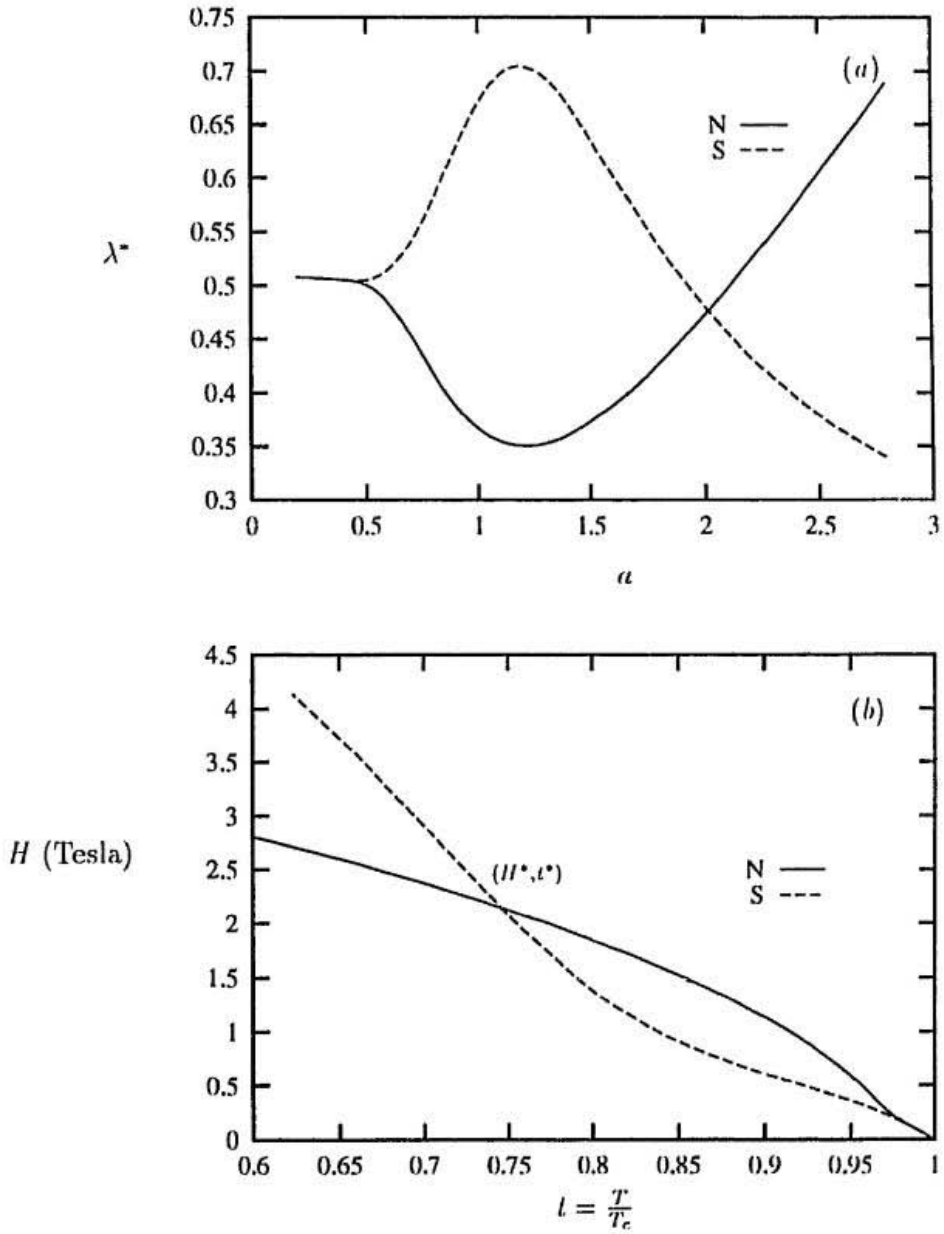

Figure 4.3: Fig. (a) shows the minimum eigenvalues found at the N and S centers, respectively. Fig. (b) shows the upper critical field, $H(T)$, and the dimensional crossover at (H^*, t^*). The higher field is defined as the upper critical field of the superlattice, $(\rho = 0.2586)$.

not observable for $t > 0$. This estimate is consistent with the experimental data in Ref. [38].

It needs to be emphasized that, in a multilayer system, the surface effect will dominate for sufficiently small H [50, 51], and the dimensional crossover observed in $H(T)$ may not correspond to the Takahashi-Tachiki effect. However, a model of the superlattice provides a simple geometry for the demonstration of the influence of the interfacial effect on $H(T)$. In the next section, we will show that the dimensional crossover will be significantly changed as the surface effect is included.

4.2 Surface Superconductivity in a Superconducting Superlattice

In the previous chapter we demonstrated how the phenomenon of surface superconductivity could be understood in terms of the location of the nucleation center at the free surface. Likewise in the previous section, we showed that the modulation of the superconducting properties of the superlattice could give rise to a discontinuous shift in the location of the nucleation center resulting in a discontinuity in the slope of the upper critical field. It is therefore interesting to explore the behavior of the nucleation center under the combined effect of a free surface and a modulation of the sample. More specifically, we ask how the phenomenon of surface superconductivity manifests itself in a multilamellar superconductor. In order to investigate the combined influence of the surface and interfacial effects, we extend our calculation to a semi-infinite superlattice geometry. The results of this calculation have appeared in two published papers [50, 51].

We apply the de Gennes-Werthamer theory to two multilamellar structures composed of N (clean) type and S (dirty) type superconductors as discussed in the previous section. In one structure, referred to as $NSN\cdots$, the initial layer (surface layer) is type N, while in the other, referred to as $SNS\cdots$, the initial layer is type

S. Both geometries are illustrated in Fig. 4.4.

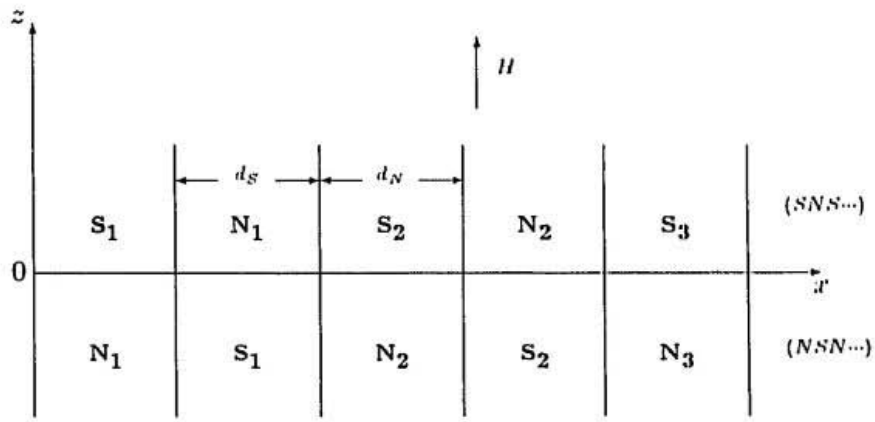

Figure 4.4: Parallel upper critical field applied to semi-infinite superlattices $(NSN\cdots)$ and $(SNS\cdots)$.

Of particular interest is the influence of competition between the surface effect and the modulation induced by the multilayer structure on the location of the nucleation site k^* and the eigenvalue $\lambda(k^*)$. The latter will determine the behavior of upper critical field $H_{\parallel}$ as a function of T. To best illustrate the modification of the temperature dependence of the upper critical field that results from the presence of a free surface we chose the parameter $\rho = 0.05$ and $d_N = d_S = d$. A more general discussion of the effects of varying the parameters ρ and d will be given in next section.

For the $(NSN\cdots)$ and $(SNS\cdots)$ structures, Eqs. (4.15) and (4.14) still hold in the N and S layers respectively. However, a surface boundary condition must be

added at $x = 0$:

$$\left.\frac{d}{dx} f_{\lambda(k)}(x-k)\right|_{x=0} = 0\,, \qquad \lim_{x\to+\infty} f_{\lambda(k)}(x-k) \to 0\,. \tag{4.24}$$

Surface plots of the eigenvalue spectrum obtained from solving the Eqs.(4.15) and (4.14) together with the newly added boundary condition (4.24) are shown in Figs. 4.5 and 4.6. The surface plots shown in Fig. 4.5 and 4.6 share a number of qualitatively similar features. In particular we find that for sufficiently small H ($\Lambda \ll \xi_H$), the detailed structure of the semi-infinite superlattice does not manifest itself in the functional dependence of the minimum eigenvalue $\lambda(k)$ on the parameter k. Instead what is observed is a smooth curve with a single minimum. The position of the minimum, k^*, and the corresponding eigenvalue, λ^*, can be evaluated in the limit $H \to 0$ (see Appendix C) as

$$\lim_{H\to 0} k^* = \sqrt{\frac{0.59010\sqrt{\rho}\,(1+\rho)}{2}}\,, \tag{4.25}$$

$$\lim_{H\to 0} \lambda^* = 0.59010\sqrt{\rho}\,, \tag{4.26}$$

This behavior is characteristic of the semi-infinite homogeneous superconductor discussed in the previous chapter, with an effective electron diffusion constant $\sqrt{D_S D_N}$. The effect of the minimum of $\lambda(k)$, induced by the presence of the free surface, is to enhance the critical field, giving rise the phenomenon of surface superconductivity [66] discussed earlier.

This rather simple behavior disappears, however, as the applied field H is increased, and the modulated structure of the superlattice is seen to manifest itself in the k dependence of the eigenvalue $\lambda(k)$. For $\Lambda \gg \xi_H$, the modulation gives rise to multiple minima located either close to the center of the clean N layers or, with increasing magnetic field, H, close to the center of the dirty S layers. Except for in the initial layer, the effect of the free surface is negligible and the dependence of the smallest eigenvalue on the wave number k^* is dominated by the modulation of the

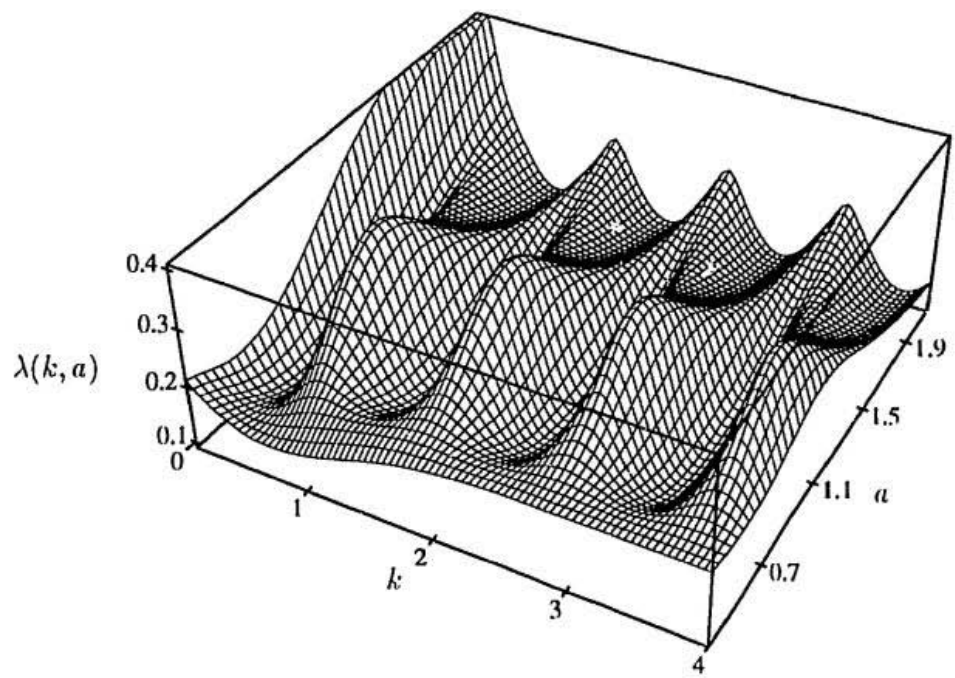

Figure 4.5: Surface plot of the eigenvalue spectrum, $\lambda(k,a)$, as a function of k and a for a $NSN\cdots$ geomrtry in parallel field case ($\rho = 0.05$). $H_{c3N1} \rightarrow H_{c2N} \rightarrow H_{c2S}$.

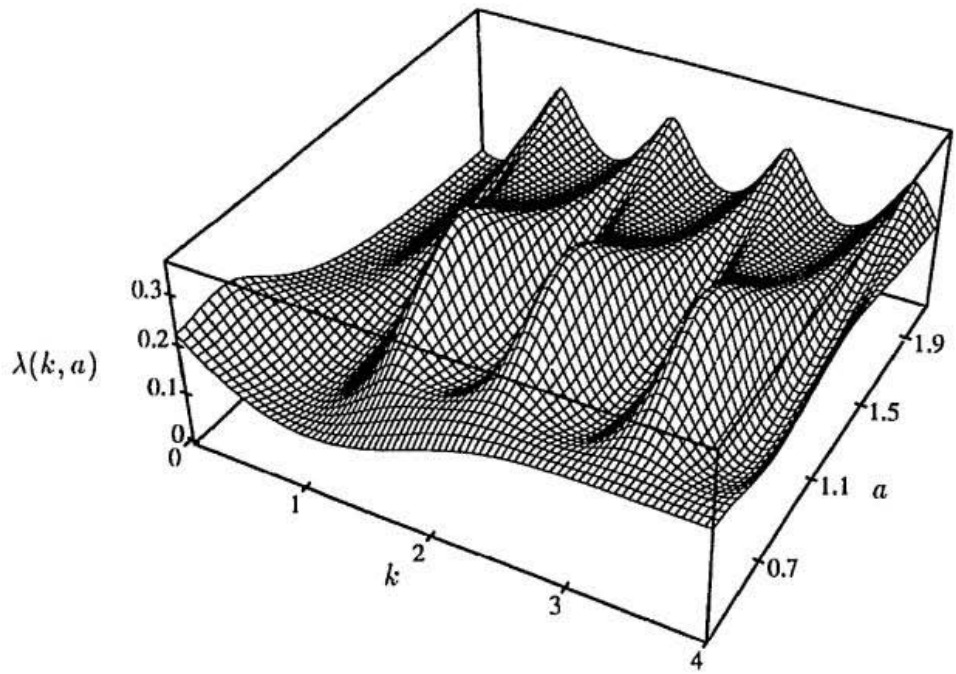

Figure 4.6: Surface plot of the eigenvalue spectrum, $\lambda(k, a)$, as a function of k and a for a $SNS\cdots$ geomrtry in parallel field case ($\rho = 0.05$). $H_{c3N2} \rightarrow H_{c3S1}$.

geometry, similar to what was found in the superlattice case discussed in the previous section.

More interesting, and indeed the substance of the present work, is the modification of the functional dependence of the eigenvalue $\lambda(k)$ on the parameter k due to the presence of the free surface in this particular regime (i.e., $\Lambda \gtrsim \xi_H$) and the corresponding values of k^* and λ^* obtained. In particular we find, not surprisingly, that in the case of the semi-infinite geometry we must distinguish between the eigenvalue spectrum shown in Fig. 4.5, obtained from the case in which the first layer is clean $(NSN\cdots)$ (see Fig. 4.4), and that shown in Fig. 4.6, obtained from the case in which the first layer is dirty $(SNS\cdots)$ (see Fig. 4.4). In the case of the former, the result obtained in the $(NSN\cdots)$ geometry shows that as $\lambda(k)$ begins to develop multiple minima with increasing magnetic field, the nucleation center is located in the first layer denoted by N_1. As the magnetic field H is increased further the nucleation center then shifts to one of the interior N layers and multiple minima with nearly degenerate eigenvalues appear. Thus we observe a crossover from nucleation at the surface to nucleation in the "bulk" of the sample. This gives rise to the very shallow discontinuity in the slope of the curve λ^* vs. H, shown in Fig. 4.7(a), in comparison with the curve for λ^* which results from a superlattice geometry.

As the magnetic field is increased further, the nucleation centers shift to the dirty S layers, giving rise to a second discontinuity in the slope of the curve λ^* vs H. The resultant critical field curve is presented in Fig. 4.7(b) and shows the effect of the two successive shifts in the nucleation center. For the particular parameters considered here, the first shift in the nucleation center at the crossover from surface nucleation to nucleation in bulk has very little quantitative effect on the calculated upper critical field curve. Nevertheless, Maj and Aarts [41] reported that a small kink qualitatively similar to that obtained from the our theoretical calculation, was

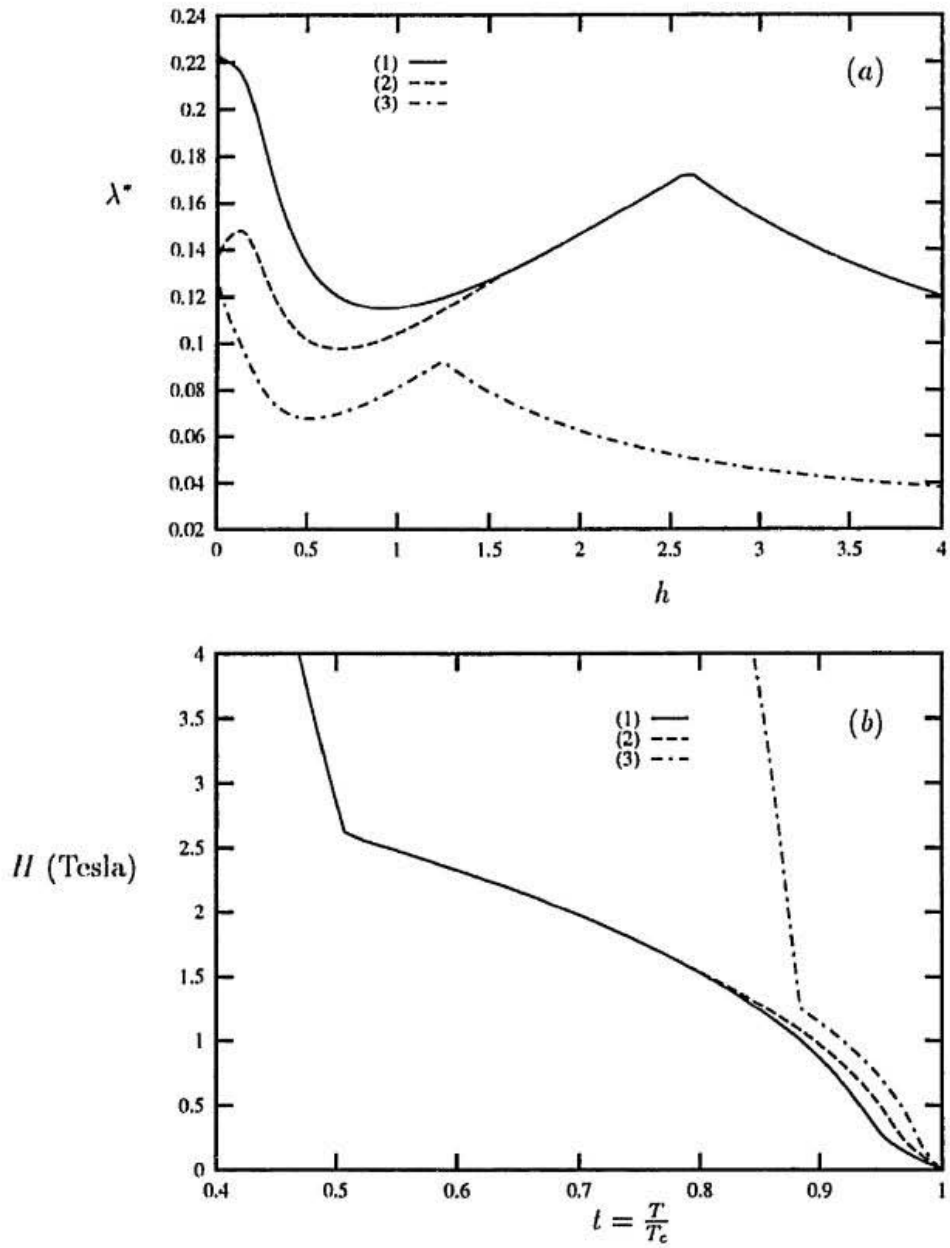

Figure 4.7: The minimum eigenvalues λ^* as a function of the applied magnetic field, for the superlattice(1) and the semi-infinite $(NSN\cdots)$(2) and $(SNS\cdots)$(3) geometries for $\rho = 0.05$ are shown in (a). The corresponding upper critical field as a function of t for the three geometries are shown in (b).

found in their experimental measurement.

In the case of the $(SNS\cdots)$ geometry, Fig. 4.6, we find that, as $\lambda(k)$ begins to develop multiple minima with increasing magnetic field H, the nucleation center k^* occurs in the N_1 layer. As the applied magnetic field is increased the nucleation center shifts from the N_1 layer to one of the interior S layers. However, due to the effect of the free surface, the shift in the nucleation center occurs at a much lower value of H than in either the $(NSN\cdots)$ geometry or the infinite superlattice geometry. The resultant critical field curves for $\rho = 0.05$ are shown in Fig. 4.7(b) and show that the discontinuity in the upper critical field curve occurs at a much lower value than in the corresponding $(NSN\cdots)$ geometry and the infinite superlattice geometry.

We have examined the effect of a free boundary on the upper critical field of a superconducting superlattice consisting of alternating layers with a particular ratio of electron diffusion constants ($\rho = 0.05$). For the parameter values studied, we find that in the $(NSN\cdots)$ geometry, in which the initial layer is a clean (N) layer, the upper critical field is very close to the value obtained for an infinite superlattice, and hence $H_{c2} \sim H_{c3}$. In particular, the temperature at which the discontinuity in the slope in the upper critical field occurs is relatively insensitive to the presence of the free surface. This is consistent with claims made in the literature regarding the interpretation of the experimental data [39, 40, 38]. Perhaps more interestingly, we find that in the case of the $(SNS\cdots)$ geometry, in which the initial layer is a dirty (S) layer, the upper critical field deviates significantly from the value calculated in the case of the infinite superconductor, and hence $H_{c3} > H_{c2}$.

We find that the surface effect is crucial in determining the site of the nucleation center, k^*, and thus the dimensional crossover in the temperature dependence of

the upper critical field. This is best demonstrated by the significant deviation between the two curves for the upper critical field $H(T)$ in the $NSN\cdots$ and $SNS\cdots$ geometries, shown in Fig. 4.7(b). This theoretical prediction has been confirmed experimentally by Maj and Aarts [41]. It should be noted that in determining the temperature dependence of the upper critical field from the minimum eigenvalue using the Werthamer equation, Eq. (4.10), a length scale given by the layer thickness d is included, as demonstrated in the previous section. This means that the temperature dependence of the upper critical field would change with the layer thickness. In our calculation, however, we used the same layer thickness for all these geometries, so the significant difference in the upper critical field between $SNS\cdots$ geometry and the superlattice and $NSN\cdots$ geometries, shown in Fig. 4.7(b), can only be due to the existence of the free surface.

4.3 Geometry and the Scaling Hypothesis

An important experimental test of the preceding arguments lies in the fact that the magnetic field is introduced into the theory only through the magnetic coherence length ξ_H. This implies that the shift in the nucleation site and the subsequent upturn in the upper critical field occur when

$$\frac{\Lambda}{\xi_H^*} = \mathcal{U}\left(\sigma = \frac{d_S}{d_N}, \rho = \frac{D_S}{D_N}\right) = const., \tag{4.27}$$

where $\Lambda = d_N + d_S$ denotes the modulation length. This in turn implies that, if the ratios σ and ρ remain fixed, then the value of the magnetic field at which this shift occurs is inversely proportional to the square of the modulation length

$$H^* \propto \frac{1}{\Lambda^2}, \tag{4.28}$$

where the constant of proportionality may be expressed in terms of the function $\mathcal{U}$ calculated for the appropriate values of σ and ρ. The occurrence of a shift in the nucleation center is, however, a necessary but not a sufficient condition for the appearance of a discontinuity in the slope of the upper critical field curve. The appearance of this discontinuity also requires that the temperature obtained from Eq. (4.10), corresponding to the eigenvalue λ^* at which the shift in the nucleation center occurs, is greater than zero. Taking the limit $T \to 0$ of Eq. (4.10), this reduces to the requirement that the modulation length Λ satisfy the inequality

$$\left(\frac{\xi_H^*}{\xi_N}\right)^2 \leq 2e^{\gamma}\lambda^* \tag{4.29}$$

where $\gamma = 0.5772$ is the Euler constant, $\xi_N = \sqrt{\hbar D_N / 2\pi k_B T_c}$, and λ^* and ξ_H^* refer to the value of the minimum eigenvalue and magnetic coherence length at which the shift in the nucleation center occurs. The latter quantities depend only on the dimensionless ratios ρ and σ and the particular geometry considered.

It should be noted that the above scaling law has a wider range of applicability than the simple superlattice geometry. Provided the composite alloys share the same bulk transition temperature, the field at which any discontinuous shift in the nucleation center induced by the spatial inhomogeneity occurs may be characterised by a similar scaling law, with Λ denoting the characteristic length scale associated with the particular geometry.

The material properties assumed in the preceding analysis have been realised to a good approximation in both Nb/NbTi [37] and Nb/NbZr [38, 39, 40, 41, 75] superlattices. Both systems exhibit a discontinuous upturn in the upper critical field that is at least in qualitative agreement with the prediction of Takahashi and Tachiki [53]. In Fig. 4.8 we plot the value of H at which the upturn is observed as a function of $\phi_0/2\pi\Lambda^2$ for three sets of data [37, 38, 40], all of which show a linear behavior consistent with the scaling law, Eq. (4.28). The values obtained for the slopes are given in Table 4.1.

Material	Reference	$(\frac{\Lambda^2}{\xi_{II}^{*2}})$
Nb/NbTi	[37]	24.5
Nb/NbZr	[40]	16.2
Nb/NbZr	[38]	6.7

Table 4.1: The value of Λ^2/ξ_{II}^{*2} at which the discontinuity in the temperature dependence of the upper critical field is observed.

In Fig. 4.9 we show the dependence of $\mathcal{U}$ on the ratio ρ for $\sigma = 1$, together with the values obtained from the data on Nb/NbZr superlattices in Refs. [38, 40].

One striking aspect of the experimental data summarized in Table 4.1 is the difference between the two values found for the Nb/NbZr superlattice structures.

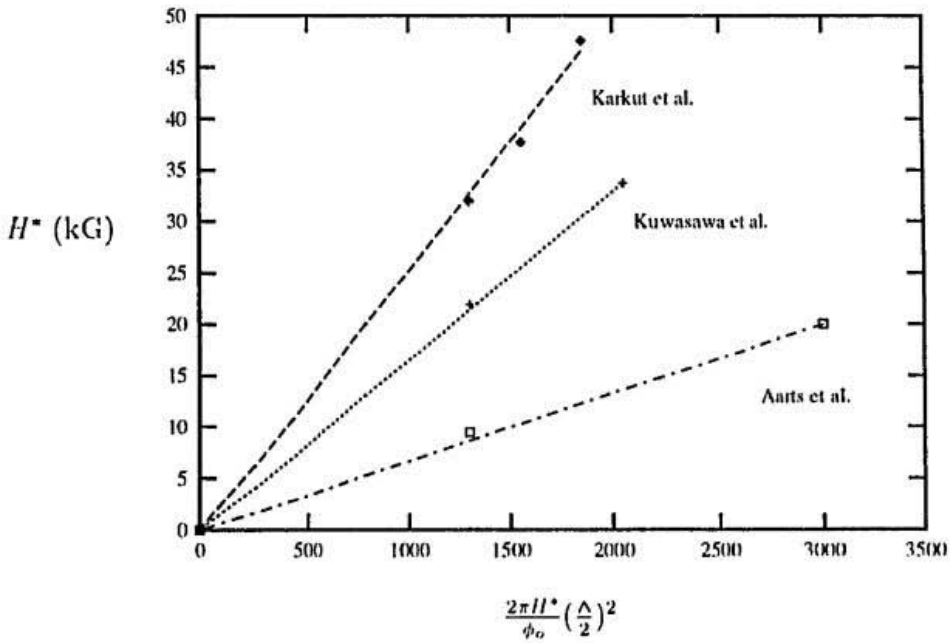

Figure 4.8: Plot showing the observed value of applied field H^*, at which the slope of the upper critical field exhibits a discontinuity.

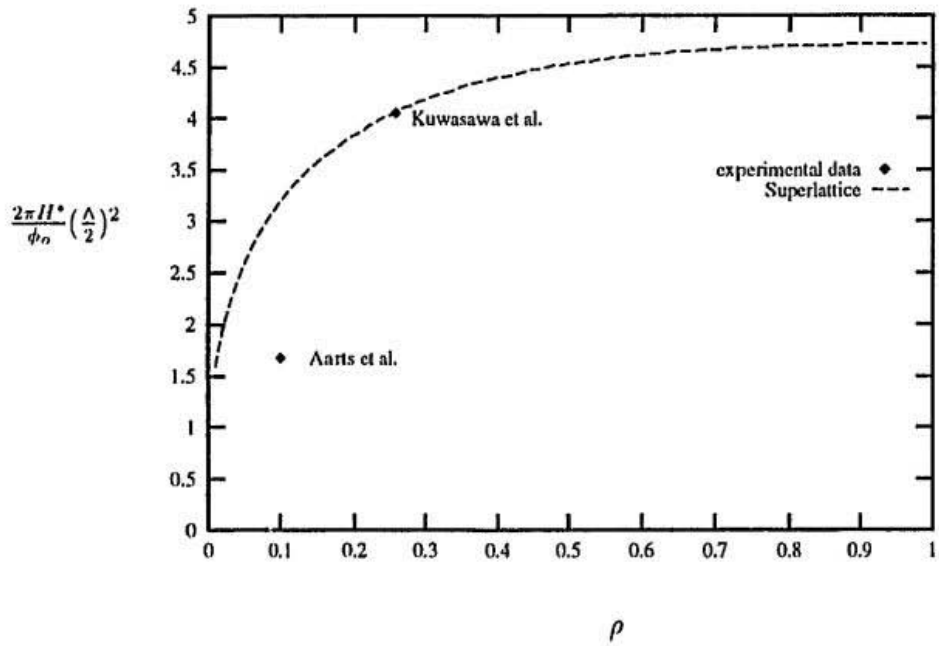

Figure 4.9: Plot showing the value of $\mathcal{U} = \frac{2\pi H^*}{\phi_o}(\frac{\Delta}{2})^2$ calculated for the superlattice as a function of ρ. Also shown are the two experimental points listed in Table (4.1).

While it should noted that the data sets correspond to different values of σ and a slightly different value of the composition in the NbZr layers, the main difference lies in the fact that in Ref. [38] the superlattice was deposited with an initial Nb layer, (an N layer in our terminology), while in Ref. [40], the superlattice was deposited with an initial NbZr layer, (an S layer in our terminology). To see this we draw what may be regarded as a phase diagram for the two semi-infinite superlattice geometries, $NSN\cdots$ (upper portion) and $SNS\cdots$ (lower portion), in Fig. 4.10. The lines indicate the values of $\frac{2\pi H^*}{\phi_o}(\frac{\Delta}{2})^2$ at which a shift in the nucleation center takes place as the applied field is increased at a fixed value of ρ.

In the $NSN\cdots$ case the nucleation center moves continuously towards the free surface as the applied field is increased until it reaches the first layer (N_1). For $\rho > 0.08$ the nucleation center remains in N_1 until the applied field exceeds a certain value whereupon it shifts discontinuously to the center of one of the interior S layers. This discontinuous shift in the nucleation center gives rise to a discontinuity in the slope of the upper critical field, which may be denoted as $H_{c3N1} \rightarrow H_{c2S}$. For $\rho < 0.08$ the situation is slightly more complicated in that, when the field reaches a certain value, the nucleation center shifts first to the center of one of the interior N layers and, as the field is further increased, the nucleation center shifts again to the center of one of the interior S layers. This results in an additional shallow discontinuity in the slope of the upper critical field, discussed in the previous section. The value of $\Lambda^2/{\xi_H^*}^2$ at which the shift in the nucleation center occurs is shown in Fig. 4.10 for $\sigma = d_S/d_N = 1$, as a function of ρ.

Note that for $\rho < 0.08$ there are two branches corresponding to the shift from the first layer (N_1) to the center of one of the interior N layers, the lower branch ($H_{c3N1} \rightarrow H_{c2N}$), and from the centers of N layers to the centers of S layers, the upper branch ($H_{c2N} \rightarrow H_{c2S}$). This last case is analogous to the effect predicted by

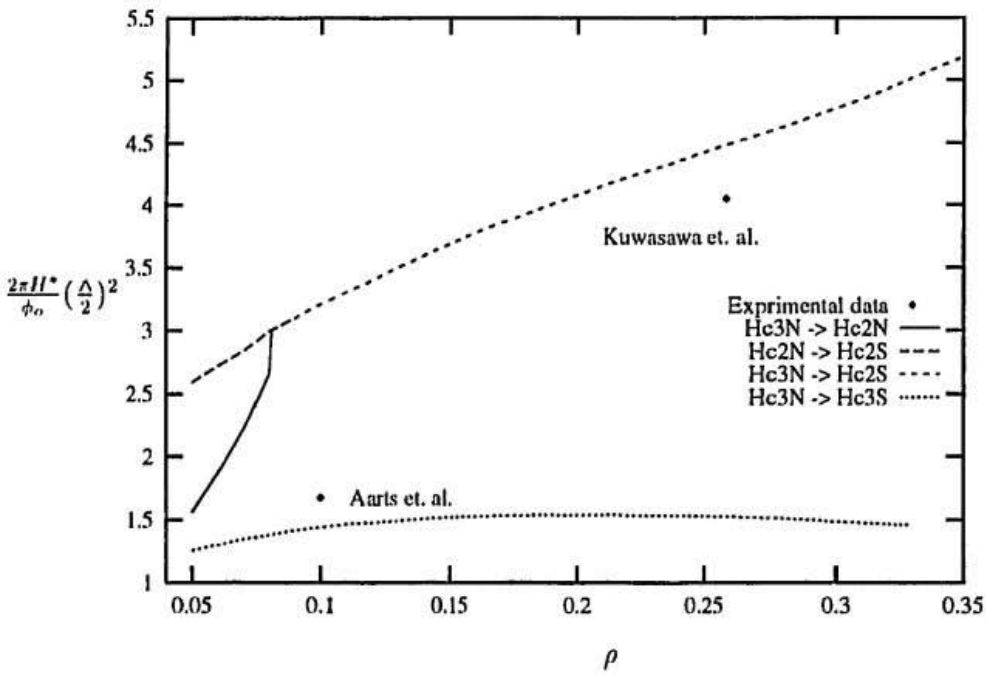

Figure 4.10: Plot of $\frac{2\pi H^*}{\phi_o}(\frac{\Delta}{2})^2$ at which the nucleation center shifts discontinuously, plotted as a function of ρ for both the $NSN\cdots$ and the $SNS\cdots$ geometries with $\sigma = d_s/d_n = 1$. $\diamond$ represents the experimental data.

Takahashi and Tachiki in the case of a superlattice.

In the case of the $SNS\cdots$ geometry, the nucleation center again moves continuously towards the free surface with increasing applied field, until it reaches the second layer (N_1). When the applied field reaches a certain value the nucleation center shifts to the first layer (S_1), producing a discontinuity in the slope of the upper critical field curve ($H_{c3N1} \rightarrow H_{c3S1}$). While this resembles the corresponding shift in the case of the infinite superlattice, the shift in the nucleation center appears at a much higher temperature and persists over a much wider range of parameters. Also included in Fig. 4.10 are the values given in Table 4.1 for the Nb/NbZr superlattices. The comparison indicates that indeed the difference between the two data sets can be largely accounted for by the fact that the two samples differ in the nature of the initial layer.

While the preceding comparison of the different measurements of the upper critical field of Nb/NbZr superlattices offers convincing evidence for the importance of surface effects in the determination of the upper critical field in layered structures, more direct evidence is provided by more recent experiments in which the upper critical field is measured for Nb/NbZr superlattice structures that differ only in the order in which the layers are grown onto the substrate [78]. The results obtained from these experiments confirm the predictions of our earlier work [50], and demonstrate quite clearly the importance of surface effects in layered superconductors.

4.4 Dependence of the Upper Critical Field on Initial Layer

Recent measurements of the parallel upper critical field of Nb/NbZr superlattice structures, in which the thickness of the first layer is varied in a systematic manner [41], show a dramatic dependence on the thickness and type (i.e., N or S) of the initial layer. These experiments not only serve to emphasize the crucial importance

of the character of the initial layer in the determination of the upper critical field, but also provide an excellent basis for a quantitative test of the application of the de Gennes-Werthamer theory of the proximity effect to superlattice structures [36, 42].

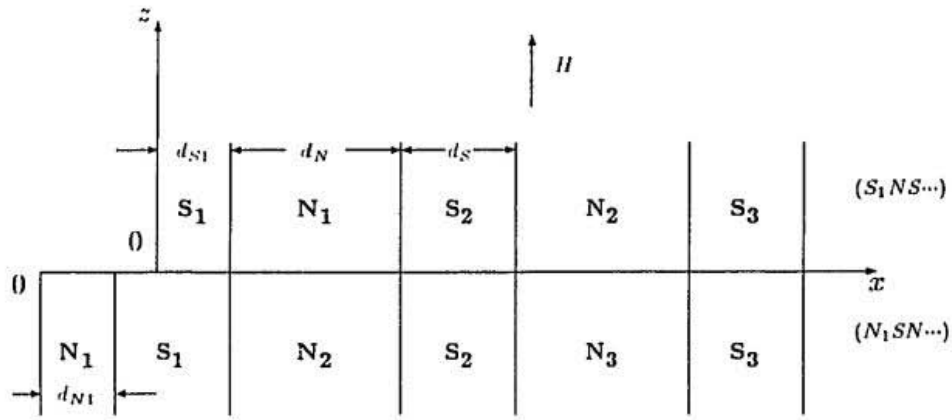

Figure 4.11: Illustration of the geometry corresponding to Maj and Aarts' experiments. $d_N = 240$ Å, $d_S = 165$ Å and $\rho = 0.1$

In order to compare the results of the de Gennes-Werthamer theory with the experimental results contained in Ref. [41], we consider two semi-infinite superlattices consisting of alternating layers of different superconducting metals. In one case we consider an initial N layer ($N_1SN\cdots$ geometry) in the other we consider an initial S layer ($S_1NS\ldots$ geometry). As in the previous discussion, both metals are assumed to have the same superconducting transition temperature in the bulk, but have different electron diffusion constants. The thicknesses of the layers are assumed constant, for all but the initial layer, and are denoted by d_N and d_S for the N and S layers respectively, as shown schematically in Fig. 4.11. The thickness of the initial layer we denote by d_{N1} and d_{S1} for the ($N_1SN\ldots$) and the ($S_1NS\ldots$) geometries respectively. The material parameters used in the calculation are chosen

to correspond to those used in the experimental studies described in Ref. [41]. We take the ratio $\sigma = d_S/d_N = 165/240$. The value of D_N is determined from the measurements of $dH_\perp/dT|_{T=T_c}$ on a single Nb layer (2,000Å), while the bulk transition temperature is $T_c = 9.2$ K. Results for a value of the ratio $\rho = 0.1$ are presented, however, calculations for several other values of ρ were performed.

In Fig. 4.12 we present the calculated temperature dependence of the upper critical field for $d_{S1} = d_S$, $0.75d_S$, $0.5d_S$ and $0.25d_S$. The corresponding curves are denoted by $S(1)NS\cdots$, $S(3/4)NS\cdots$, $S(1/2)NS\cdots$ and $S(1/4)NS\cdots$ respectively. Also included is the curve obtained for the $N_1SN\cdots$ geometry with $d_{N1} = d_N$. A comparison of the calculated results shown in Fig. 4.12 with the corresponding experimental results given in Ref. [41] indicates that the preceding analysis provides a good qualitative account of the temperature dependence of the upper critical field. In particular we see that T^*, where T^* denotes the temperature at which the shift in the nucleation center occurs, is reduced for decreasing values of the thickness d_{S1}, and that for $T > T^*$ the temperature dependence of the upper critical field is little affected by the thickness of the first layer. Roughly speaking, this result may be understood as resulting from the fact that, for $T > T^*$, the nucleation center is located in the second layer and the presence of the free surface has little effect on the value of the eigenvalue. On the other hand, for $T < T^*$ the nucleation center is located in the first layer, where the value of the eigenvalue is strongly dependent on the presence of the free surface. The temperature dependence of the upper critical field consequently exhibits a strong dependence on the thickness of the initial layer.

It is also interesting to note that there is no discontinuity in the slope of the upper critical field curve for the $S(1/2)NS\cdots$ geometry. Instead there is a continuous, but rapid, increase in the slope around $t = 0.55$, reflecting the fact that the nucleation center moves continuously from N_1 layer to the initial S_1 layer as the applied field

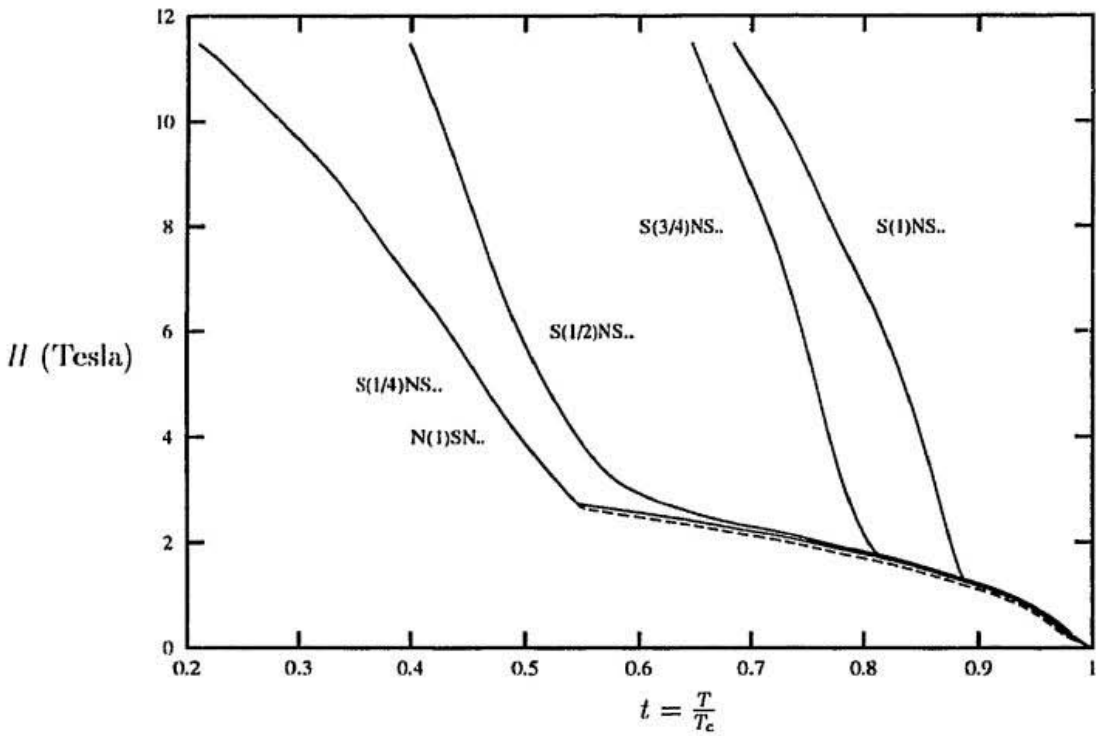

Figure 4.12: The upper critical field as a function of temperature for the $SNS\cdots$ geometry for $d_{S1} = d_S, 0.75d_S, 0.5d_S$, and $0.25d_S$. The dashed line is the upper critical field calculated for the $N(1)SN$ geometry.

H is increased.

In Fig. 4.13 we present the calculated temperature dependence of the upper critical field for the $N_1SN\cdots$ geometry, with $d_{N1} = d_N$, $0.75d_N$, $0.5d_N$ and $0.25d_N$. The corresponding curves are denoted by $N(1)SN\cdots$, $N(3/4)SN\cdots$, $N(1/2)SN\cdots$ and $N(1/4)SN\cdots$ respectively. Also included is the curve obtained for the $S_1NS\cdots$ geometry with $d_{S1} = d_S$. The qualitative character of the curves may be understood in terms of the dependence of the nucleation center k^* on the applied field H and the reduced temperature $t = T/T_c$. For the $N(1)SN\cdots$ and $N(3/4)SN\cdots$ geometries the nucleation center moves continuously towards the free surface with decreasing temperature, until it reaches the first layer (N_1). The nucleation center remains in the first layer (N_1) until $T = T^*$ whereupon it shifts to the second layer (S_1), with $T^*/T_c = 0.55$ and 0.5 for the $N(1)SN\cdots$ and the $N(3/4)SN\cdots$ geometries respectively. For the $N(1/2)SN\cdots$ geometry the nucleation center does not move continuously towards the free surface with decreasing temperature but is "trapped" in the second layer (S_1) until it jumps to the first layer (N_1) at $t = 0.96$. As the temperature is further reduced the nucleation center shifts from the first layer (N_1) to the second layer (S_1) at $T = T^* = 0.45T_c$. Similarly with the $N(1/4)SN\cdots$ geometry the nucleation center does not shift continuously towards the surface but is "trapped" in the third layer (N_2) close to the interface with the second layer (S_1) until it jumps to the first layer (N_1) as the temperature is further reduced, where it remains as the temperature is reduced to zero.

One striking feature of the above analysis is the sensitivity of the location of the nucleation center, and consequently the temperature dependence of the upper critical field, on the boundary condition at the surface of the superlattice and the detailed nature of the geometry considered. That such a sensitivity has some basis in reality, and is not simply an artifact of the formalism used in the analysis, is

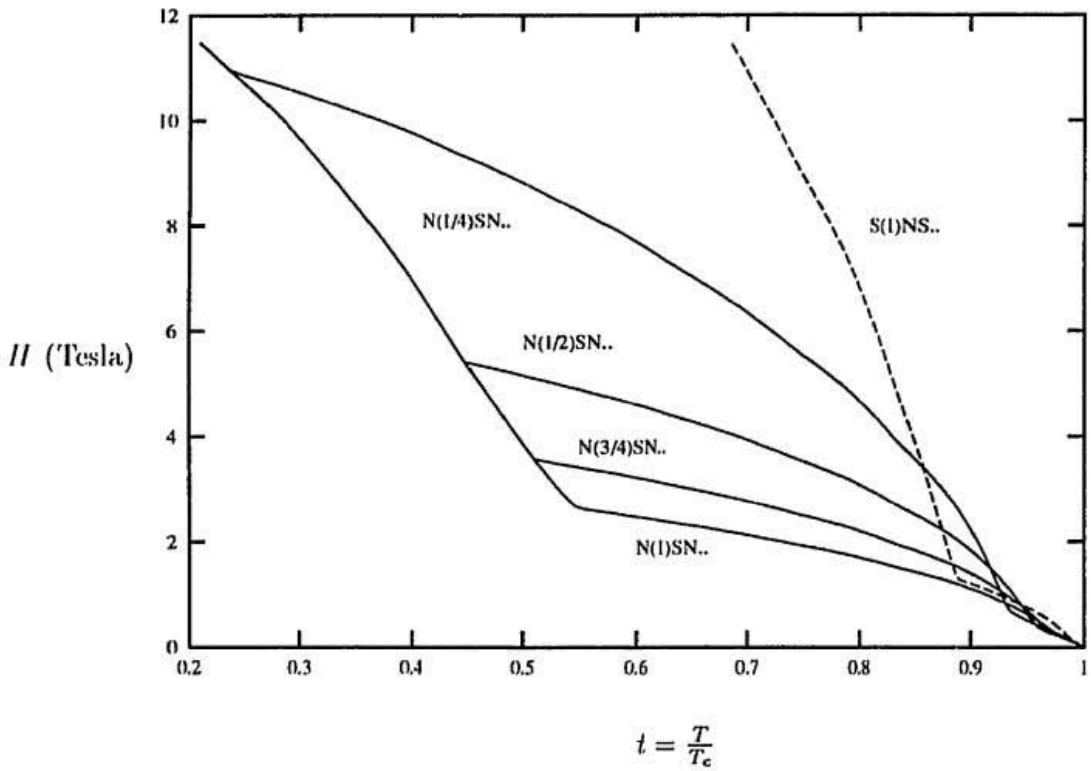

Figure 4.13: The upper critical field as a function of temperature for the $NSN\cdots$ geometry for $d_{N1} = d_N, 0.75d_N, 0.5d_N$, and $0.25d_N$. The dashed line is the upper critical field calculated for the $S(1)NS$ geometry.

supported by the fact that the results shown in Figs. 4.12 and 4.13 provide a good qualitative account of the corresponding experimental results presented in Ref. [41]. This indicates that the subtle geometric effects manifested within the de Gennes-Werthamer theory are at least consistent with observation. Similarly with the $N(1/4)SN\cdots$ geometry the nucleation center does not shift continuously towards the surface but is "trapped" in the third layer (N_2) close to the interface with the second layer (S_1) until it jumps to the first layer (N_1) as the temperature is further reduced, where it remains as the temperature is reduced to zero.

One striking feature of the above analysis is the sensitivity of the location of the nucleation center, and consequently the temperature dependence of the upper critical field, on the boundary condition at the surface of the superlattice and the detailed nature of the geometry considered. That such a sensitivity has some basis in reality, and is not simply an artifact of the formalism used in the analysis, is supported by the fact that the calculated results obtained from the present analysis shown in Figs. 4.12 and 4.13 provide a good qualitative account of the corresponding experimental results given in Ref. [41]. This indicates that the subtle geometric effects manifested within the de Gennes-Werthamer theory are at least consistent with observation.

4.5 Effect of Spin Paramagnetism

For the particular choice of parameters used in the preceding analysis we find the zero temperature critical field to be substantially higher than the observed value for all the geometries considered. While a lower value of the upper critical field may be obtained by modifying the parameters used in the analysis, this results in other discrepancies between the observed data and the calculated upper critical field curves.

The large value of the critical field at low temperatures suggests that pair breaking effects induced by the electron spin paramagnetism may substantially modify the results of the preceding analysis. In fact, the upper critical field at low temperatures is comparable with the paramagnetic limiting field at $T = 0$, which is given by [79, 80]

$$H_p(0) \approx 2.5 \frac{k_B T_c}{g\mu_B} = 18.57\,\text{Tesla}\,. \tag{4.30}$$

This indicates that the polarization energy of the electrons is a substantial fraction of the condensation energy.

A general theory including spin paramagnetism and spin-orbit impurity scattering, developed by Maki [10, 67] and Werthamer [81] in the dirty limit, has been extended to the case of spatially modulated systems [36, 42]. Neglecting the effect of spin orbit scattering, the effect of spin paramagnetism may be included in the preceding analysis by replacing the expression for the transition temperature given by Eq. (4.10) by the relation

$$\tilde{\chi}\left(\frac{\varepsilon}{2\pi k_B T} + i\frac{\mu_B H_{\|}}{\pi k_B T}\right) + \ln t = 0\,, \tag{4.31}$$

where $\tilde{\chi}$ is defined as

$$\tilde{\chi}(z) = \Re\left[\psi(\frac{1}{2} - \frac{1}{2}z) - \psi(\frac{1}{2})\right]. \tag{4.32}$$

The results of calculations including the effect of electron spin paramagnetism on the $(N_1SN\cdots)$ and $(S_1NS\cdots)$ geometries, for $\rho = 0.1$, are shown in Figs. 4.14 and 4.15 respectively. While the results obtained including electron spin paramagnetism are qualitatively similar to those presented in the previous section, the effect of the spin paramagnetism nevertheless leads to significant quantitative modification of the upper critical field curves, particularly at low temperature. The resultant upper critical field curves are also in excellent agreement with experimental data presented

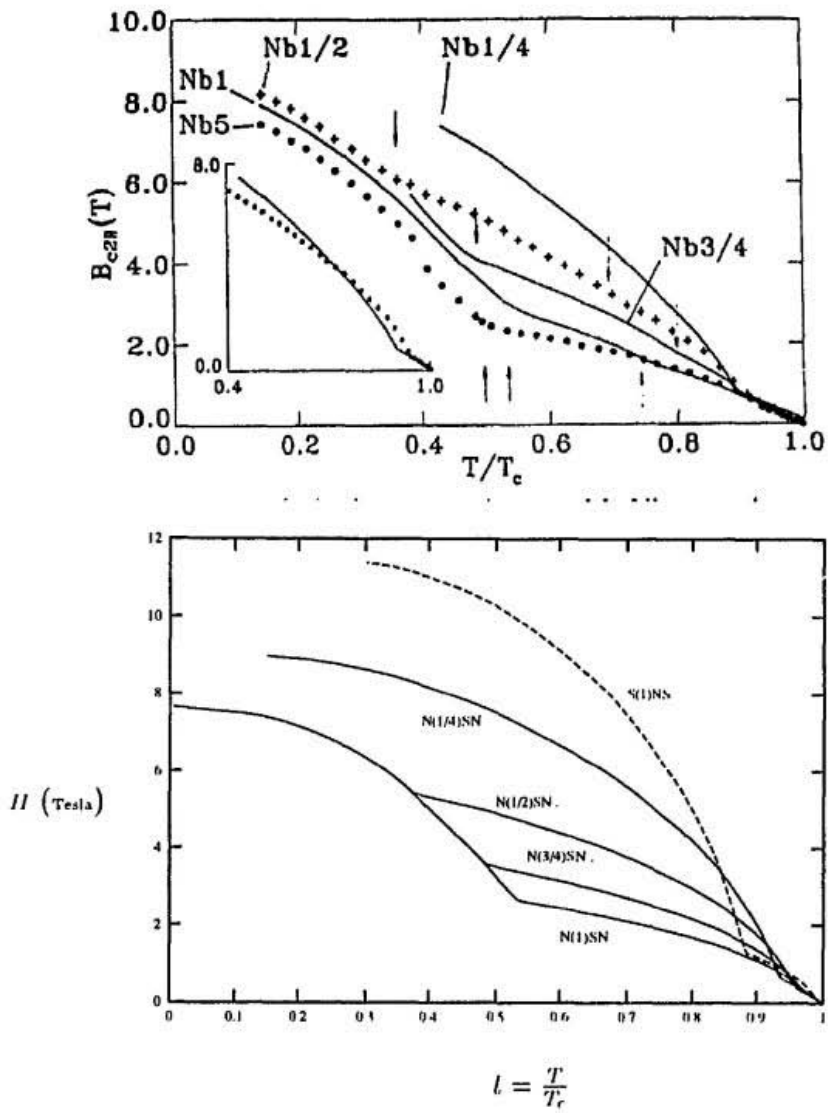

Figure 4.14: The upper critical field calculated as a function of temperature for the $NSN\cdots$ geometry for $d_{N1} = d_N, 0.75d_N, 0.5d_N$, and $0.25d_N$, including the effect of electron spin paramagnetism. The dashed line corresponds to $SNS\cdots$ geometry with $d_{S1} = d_S$. Also included is the experimental data of W. Maj and J. Aarts [41] (reprinted by permission from J. Aarts).

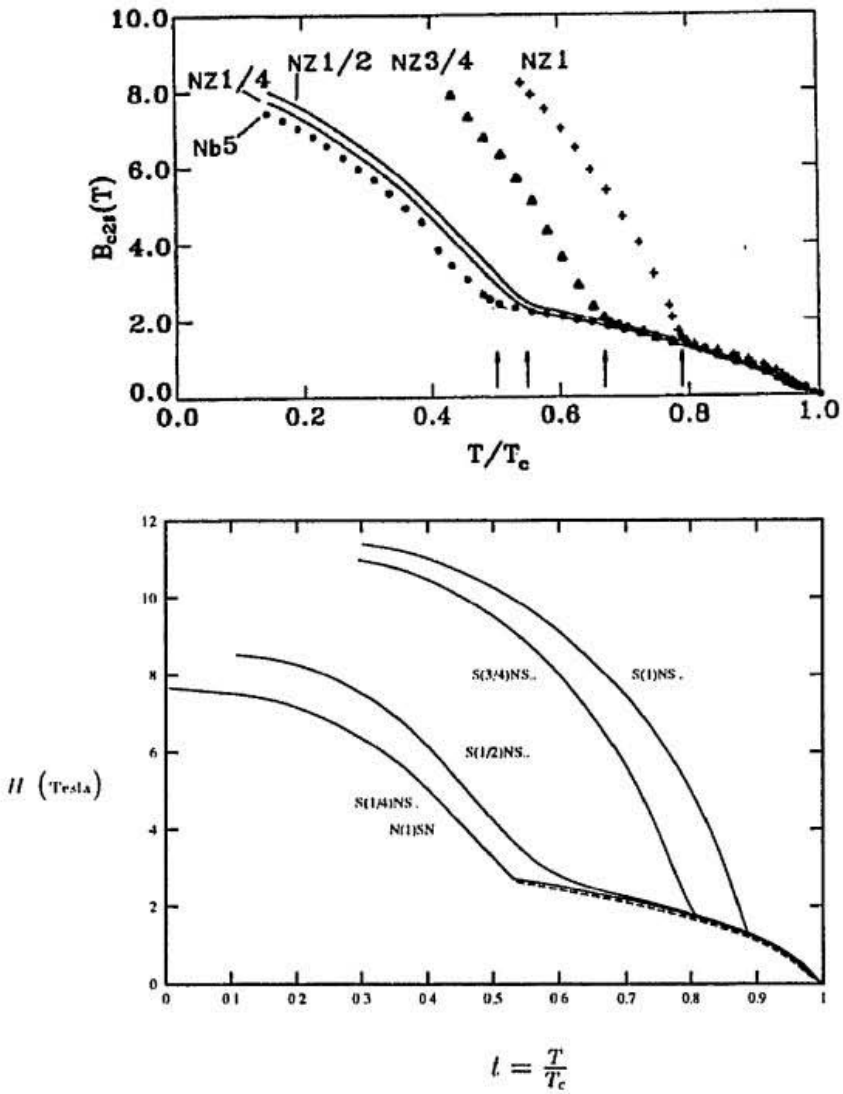

Figure 4.15: The upper critical field calculated as a function of temperature for the $SNS\cdots$ geometry for $d_{S1} = d_S, 0.75d_S, 0.5d_S$, and $0.25d_S$, including the effect of electron spin paramagnetism. The dashed line corresponds to $NSN\cdots$ geometry with $d_{N1} = d_N$. Also included is the experimental data of W. Maj and J. Aarts [41] (reprinted by permission from J. Aarts).

by Maj and Aarts [41] and reproduced in Figs. 4.14 and 4.15. The various features of the upper critical field for those geometries studied by Maj and Aarts are summarized in the Table 4.2.

Geometry	Thickness of 1st Layer	Dimensional Crossover
$N_1SN\cdots$	$d_{N1} = 1.00d_N$	$H_{c3N1} \rightarrow H_{c2S}$
$N_1SN\cdots$	$d_{N1} = 0.75d_N$	$H_{c3N1} \rightarrow H_{c2S}$
$N_1SN\cdots$	$d_{N1} = 0.50d_N$	$H_{c3S2} \rightarrow H_{c3N1} \rightarrow H_{c2S}$
$N_1SN\cdots$	$d_{N1} = 0.25d_N$	$H_{c3N3} \rightarrow H_{c3N1} \rightarrow H_{c2S}$
$S_1NS\cdots$	$d_{S1} = 1.00d_S$	$H_{c3N2} \rightarrow H_{c3S1}$
$S_1NS\cdots$	$d_{S1} = 0.75d_S$	$H_{c3N2} \rightarrow H_{c3S1}$
$S_1NS\cdots$	$d_{S1} = 0.50d_S$	H_{c3}
$S_1NS\cdots$	$d_{S1} = 0.25d_S$	$H_{c3N2} \rightarrow H_{c2S}$

Table 4.2: Dimensional crossover of the upper critical field in the $N_1SN\cdots$ and $S_1NS\cdots$ geometries composed of Nb and NbZr in Maj and Aarts' experiment [41]. $d_S = 165$ Å, $d_N = 240$ Å, and $\rho = 0.1$.

4.6 Conclusions

In this chapter we have examined the parallel upper critical field in a number of superlattice geometries, in which the component metals shared a common BCS coupling constant, density of states at the Fermi surface, and Debye temperature, but differed in the size of the electron diffusion constant. A number of systems have been studied experimentally for which this is a reasonably good description. One of the more intriguing features in these systems arises from the discontinuous shift in the nucleation site of the superconducting order parameter, induced by the discontinuous change in the slope of the upper critical field. This effect, first predicted by Takahashi and Tachiki [53], has been confirmed by a number of experiments [37, 38, 39, 40, 75].

Of particular interest in our research are the effects which may be attributed

to the presence of the insulating substrate, which we represent by a free surface, through the boundary condition given by Eq. (4.24). One important aspect of the present analysis is the sensitivity of the location of the nucleation center to the presence of the free surface, notably in the $NSN\cdots$ and $SNS\cdots$ geometry discussed in Section 4.2. This gives rise to two important results, the first is that the ratio of the upper critical fields, H_{c3}/H_{c2}, shows a complicated dependence on temperature and geometry and can yield values considerably higher than those obtained in the case of a homogeneous system. The second result is that the upper critical field curve depends strongly on the nature of the initial layer.

The experimental evidence for this predicted sensitivity comes from a detailed comparison of different data sets for Nb/NbZr superlattices. Those superlattice differ principally in the order in which the layers are deposited on an insulating substrate [41], and differ in the thickness of the initial layer, denoted by $N_1SN\cdots$ and $S_1NS\cdots$. Both of the results represent a critical test of the de Gennes-Werthamer theory of the proximity effect. In the former case, the field at which the nucleation shift is observed to occur is shown to satisfy the scaling law given by Eq. (4.28) for three different geometries. Moreover it is shown that the constant, which depends on the detailed nature of the geometry, can be calculated using de Gennes-Werthamer theory with parameters determined from the bulk properties of the component metals for the Nb/NbZr superlattices. In the case of the experiments of Maj and Aarts [41], it is significant that the complexity regarding the location of the nucleation center is reflected in the calculated upper critical field curves, which are qualitatively similar to those observed experimentally [78]. This suggests that the subtle effects arising from the interplay of the free surface and the layered structure in determining the nucleation center are at least consistent with observation.

Another result that emerges from the present analysis is the importance of the

pair breaking due to the electron spin paramagnetism in the case of the layered Nb/NbZr structures. This effect substantially reduces the calculated value of the upper critical field at low temperatures. With the inclusion of the spin paramagnetism the agreement between the calculated upper critical field curves for both the $(N_1SN\cdots)$ and the $(S_1NS\cdots)$ geometries and the corresponding experimental curves [41] is good.

The present analysis demonstrates that, provided the geometric effect of the free surface and the pair breaking effect of the electron spin paramagnetism are included, the de Gennes-Werthamer theory of the proximity effect provides a very satisfactory quantitative description of the parallel upper critical field in layered Nb/NbZr systems. It should be noted that all of the parameters used in obtaining the curves presented in Figs. 4.14 and 4.15, on which this conclusion is based, may be determined independently. The close accord between theory and experiment obtained within this work suggests that a quantitative study of other aspects of the superconducting properties of layered structures such as Nb/NbZr would be of considerable value. One such study concerns the angular dependence of the upper critical field at a fixed temperature, analogous to our work on superconducting films presented in chapter 3. This research is presently in progress.

Chapter 5

Summary and Conclusions

We have rederived the de Gennes-Werthamer dirty limit theory from the microscopic BCS theory using the Green's function method. The application of this theory to inhomogeneous superconductors has been examined for both superconducting films and multilayer systems. Studies of the angular dependence of the upper critical field ($0 \leq \theta \leq 90°$) for the former geometry reveal the importance of the surface effect [19] and the size effect in determining the upper critical field, while for the latter case, detailed studies of the upper critical field lead to a number of experimentally testable theoretical predictions. The results of our numerical calculations show excellent quantitative agreement with existing experimental data.

In this chapter, we will briefly review the basic properties of the de Gennes theory and summarize the key results obtained from the research described in this thesis. We then draw a number of conclusions based on this work and discuss what related problems require further analysis and investigation.

A detailed review of the microscopic theory for conventional superconductors was presented in Chapter 2. We derived the linearized Gor'kov integral equation, Eq. (2.61),

$$\Delta^{\dagger}(\mathbf{x}) = V\,\beta^{-1} \int d^3y \sum_{\omega} Q_{\omega}(\mathbf{x},\mathbf{y})\,\Delta^{\dagger}(\mathbf{y}) ,$$

for a homogeneous superconductor from the BCS theory. We then went on to examine how to evaluate the kernel, Q_{ω}, in the linearized Gor'kov equation for the case of electrons in a randomly distributed impurity potential, by means of

the Green's function method. The solution for the kernel in momentum space, Eq. (2.96), was given by

$$Q_\omega(\mathbf{q}) = 2\pi N(0) \left\{ \left[\frac{1}{v_F q} \tan^{-1}\left(\frac{v_F q}{2|\Gamma|}\right) \right]^{-1} - \tau^{-1} \right\}^{-1} ,$$

where τ denotes the electron collision time.

Applying the long wave length approximation, $|\mathbf{q}| \sim 0$, to this kernel, we showed that it reduces to the result proposed by de Gennes for a dirty superconducting alloy, which satisfies the three-dimensional diffusion equation, Eq. (2.100),

$$(2|\omega| - D\nabla^2)\, Q_\omega(\mathbf{x} - \mathbf{x}') = 2\,\pi\, N\, \delta(\mathbf{x} - \mathbf{x}') .$$

The consistency between the kernel in the linearized Gor'kov equation under the long-wavelength approximation and de Gennes' kernel suggests that the original Gor'kov theory for a homogeneous superconductor may be readily extended to include inhomogeneous superconductors, provided the boundary conditions and continuity conditions of the kernel in de Gennes' proximity theory are incorporated.

Following de Gennes' work, we examined the influence of a planar surface and a planar interface on the kernel Q_ω and showed how the effects could be described by supplementing the de Gennes diffusion equation with certain boundary and continuity conditions. Using the linearized Gor'kov equation, the boundary and continuity conditions obtained for the kernel result in certain boundary and continuity conditions on the gap function. The theory was then generalized to include the effect of an applied field through the semi-classical phase integral approximation, which is equivalent to the replacement

$$\nabla \rightarrow \mathbf{\Pi} = \nabla - i\frac{2\pi}{\phi_o}\mathbf{A} .$$

While this theory may be readily applied to an inhomogeneous superconductor, a single film and multilayer systems, two assumptions made in obtaining this theory should be emphasized.

The first is the long-wavelength approximation, $|\mathbf{q}| \sim 0$. In applying this theory to an inhomogeneous system, e.g. a bilayer, this approximation requires that the eigenvalue used in Werthamer equation, Eq. (3.8), should be small. Certain results for the transition temperature at zero field in a bilayer system, based on the de Gennes-Werthamer theory, are inconsistent with this approximation [44].

The second is the assumption that de Gennes' continuity condition, derived in the case of a single interface, is applicable to a system with multiple interfaces. While we have not examined the validity of this assumption theoretically, the quantitative comparison of the theoretical results of our calculation with experimental data suggests that it is indeed valid for a wide class of multilayer systems.

In the last part of chapter 2, we reviewed briefly the recent development of de Gennes-Werthamer theory, notably the Takahashi-Tachiki formalism. For the particular case of a two component multilayer system, in which the component metals share the same transition temperature at zero field, e.g. Nb/NbZr, the Takahashi-Tachiki formalism reduces to the de Gennes-Werthamer theory. While this is an interesting and important case, it does not really provide an adequate test of the Takahashi-Tachiki formalism and other recent generalizations of the de Gennes theory. A more demanding and revealing test would be the careful and systematic comparison of the Takahashi-Tachiki formalism with the large amount of existing experimental data.

In chapter 3, we applied the de Gennes-Werthamer theory to a superconducting film to study the temperature dependence of the upper critical field in the parallel field case and the angular dependence of the upper critical field at fixed temperature.

The non-trivial dependence of the eigenvalue, λ, on the wave number, k, in the parallel field case is clearly shown by the numerical result of Fig. 3.2. For thin films we found that the minimum eigenvalue, λ^*, found at $k^* = 0$ can be analytically

expressed as

$$\lambda^* = \frac{1}{3}\,h\,\left(1 - \frac{8}{315}\,h^2\right)$$

through the mean field approximation. This expression also shows that the eigenvalue in the thin film limit, $\lambda^* = \frac{1}{3}h$, is applicable to a wider range of film thickness, $2a_r \lesssim \sqrt{2}\xi_H$, instead of $2a_r \ll \xi_H$ as Maki [67] suggested. The distinct temperature dependence of the upper critical field in the thin film case and for the infinite geometry are given by Eq. (3.2) and Eq. (3.3). The rest of chapter 3 was devoted to a detailed analysis of the angular dependence of the upper critical field for a superconducting film.

A general framework for calculating the angular dependence of minimum eigenvalue was established in terms of an eigenfunction expansion method. The formula serving as the basis of our numerical calculation was given by

$$\det\left|\langle j,m|\hat{\mathcal{L}}(k)|i,n\rangle - \varepsilon(k)\right| = 0\,,$$

with matrix element

$$\begin{aligned}\langle j,m|\hat{\mathcal{L}}(k)|i,n\rangle &= \left[\lambda_j + \lambda_m + k^2\right]\,\delta_{ij}\,\delta_{mn} - \sqrt{\sin\theta\,\cos\theta}\,\mathcal{X}_{ij}\,\mathcal{Z}_{mn} \\ &+ k\left[\mathcal{X}_{ij}\,\delta_{mn}\,\sqrt{2\cos\theta} - \mathcal{Z}_{mn}\,\delta_{ij}\,\sqrt{2\sin\theta}\right]\,.\end{aligned}$$

Using this formula, our numerical results showed that the underlying eigenvalue problem for the finite-angle case differs qualitatively from that applicable to the parallel field case. This is best seen from the fact that the minimum eigenvalue in the tilted field case, presented in Fig. 3.6, is independent of wave number, in contrast with the non-trivial dependence of the minimum eigenvalue on wave number in the parallel field case presented in Fig. 3.2.

The full angular dependence of the upper critical field at fixed temperature was obtained using the de Gennes-Werthamer formalism from the minimum eigenvalue

calculated from Eq. (3.95). This calculation is valid for both thin and thick films and all angles in the range $0 < \theta < \pi/2$. The calculation of the full angular dependence for a semi-infinite geometry is also given for the limiting case of a thick film. While our results were consistent with Tinkham's results for thin films, we were able to show that Tinkham's formula, given by Eq. (3.55), is not valid in the case of thick films, even if the experimental values of $H_{\parallel}$ and $H_{\perp}$ are used. In comparing the full angle-dependent upper critical field of a thick film with that of a semi-infinite geometry, a dimensional crossover was found from our theoretical calculation presented in Fig. 3.11. This dimensional crossover reflects a transition from surface effect to size effect as the angle increases.

The upper critical field in the limit $\theta \to 0$ was studied in detail by computing the quantity, $\lim_{\theta \to 0} \frac{1}{H} \frac{\partial H}{\partial \theta}\Big|_T$, as a function of the reduced applied field, h. The numerical results are consistent with the expression obtained by Thompson [24] and Takanaka [56] in the superconducting film case. Our calculation shows that, within the numerical precision we reached, $\lim_{\theta \to 0} \frac{1}{H} \frac{\partial H}{\partial \theta}\Big|_T$ is very close to zero at $h = h_c = 1.62$. This result contradicts the earlier work of Saint-James [21] and supports Thompson's theoretical analysis.

While the existing experimental data show the presence of a cusp, as predicted by Saint-James [21] and Thompson [24], a quantitative comparison between the theoretical results and experimental data show significant differences. The earlier experimental data [71, 23] were in good agreement with Saint-James' theoretical prediction. However, later experiments carried out by Harper and Tinkham [69] showed that the value of $\lim_{\theta \to 0} \frac{1}{H} \frac{\partial H}{\partial \theta}\Big|_T$ at the cusp lies between Saint-James' and Thompson's result. Harper and Tinkham's measurement is obviously in contradiction of Saint-James' theoretical result. Its deviation from Thompson's prediction and our calculation may be attributed to imprecision in the measurement of the

slope, due to limitations in the angular resolution in the experiments. The possible error involved in the measurement of the quantity, $\lim_{\theta\to 0}\frac{1}{H}\left.\frac{\Delta H}{\Delta\theta}\right|_T$, caused by limitations in the angular resolution was estimated using Eq. (3.110) and the results were presented in Fig. 3.14.

In chapter 4, we studied the temperature dependence of the upper critical field in a multilayer system. In this class of systems the effects of geometry arise as a consequence of the inherent modulation imposed by the layered structure and surface effects. Both play an important role in determining the upper critical field. Particular attention is paid to the Nb/NbZr multilayer system as it satisfies, to a good approximation, the requirement that $T_{cS} = T_{cN}$, and is used in a number of experimental studies.

We calculated the upper critical field of a superlattice model, Nb/NbZr, corresponding to the sample prepared by Kuwasawa et al. [38]. The detailed dependence of the eigenvalue on wave number was presented in Fig. 4.2, which explicitly show the shift in the nucleation center at the critical reduced thickness, $a^* = 2.05$. Using the de Gennes-Werthamer formula, with the minimum eigenvalue presented in Fig. 4.3 (a), the temperature dependence of the upper critical field for this superlattice model shown in Fig. 4.3 (b) are in good quantitative agreement with the experimental data of Kuwasawa et al. [38]. The investigation of the upper critical behavior was then extended to a semi-infinite superlattice with one free surface. Of particular interest in this type of geometry are effects attributed to the presence of a free surface and the interplay between the surface effect and the effect of the modulation.

For a sample with a ratio of diffusion constants given by $\frac{D_S}{D_N} = 0.05$, we showed, in Fig. 4.5, that the $NSN\cdots$ geometry undergoes a shift in the nucleation site from the surface to the center of one interior N layer at low applied field, and then from

the center of one interior N layer to the center of one interior S layer as the applied field increases. The second nucleation site shift corresponds to the interfacial effect found in a superlattice geometry, which indicates the presence of the Takahashi-Tachiki effect in this semi-infinite superlattice. The first shift in the nucleation site corresponds to a transition from a pure surface superconducting state to a bulk superconducting state. Both shifts in the nucleation site manifest themselves as discontinuities in the slope of the temperature-dependent upper critical field presented by curve (2) in Fig. 4.7. We describe the transitions corresponding to the discontinuous slopes by $H_{c3N} \rightarrow H_{c2N} \rightarrow H_{c2S}$. The first transition, denoted by $H_{c3N} \rightarrow H_{c2N}$, shows only a very shallow discontinuity in the slope of the curve and therefore is difficult to detect from measurements of the upper critical field. However, recent experimental measurements of the logarithmic derivative of the upper critical field for the multilayer Nb/NbZr system, carried out by Kuwasawa et al. [82], show clearly that two distinct upper critical fields are found at temperatures T_1^* and T_2^* at which the logarithmic derivative of the upper critical field changes abruptly.

For the $SNS\cdots$ geometry, the nucleation site undergoes only one shift from a surface to the center of one interior S layer, as shown in Fig. 4.6. The temperature dependence of the upper critical field is presented by curve (3) in Fig. 4.7. We describe the upturn of the upper critical field in this geometry by $H_{c3S} \rightarrow H_{s2S}$.

Comparing the results obtained for the $NSN\cdots$ geometry with that for the $SNS\cdots$ geometry, we conclude that the surface effect is crucial in determining the upper critical field of a multilayer system. The importance of the surface effect is best shown by the two distinct upper critical field curves presented in Fig. 4.7, corresponding to the $SNS\cdots$ and $NSN\cdots$ geometries, respectively. This theoretical prediction was confirmed by the experiment carried out by Maj and Aarts [41] in the Netherlands, who arrived at this conclusion independently through their systematic

experimental work.

Through a careful examination of the wave number dependence of the eigenvalue calculated for the given geometry, we found that the shift in the nucleation site and the subsequent upturn in the upper critical field occur when

$$\frac{\Lambda}{\xi_{II}^*} = \mathcal{U}\left(\sigma = \frac{d_S}{d_N}, \rho = \frac{D_S}{D_N}\right) ,$$

where the function $\mathcal{U}$ can be calculated numerically for a given geometry. This implies a scaling law that the upper critical field, H^*, at which the upturn occurs, is inversely proportional to the square of the modulation length

$$H^* \propto \frac{1}{\Lambda^2} .$$

This scaling law was shown to be satisfied by several sets of experimental data, presented in Table 4.1.

We calculated $\mathcal{U}$ as a function of ρ for $\sigma = 1$, for the $NSN\cdots$, $SNS\cdots$ and the superlattice geometries. The results were shown in Fig. 4.10. In the case of the $(NSN\cdots)$ geometry, the shift in the nucleation centre, $H_{c3N} \rightarrow H_{c2S}$, is described by the upper curve for $\rho > 0.08$, while for $\rho < 0.08$, the two branches of the upper curve describe two successive shifts in the nucleation site, denoted by $H_{c3N} \rightarrow H_{c2N} \rightarrow H_{c2S}$. The lower curve corresponds to the shift in the nucleation site $H_{c3S} \rightarrow H_{c2S}$ in $SNS\cdots$ geometry. While for a given multilayer system containing sufficient layers with $\sigma = 1$ and $T_S = T_N$, the magnitude of the applied field at which the upturn of the temperature dependent parallel upper critical field occur for both $NSN\cdots$ and $SNS\cdots$ geometries are predicted by the upper and lower curves in Fig. 4.10, to observe the upturn of the upper critical field in experiment, the inequality, Eq. (4.29), has to be satisfied.

The last part of chapter 4 consists of a detailed quantitative examination of the

de Gennes-Werthamer formalism to multilayer systems. The temperature dependence of the upper critical field as well as the upturn in upper critical field for two sets of multilayer systems, corresponding to the samples studied experimentally by Maj and Aarts [41] and illustrated schematically in Fig. 4.11, were examined. For those two sets of samples, the surface effect was investigated systematically by varying the thickness of the first layer for both $NSN\cdots$ and $SNS\cdots$ geometries, and a quantitative comparison with the experiment data of Maj and Aarts was made. The results of our calculation for the upper critical field, shown in Fig. 4.12 and 4.13, are in excellent agreement with the experimental measurements over the entire temperature range, provided the effect of the spin paramagnetism is included. While most of the upper critical field curves in Fig. 4.12 and 4.13 exhibit a discontinuity in the slope that arises as a consequence of the shift in the nucleation site, it is worth noting that the $S(1/2)NS\cdots$ geometry exhibits a smooth upper critical field curve. In this geometry, the nucleation site moves continuously from the N_1 layer to the S_1 layer as the applied field increases, reflecting the fact that a superconducting sheath exists over the entire temperature region. The various features of the upper critical field for those samples prepared by Maj and Aarts [41] are summarized in Table 4.2.

Certain conclusions may be drawn from our theoretical studies. First the discrepancies between the earlier theoretical studies on the angular dependence of the upper critical field of superconducting films may be attributed to non-analytical behaviour of the eigenvalue problem in the limit $\theta \rightarrow 0$. The validity of the approximations used by previous authors may be examined in the light of our exact numerical results. It was also shown that the non-analytical nature of the angular dependence in the limit $\theta \rightarrow 0$, would also make the precise experimental determination of the slope, $\lim_{\theta\rightarrow 0} \frac{\partial H}{\partial \theta}\Big|_T$, difficult. It is interesting to note that the size effect, introduced by the thickness of the film, manifests itself in both the temperature

dependence and the angular dependence of the upper critical field and leads to a dimensional crossover from two dimensional behavior to three-dimensional behavior, which should be observable experimentally. Finally, our theoretical result, within the framework of DW theory, extends the knowledge of the second order phase transition in superconductivity for a superconducting film from a co-existence curve to a co-existence surface in the phase space spanned by $(H_{\parallel}, H_{\perp}, t)$.

For all the multilayer cases we studied, our calculations show the importance of the surface superconducting state in determining the upper critical field. The persistence of this surface superconducting state stems from the macroscopic nature of the superconducting order parameter and can manifest itself in an enhanced parallel upper critical field. In addition to the influence of the surface effect on the macroscopic superconducting order parameter, the modulation of the multilayer system also plays an important role in determining the spatial variation of the order parameter. This was shown in our work by the complex dependence of the nucleation site on the magnetic field and resultant temperature dependence of the upper critical field in the multilayer system. One consequence of this was that our calculations showed that the upper critical field was extremely sensitive to the properties of the initial layer. The fact that this sensitivity was also present in the corresponding experiments of Maj and Aarts is of some importance as it suggests that this sensitivity is not simply an artifact of the de Gennes formalism. These calculations taken together with the experimental results therefore provide a critical test of the de Gennes boundary and continuity conditions.

There are a number of interesting and important extensions to the research presented in this thesis. One obvious extension is the evaluation of the angular dependence of the upper critical field in the case of the superlattice, particularly in the limit $\theta \rightarrow 0$. Recent experimental data [82] show discontinuities in the logarithmic

derivative of the angular dependence of the upper critical field, $\lim_{\theta \to 0} \frac{\partial H}{\partial \theta}\Big|_T$, that are possibly correlated with shifts in the nucleation site. Also, while we have been able to obtain good agreement between theory and experiment for multilayer systems, it should be noted that we have restricted our consideration to the case where both the composite metals share the same transition temperature. A far more demanding and possibly revealing test of the de Gennes formalism would be the extension of these studies to the case $T_{cS} \neq T_{cN}$ or to the case in which one of the components contained magnetic impurities. It would also be feasible to extend this work to examine the region just below the upper critical field. This would be carried out by an appropriate application of Abrikosov's theory of the vortex lattice [7] based on the eigenvalue solutions obtained for the superlattice. It would be interesting to discover whether the vortex lattice would be commensurate or incommensurate with the superlattice and what consequences this would have for the magnetization curve and the critical current.

Finally we note that all the discussion contained in this thesis has been directed towards so called conventional superconductors. While there have been a number of experiments done on synthetically modulated high T_c compounds, the theory of the superconducting state in these compounds is not well understood and it is far from obvious that the de Gennes theory of the proximity effect is applicable to them. However it should be noted that these compounds do exhibit a second order phase transition at the upper critical field. It would be interesting, therefore, if certain phenomena observed in the high T_c compounds were also present in multilamellar structures composed of conventional superconductors.

Appendix A

A.1 Gor'kov Equation and the BCS Gap Equation

In section 2.2 of chapter 2, we obtained the Gor'kov equation, Eqs. (2.56) and (2.55). We wish to show how the Gor'kov equation may be reduced to the BCS gap equation [9], and how the formula for the transition temperature in BCS theory may be recovered by solving Eqs. (2.56) and (2.56) for a spatially homogenous superconductor in the zero applied field case, specified by

$$\begin{aligned} \mathbf{A}(\mathbf{x}) &= 0 \,, \\ U(\mathbf{x}) &= 0 \,, \\ \Delta(\mathbf{x}) &= \Delta \,. \end{aligned} \tag{A.1}$$

Eqs. (2.56) and (2.56) can be written, in this case, as

$$\left[i\hbar\omega_n - \frac{1}{2m}(-i\hbar\nabla)^2 + \mu\right] \mathcal{G}(\mathbf{x}, \mathbf{x}'\omega_n) + \Delta\mathcal{F}^\dagger(\mathbf{x}, \mathbf{x}', \omega_n) = h\delta(\mathbf{x} - \mathbf{x}') \,, \tag{A.2}$$

$$\left[-i\hbar\omega_n - \frac{1}{2m}(i\hbar\nabla)^2 + \mu\right] \mathcal{F}^\dagger(\mathbf{x}, \mathbf{x}', \omega_n) - \Delta^\dagger\mathcal{G}(\mathbf{x}, \mathbf{x}', \omega_n) = 0 \,. \tag{A.3}$$

The translational invariance of the above equations implies that

$$\begin{aligned} \mathcal{G}(\mathbf{x}, \mathbf{x}', \omega_n) &= \mathcal{G}(\mathbf{x} - \mathbf{x}', \omega_n) \,, \\ \mathcal{F}^\dagger(\mathbf{x}, \mathbf{x}', \omega_n) &= \mathcal{F}^\dagger(\mathbf{x} - \mathbf{x}', \omega_n) \,, \end{aligned} \tag{A.4}$$

and hence we have the Fourier transformation of the Matsubara functions with respect to spatial coordinates

$$\mathcal{G}(\mathbf{x} - \mathbf{x}', \omega_n) = (2\pi)^{-3} \int d^3k \, e^{i\mathbf{k}\cdot(\mathbf{x}-\mathbf{x}')} \mathcal{G}(\mathbf{k}, \omega_n) \,, \tag{A.5}$$

$$\mathcal{F}^{\dagger}(\mathbf{x}-\mathbf{x}',\omega_n) = (2\pi)^{-3}\int d^3k\, e^{i\mathbf{k}\cdot(\mathbf{x}-\mathbf{x}')}\mathcal{F}^{\dagger}(\mathbf{k},\omega_n)\,. \tag{A.6}$$

Substituting Eqs. (A.5) and (A.6) into (A.2) and (A.3), we get

$$[ih\omega_n - \epsilon_{\mathbf{k}}]\mathcal{G}(\mathbf{k},\omega_n) + \Delta\mathcal{F}^{\dagger}(\mathbf{k},\omega_n) = \hbar\,, \tag{A.7}$$

$$[-ih\omega_n - \epsilon_{\mathbf{k}}]\mathcal{F}^{\dagger}(\mathbf{k},\omega_n) - \Delta^{*}\mathcal{G}(\mathbf{k},\omega_n) = 0\,. \tag{A.8}$$

where the order parameter Δ is of the form

$$\Delta^{*} = V(\beta h)^{-1}\sum_n e^{-i\omega_n 0^{+}}\mathcal{F}^{\dagger}(\mathbf{x}=0,\omega_n)\,. \tag{A.9}$$

The solutions of the Eqs. (A.7) and (A.8) are given by

$$\mathcal{G}(\mathbf{k},\omega_n) = \frac{-h(ih\omega_n + \epsilon_{\mathbf{k}})}{h^2\omega_n^2 + \epsilon_{\mathbf{k}}^2 + |\Delta|^2}\,, \tag{A.10}$$

$$\mathcal{F}^{\dagger}(\mathbf{k},\omega_n) = \frac{h\Delta^{*}}{h^2\omega_n^2 + \epsilon_{\mathbf{k}}^2 + |\Delta|^2}\,, \tag{A.11}$$

so the self-consistent equation for the order parameter is

$$\Delta = V(h\beta)^{-1}\sum_n\int \frac{d^3k}{(2\pi)^3}\frac{h\Delta}{(h\omega_n)^2 + E_{\mathbf{k}}^2}\,, \tag{A.12}$$

with

$$E_{\mathbf{k}} = (\epsilon_{\mathbf{k}}^2 + \Delta^2)^{\frac{1}{2}}\,. \tag{A.13}$$

We eliminate the common factor Δ in Eq. (A.12) and complete the summation over ω_n using the following formula,

$$\lim_{\eta\to 0}\sum_n \frac{e^{i\omega_n\eta}}{i\omega_n - z} = \mp\frac{\beta}{e^{\beta z}\mp 1}\,, \tag{A.14}$$

where $\mp$ corresponds to Boson and Fermion, respectively. We obtain

$$\begin{aligned}
\sum_n \frac{1}{(\omega_n)^2 + E_{\mathbf{k}}^2} &= \sum_n \frac{1}{2E_{\mathbf{k}}}\left[\frac{1}{i\omega_n + E_{\mathbf{k}}} - \frac{1}{i\omega_n - E_{\mathbf{k}}}\right] \\
&= \frac{1}{2E_{\mathbf{k}}}\left[\frac{\beta}{e^{-\beta E_{\mathbf{k}}}+1} - \frac{\beta}{e^{\beta E_{\mathbf{k}}}+1}\right] \\
&= \frac{\beta}{2E_{\mathbf{k}}}\frac{e^{\frac{1}{2}\beta E_{\mathbf{k}}} - e^{-\frac{1}{2}\beta E_{\mathbf{k}}}}{e^{\frac{1}{2}\beta E_{\mathbf{k}}} + e^{-\frac{1}{2}\beta E_{\mathbf{k}}}} \\
&= \frac{\beta}{2E_{\mathbf{k}}}\tanh\frac{1}{2}\beta E_{\mathbf{k}}\,.
\end{aligned} \tag{A.15}$$

Eq. (A.12) is thus written as

$$1 = V(2\pi)^{-3} \int d^3k\, (2E_{\mathbf{k}})^{-1} \tanh(\beta E_{\mathbf{k}}/2)\ . \tag{A.16}$$

This equation determines the transition temperature and order parameter $\Delta(T)$. At $T = T_c$, the system goes to the normal state so that $\Delta(T_c) = 0$, and Eq. (A.16) is of the form

$$1 = VN \int_0^{\hbar\omega_D} \frac{d\epsilon}{\epsilon} \tanh(\beta_c \epsilon/2)\ , \tag{A.17}$$

This equation allows us to write down the expression for transition temperature T_c in the bulk superconductor as

$$T_c = \frac{2e^{\gamma}}{\pi} \hbar\omega_D \exp(-1/NV) \tag{A.18}$$

where γ is Euler's constant. This is the same result as that of BCS theory, obtained by means of a variational method [9].

Another interesting limiting case is the value of the order parameter at $T = 0$. In this case, Eq. (A.16) becomes

$$1 = VN \int_0^{\hbar\omega_D} \frac{d\epsilon}{(\epsilon^2 + \Delta^2)^{\frac{1}{2}}} = VN \ln(\frac{2\omega_D}{\Delta})\ , \tag{A.19}$$

so that

$$\Delta(0) = 2\hbar\omega_D \exp(-1/NV)\ . \tag{A.20}$$

The more general relation between the order parameter and temperature requires numerical calculation and we do not discuss it here.

A.2 Spatial Representation of $\mathcal{G}_o$

To obtain the spatial variation of the one-particle Green's function in the absence of the impurity potential and magnetic field, we write down Eq. (2.64)

$$\mathcal{G}_o(\mathbf{x} - \mathbf{x}', \omega) = (2\pi)^{-3} \int d^3p \frac{e^{i\mathbf{p}\cdot(\mathbf{x}-\mathbf{x}')}}{i\omega - \xi}\ , \tag{A.21}$$

and define the following variables

$$\begin{aligned}
\xi &= \frac{1}{2m}(p^2 - p_F^2) \\
d\xi &= p\,dp/m \\
p &= p_F + \xi/v_F \\
N &= \frac{mp_F}{2\pi^2} \\
d^3p &= p_F p\,dp\,d\Omega \\
&= 2\pi^2 N\,d\xi\,d\Omega\,.
\end{aligned} \tag{A.22}$$

Thus we obtain

$$\begin{aligned}
\mathcal{G}_o(\mathbf{x}-\mathbf{x}',\omega) &= (2\pi)^{-3}2\pi^2 N \int_0^{2\pi} d\phi \int_{-\mu}^{\infty} \frac{d\xi}{i\omega-\xi} \int_{-1}^{1} dz e^{i|\mathbf{p}||\mathbf{x}-\mathbf{x}'|z} \\
&= \frac{N}{2}\frac{1}{ip_F x}\int_{-\infty}^{\infty}\frac{d\xi}{i\omega-\xi}\left[e^{i(p_F+\frac{\xi}{v_F})x} - e^{-i(p_F+\frac{\xi}{v_F})x}\right]
\end{aligned} \tag{A.23}$$

with $x = |\mathbf{x}-\mathbf{x}'|$.

Choosing the contour in the upper half plane

$$(2\pi i)^{-1}\int_{-\infty}^{\infty}\frac{-d\xi}{i\omega-\xi}e^{i\frac{\xi}{v_F}x} = \begin{cases} e^{-\frac{\omega}{v_F}x} & \omega > 0 \\ 0 & \omega < 0 \end{cases} \tag{A.24}$$

$$(2\pi i)^{-1}\int_{-\infty}^{\infty}\frac{-d\xi}{i\omega-\xi}e^{-i\frac{\xi}{v_F}x} = \begin{cases} e^{-\frac{|\omega|}{v_F}x} & \omega < 0 \\ 0 & \omega > 0\,, \end{cases} \tag{A.25}$$

Finally,

$$\mathcal{G}_o(\mathbf{x};\mathbf{x}',\omega) = -\frac{\pi N}{p_F|\mathbf{x}-\mathbf{x}'|}e^{-\frac{|\omega|}{v_F}|\mathbf{x}-\mathbf{x}'|}\,e^{ip_F|\mathbf{x}-\mathbf{x}'|sgn\omega} \tag{A.26}$$

A.3 Diagrammatic Representation for Fourth Order Term

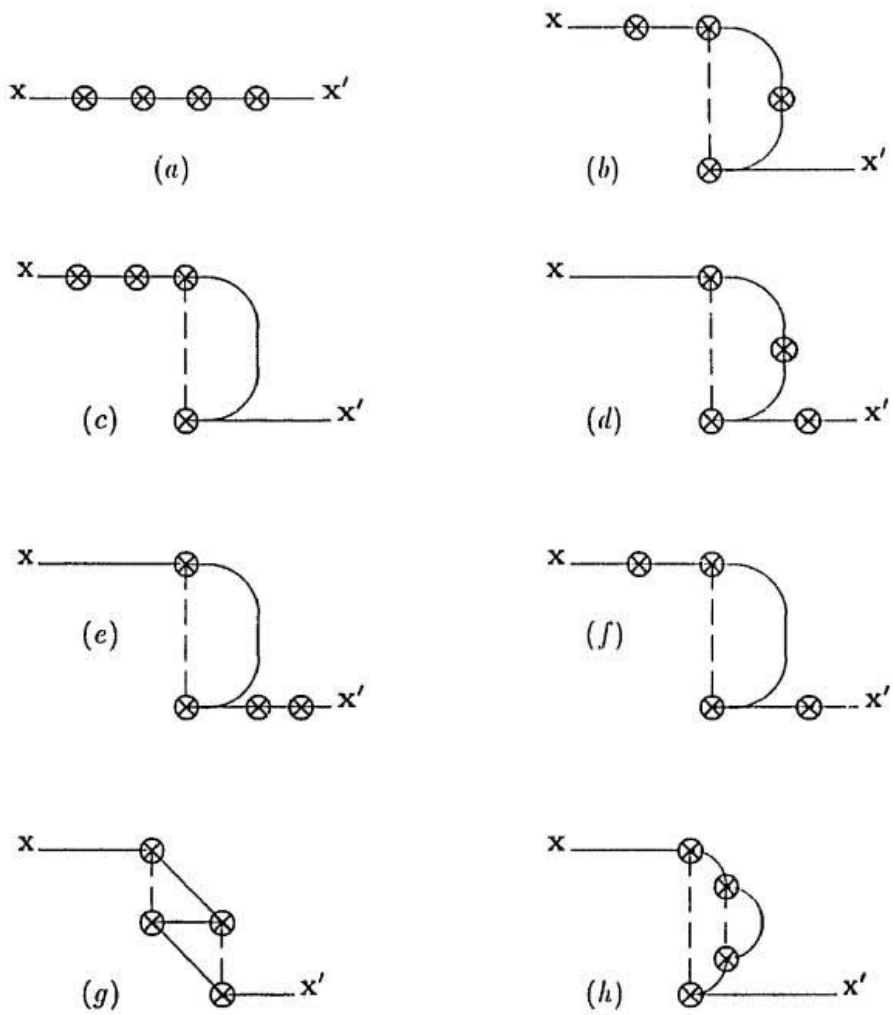

Figure A.1: Diagramatic representation of the fourth order term in the perturbation expansion of Eq. (2.74).

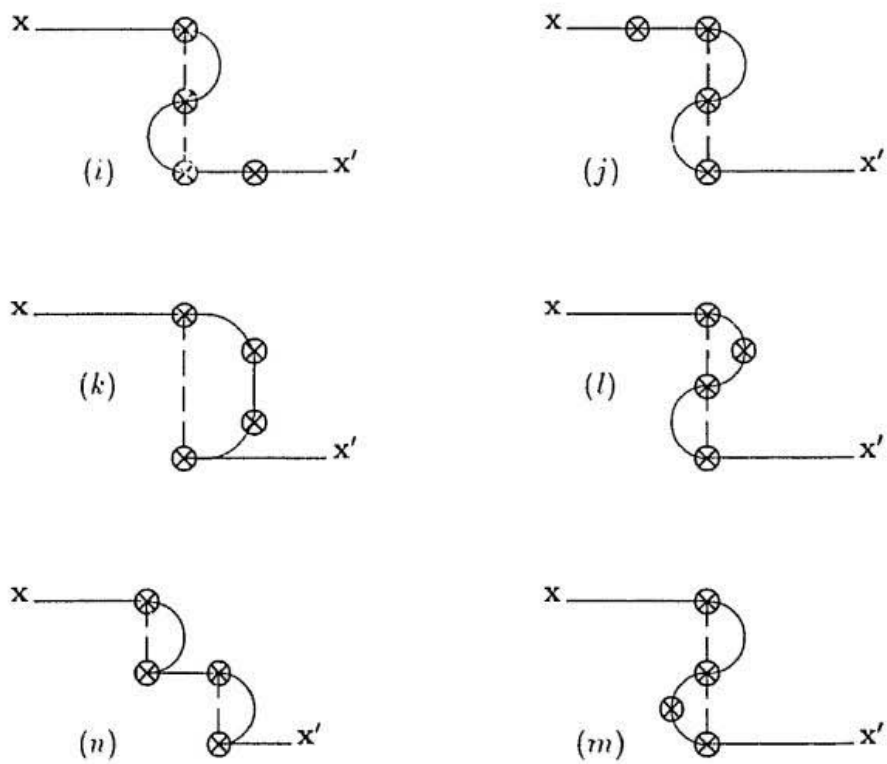

Figure A.2: Diagramatic representation of the fourth order term in the perturbation expansion of Eq. (2.74) (continued).

Appendix B

B.1 Non-Analytical Behavior of the Eigenvalue Equation

In this section, the non-analytical behavior of the eigenvalue equation, Eq. (3.44), corresponding to the limit $\theta \to 0$ is discussed. In section B.1.1, a perturbation potential characterised by a small parameter α is introduced which modifies the eigenvalue equation. In section B.1.2 and B.1.3, the orthonormal basis used to solve the partial differential equation is chosen. Finally, in section B.1.4, it is shown that the secular equation approaches for $\theta \to 0$ differently for $\alpha = 0$ and $\alpha \neq 0$.

B.1.1 Eigenvalue Equation

We wish to find the lowest eigenvalue of the partial differential equation

$$\left\{-\frac{\partial^2}{\partial x^2} - \left[i\frac{\partial}{\partial y} + (x\cos\theta - z\sin\theta)\right]^2 - \frac{\partial^2}{\partial z^2}\right\}\mathcal{F}(x,y,z) = \varepsilon\mathcal{F}(x,y,z)\,, \qquad (B.1)$$

subject to the boundary conditions

$$\frac{\partial}{\partial x}\mathcal{F}\bigg|_{x=\pm a} = 0. \qquad (B.2)$$

The solution is of the form

$$\mathcal{F}(x,y,z) = e^{-iky}\psi(x,z)\,, \qquad (B.3)$$

where $\psi(x,z)$ satisfies the eigenvalue equation

$$\left[-\frac{\partial^2}{\partial x^2} + (-k - x\cos\theta + z\sin\theta)^2 - \frac{\partial^2}{\partial z^2}\right]\psi(x,z) = \varepsilon\psi(x,z)\,, \qquad (B.4)$$

subject to the boundary conditions

$$\left.\frac{\partial\psi}{\partial x}\right|_{x=\pm a} = 0. \tag{B.5}$$

In order to show the non-analytical behavior of the eigenvalue equation in the limit $\theta \to 0$, we modify the above eigenvalue equation by introducing an small perturbation potential αz^2 to give

$$\left[-\frac{\partial^2}{\partial x^2} + (-k - x\cos\theta + z\sin\theta)^2 - \frac{\partial^2}{\partial z^2} + \alpha^2 z^2\right]\psi_\alpha(x,z) = \varepsilon_\alpha\psi_\alpha(x,z)\,. \tag{B.6}$$

We are obviously interested in the limit

$$\varepsilon = \lim_{\alpha\to 0}\epsilon_\alpha\,. \tag{B.7}$$

We expand the eigenfunction $\psi_\alpha(x,z)$ as

$$\psi_\alpha(x,z) = \sum_{j,m} A_{jm}\, f_j(x)\, g_m^\alpha(z)\,, \tag{B.8}$$

where $f_j(x)$ satisfies the Weber equation (3.81) and the subscript j denotes the eigenvalue λ_j.

B.1.2 Harmonic Oscillator Equation

The functions $g_m^\alpha(z)$ satisfy the equation

$$\left[-\frac{d^2}{dz^2} + (z\sin\theta - k)^2 + \alpha^2 z^2\right] g_m^\alpha(z) = \lambda_m^\alpha g_m^\alpha(z)\,. \tag{B.9}$$

The potential part may be written as

$$\begin{aligned}
&(z\sin\theta - k)^2 + \alpha^2 z^2 \\
&= (\sin^2\theta + \alpha^2)\left[z - \frac{k\sin\theta}{\sin^2\theta + \alpha^2}\right]^2 + k^2\left[1 - \frac{\sin^2\theta}{\sin^2\theta + \alpha^2}\right] \\
&= (\sin^2\theta + \alpha^2)\left[z - \frac{k\sin\theta}{\sin^2\theta + \alpha^2}\right]^2 + \frac{k^2\alpha^2}{\sin^2\theta + \alpha^2}\,.
\end{aligned} \tag{B.10}$$

A translational transformation

$$z' = z - \frac{k \sin\theta}{\sin^2\theta + \alpha^2} \tag{B.11}$$

can be made, and the equation now becomes

$$\left[-\frac{d^2}{dz'^2} + (\sin^2\theta + \alpha^2) z'^2\right] g_m^\alpha(z') = \left(\lambda_m^\alpha - \frac{k^2\alpha^2}{\sin^2\theta + \alpha^2}\right) g_m^\alpha(z') . \tag{B.12}$$

We further define a scaling transformation

$$\tau = (\sin^2\theta + \alpha^2)^{\frac{1}{4}} z' = \sqrt{\sigma} z'; \quad \sigma = \sqrt{\sin^2\theta + \alpha^2} , \tag{B.13}$$

and the equation becomes

$$\left[-\frac{d^2}{d\tau^2} + \tau^2\right] \varphi_m(\tau) = \left(\lambda_m^\alpha - \frac{k^2\alpha^2}{\sigma^2}\right) \frac{\varphi_m(\tau)}{\sigma} = (2m+1)\varphi_m(\tau) , \tag{B.14}$$

where $\varphi_m \propto g_m$. We note that the scaled function φ_m is independent of α since the boundary conditions are not changed by the scaling. The eigenvalues may be readily found to be

$$\begin{aligned} \lambda_m^\alpha &= (2m+1)\sqrt{\sin^2\theta + \alpha^2} + \frac{k^2\alpha^2}{\sin^2\theta + \alpha^2} \\ &= (2m+1)\sigma + \frac{k^2\alpha^2}{\sigma^2} . \end{aligned} \tag{B.15}$$

Using Eq. (B.12) and the eigenvalues (B.15), it can be verified that

$$\begin{aligned} g_m^\alpha(z') &= N_m \exp\left(-\frac{1}{2} z'^2 \sqrt{\sin^2\theta + \alpha^2}\right) H_m\left(z' \sqrt[4]{\sin^2\theta + \alpha^2}\right) \\ &= N_m \exp\left(-\frac{1}{2} z'^2 \sigma\right) H_m\left(z'\sqrt{\sigma}\right) \\ &= N_m \exp\left(-\frac{1}{2}\tau^2\right) H_m(\tau) \\ &= g_m^\alpha\left(z - \frac{k\sin\theta}{\sin^2\theta + \alpha^2}\right) \end{aligned} \tag{B.16}$$

satisfies the Eq. (B.12). The normalization of the eigenfunction yields

$$N_m = \frac{\sqrt[4]{\sigma}}{\sqrt[4]{\pi}} \frac{1}{\sqrt{2^m m!}} \tag{B.17}$$

and

$$\varphi_m(\tau) = \frac{1}{\sqrt[4]{\pi}\,\sqrt{2^m\, m!}} \exp\left(-\frac{1}{2}\tau^2\right) H_m(\tau)\ . \tag{B.18}$$

Now we use

$$\int_{-\infty}^{\infty} \varphi_m^{\alpha}(\tau)\,\tau d\tau\,\varphi_n^{\alpha}(\tau) = \frac{1}{\sqrt{2}}\left[\sqrt{n+1}\,\delta_{m,n+1} + \sqrt{n}\,\delta_{m,n-1}\right], \tag{B.19}$$

and the matrix element is expressed as

$$\begin{aligned} Z_{mn} &= \int_{-\infty}^{\infty} dz\, g_m^{\alpha}(z)\, z\, g_n^{\alpha}(z) \\ &= \int_{-\infty}^{\infty} dz'\, g_m^{\alpha}(z') \left(z' + \frac{k\sin\theta}{\sin^2\theta + \alpha^2}\right) g_n^{\alpha}(z') \\ &= \int_{-\infty}^{\infty} \sqrt[4]{\sigma}\varphi_m^{\alpha}(\tau)\,\frac{\tau d\tau}{\sigma}\ \sqrt[4]{\sigma}\varphi_n^{\alpha}(\tau) + \frac{k\sin\theta}{\sin^2\theta + \alpha^2}\,\delta_{mn} \\ &= \frac{1}{\sqrt{2\sigma}}\left[\sqrt{n+1}\,\delta_{m,n+1} + \sqrt{n}\,\delta_{m,n-1}\right] + \frac{k\sin\theta}{\sin^2\theta + \alpha^2}\,\delta_{mn}\ , \\ &= \frac{1}{\sqrt{2\sigma}}\mathcal{Z}_{mn} + \frac{k\sin\theta}{\sigma^2}\,\delta_{mn}\ , \end{aligned} \tag{B.20}$$

with

$$\mathcal{Z}_{mn} = \left[\sqrt{n+1}\,\delta_{m,n+1} + \sqrt{n}\,\delta_{m,n-1}\right]\ . \tag{B.21}$$

B.1.3 Eigenfunctions for Weber Equation

In this section, we derive the matrix element Υ_{ij}, given by Eq. (3.90), in terms of the Kummer function [70]. The equation

$$\left[-\frac{d^2}{dx^2} + x^2\cos^2\theta\right] f_j(x) = \lambda_j f_j(x)$$

may be written as

$$\left[-\frac{d^2}{d(x\sqrt{2\cos\theta})^2} + \frac{1}{4}(x\sqrt{2\cos\theta})^2\right] f_j(x) = (\nu_j + \frac{1}{2})\, f_j(x) \tag{B.22}$$

with

$$\lambda_j = (2\nu_j + 1)\cos\theta\,. \tag{B.23}$$

The parity of f_j is specified by

$$\begin{cases} f_j(x) = f_j(-x)\,; & j = 0, 2, 4, \cdots \\ f_j(x) = -f_j(-x)\,; & j = 1, 3, 5, \cdots \end{cases} \tag{B.24}$$

In terms of the Weber and Kummer functions [70], we write the unnormalized eigenfunctions as

$$\begin{aligned} f_j(x) &= y_1(a, x\sqrt{2\cos\theta})\,; \qquad (j = 0, 2, 4, \cdots) \\ &= e^{-\frac{1}{4}(x\sqrt{2\cos\theta})^2}\, M\left[\frac{1}{2}a + \frac{1}{4}, \frac{1}{2}, \frac{1}{2}(x\sqrt{2\cos\theta})^2\right] \\ &= e^{-\frac{1}{4}(x\sqrt{2\cos\theta})^2}\, M\left[-\frac{\nu_j}{2}, \frac{1}{2}, \frac{1}{2}(x\sqrt{2\cos\theta})^2\right], \end{aligned} \tag{B.25}$$

$$\begin{aligned} f_j(x) &= y_2(a, x\sqrt{2\cos\theta})\,; \qquad (j = 1, 3, 5, \cdots) \\ &= x\sqrt{2\cos\theta}\, e^{-\frac{1}{4}(x\sqrt{2\cos\theta})^2}\, M\left[\frac{1}{2}a + \frac{3}{4}, \frac{3}{2}, \frac{1}{2}(x\sqrt{2\cos\theta})^2\right] \\ &= x\sqrt{2\cos\theta}\, e^{-\frac{1}{4}(x\sqrt{2\cos\theta})^2}\, M\left[\frac{1-\nu_j}{2}, \frac{3}{2}, \frac{1}{2}(x\sqrt{2\cos\theta})^2\right] \end{aligned} \tag{B.26}$$

where $a = -(\nu_j + \frac{1}{2})$.

The recurrence relation of the Weber functions

$$y_1'(a,t) = -\frac{1}{2}\, t\, y_1(a,t) + (a + \frac{1}{2}) y_2(a+1,t) \tag{B.27}$$

$$y_2'(a,t) = -\frac{1}{2}\, t\, y_2(a,t) + y_1(a+1,t) \tag{B.28}$$

with $t = x\sqrt{2\cos\theta}$ gives rise to

$$y_1'(a,t) = -t\,e^{-\frac{1}{4}t^2}\left\{\frac{1}{2}\,M\left[-\frac{\nu_j}{2},\frac{1}{2},\frac{1}{2}t^2\right] + \nu_j\,M\left[1-\frac{\nu_j}{2},\frac{3}{2},\frac{1}{2}t^2\right]\right\} \quad \text{(B.29)}$$

$$y_2'(a,t) = e^{-\frac{1}{4}t^2}\left\{-\frac{1}{2}\,t^2\,M\left[\frac{1-\nu_j}{2},\frac{3}{2},\frac{1}{2}t^2\right] + M\left[\frac{1-\nu_j}{2},\frac{3}{2},\frac{1}{2}t^2\right]\right\}. \quad \text{(B.30)}$$

These two equations determine the eigenvalues of the eigenfunctions f_j through the boundary condition

$$\frac{d}{dx}f_j(x)\Big|_{x=\pm a} = 0\,,$$

which are written explicitly as

$$P(\nu_j) = 0 \quad \text{(B.31)}$$
$$= \frac{1}{2}\,M\left[-\frac{\nu_j}{2},\frac{1}{2},\frac{1}{2}(a\sqrt{2\cos\theta})^2\right] + \nu_j\,M\left[1-\frac{\nu_j}{2},\frac{3}{2},\frac{1}{2}(a\sqrt{2\cos\theta})^2\right],$$

$$O(\nu_j) = 0 \quad \text{(B.32)}$$
$$= \frac{-1}{2}(a\sqrt{2\cos\theta})^2 M\left[\frac{1-\nu_j}{2},\frac{3}{2},\frac{1}{2}(a\sqrt{2\cos\theta})^2\right] + M\left[\frac{1-\nu_j}{2},\frac{3}{2},\frac{1}{2}(a\sqrt{2\cos\theta})^2\right],$$

where zeros of $P(\nu_j)$ and $O(\nu_j)$ give rise to the eigenvalues ν_j for even and odd eigenfunctions.

The normalization constant of the Weber function may be expressed as

$$C_j^{+-2} = \int_{-a}^{a} f_j^2(x)\,dx \quad \text{(B.33)}$$
$$= \int_{-a}^{a} y_1^2(a, x\sqrt{2\cos\theta})\,dx$$
$$= \frac{1}{\sqrt{2\cos\theta}}\int_{-a\sqrt{2\cos\theta}}^{a\sqrt{2\cos\theta}} y_1^2(a,t)\,dt$$
$$= \int_{-a}^{a} e^{-\frac{1}{2}(x\sqrt{2\cos\theta})^2}\,M^2\left[-\frac{\nu_j}{2},\frac{1}{2},\frac{1}{2}(x\sqrt{2\cos\theta})^2\right]dx$$
$$= \frac{1}{\sqrt{2\cos\theta}}\int_{-a\sqrt{2\cos\theta}}^{a\sqrt{2\cos\theta}} e^{-\frac{1}{2}t^2}\,M^2\left[-\frac{\nu_j}{2},\frac{1}{2},\frac{1}{2}t^2\right]dt\,; \quad (j=0,2,4,\cdots),$$

and

$$
\begin{aligned}
C_j^{-2} &= \int_{-a}^{a} f_j^2(x)\,dx \qquad (B.34)\\
&= \int_{-a}^{a} y_2^2(a, x\sqrt{2\cos\theta})\,dx\\
&= \frac{1}{\sqrt{2\cos\theta}} \int_{-a\sqrt{2\cos\theta}}^{a\sqrt{2\cos\theta}} y_2^2(a,t)\,dt\\
&= \int_{-a}^{a} (x\sqrt{2\cos\theta})^2 e^{-\frac{1}{2}(x\sqrt{2\cos\theta})^2} M^2\left[\frac{1-\nu_j}{2}, \frac{3}{2}, \frac{1}{2}(x\sqrt{2\cos\theta})^2\right] dx\\
&= \frac{1}{\sqrt{2\cos\theta}} \int_{-a\sqrt{2\cos\theta}}^{a\sqrt{2\cos\theta}} t^2\, e^{-\frac{1}{2}t^2} M^2\left[\frac{1-\nu_j}{2}, \frac{3}{2}, \frac{1}{2}t^2\right] dt\,; \quad (j = 1,3,5,\cdots).
\end{aligned}
$$

The normalized eigenfunction are expressed as

$$
\begin{aligned}
f_j(x) &= C_j^{+}\, y_1(a, x\sqrt{2\cos\theta}) \qquad (B.35)\\
&= C_j^{+}\, e^{-\frac{1}{4}(x\sqrt{2\cos\theta})^2} M\left[-\frac{\nu_j}{2}, \frac{1}{2}, \frac{1}{2}(x\sqrt{2\cos\theta})^2\right],\\
f_j(x) &= C_j^{-}\, y_2(a, x\sqrt{2\cos\theta})\\
&= C_j^{-}\, x\sqrt{2\cos\theta}\, e^{-\frac{1}{4}(x\sqrt{2\cos\theta})^2} M\left[\frac{1-\nu_j}{2}, \frac{3}{2}, \frac{1}{2}(x\sqrt{2\cos\theta})^2\right]. \qquad (B.36)
\end{aligned}
$$

with

$$
C_j^{+} = \sqrt[4]{2\cos\theta}\left\{\int_{-a\sqrt{2\cos\theta}}^{a\sqrt{2\cos\theta}} e^{-\frac{1}{2}t^2} M^2\left[-\frac{\nu_j}{2}, \frac{1}{2}, \frac{1}{2}t^2\right] dt\right\}^{-\frac{1}{2}} \qquad (B.37)
$$

$$
C_j^{-} = \sqrt[4]{2\cos\theta}\left\{\int_{-a\sqrt{2\cos\theta}}^{a\sqrt{2\cos\theta}} t^2\, e^{-\frac{1}{2}t^2} M^2\left[\frac{1-\nu_j}{2}, \frac{3}{2}, \frac{1}{2}t^2\right] dt\right\}^{-\frac{1}{2}} \qquad (B.38)
$$

In terms of the normalized eigenfunctions, the matrix element is expressed as

$$
\begin{aligned}
X_{ij} &= \int_{-a}^{a} f_i(x)\, f_j(x)\, x\, dx\\
&= C_i^{+} C_j^{-} \int_{-a\sqrt{2\cos\theta}}^{a\sqrt{2\cos\theta}} e^{-\frac{1}{2}t^2} M\left[\frac{1-\nu_j}{2}, \frac{3}{2}, \frac{1}{2}t^2\right] \frac{t^2\,dt}{2\cos\theta} M\left[\frac{-\nu_i}{2}, \frac{1}{2}, \frac{1}{2}t^2\right]\\
&= \frac{1}{\sqrt{2\cos\theta}} \frac{\int e^{-\frac{1}{2}t^2} M\left[\frac{1-\nu_j}{2}, \frac{3}{2}, \frac{1}{2}t^2\right] M\left[\frac{-\nu_i}{2}, \frac{1}{2}, \frac{1}{2}t^2\right] t^2\,dt}{\sqrt{\int e^{-\frac{1}{2}t^2} M^2\left[\frac{-\nu_i}{2}, \frac{1}{2}, \frac{1}{2}t^2\right] dt}\sqrt{\int e^{-\frac{1}{2}t^2} M^2\left[\frac{1-\nu_j}{2}, \frac{3}{2}, \frac{1}{2}t^2\right] t^2 dt}}\\
&= \frac{1}{\sqrt{2\cos\theta}}\, \mathcal{X}_{ij}, \qquad (B.39)
\end{aligned}
$$

where we have used

$$
X_{2i,2j} = X_{2i+1,2j+1} = X_{i,i} = 0, \qquad X_{i,j} = X_{j,i} \qquad (B.40)
$$

B.1.4 Matrix Element and Secular Equation

In the Hilbert space spanned by the chosen eigenbasis $|j,m\rangle = f_j(x)\,g_m(z)$, the matrix representation of the differential operator

$$\begin{aligned}\hat{\mathcal{L}} &= \left[-\frac{\partial^2}{\partial x^2} + (-k - x\cos\theta + z\sin\theta)^2 - \frac{\partial^2}{\partial z^2} + \alpha^2 z^2\right] \\ &= \left[-\frac{d^2}{dx^2} + x^2\cos^2\theta\right] \\ &+ \left[-\frac{d^2}{dz^2} + \alpha^2 z^2 + (z\sin\theta - k)^2\right] \\ &- 2x\,\cos\theta\,(z\sin\theta - k) \end{aligned} \tag{B.41}$$

is written as

$$\begin{aligned}\langle j,m|\hat{\mathcal{L}}|i,n\rangle &= \int_{-a}^{a} dx \int_{-\infty}^{\infty} dz\; f_j(x)\,g_m^{\alpha}(z)\;\hat{L}\;f_i(x)\,g_n^{\alpha}(z) \\ &= \left(\lambda_j\cos\theta + (2m+1)\sqrt{\sin^2\theta+\alpha^2} + \frac{k^2\alpha^2}{\sin^2\theta+\alpha^2}\right)\delta_{ij}\,\delta_{mn} \\ &+ 2\cos\theta\int_{-a}^{a} dx\; f_i(x)\,x\,f_j(x)\int_{-\infty}^{\infty} dz\,g_n^{\alpha}(z)\,[k - z\sin\theta]\,g_m^{\alpha}(z) \\ &= \left(\lambda_j\cos\theta + (2m+1)\sqrt{\sin^2\theta+\alpha^2} + \frac{k^2\alpha^2}{\sin^2\theta+\alpha^2}\right)\delta_{ij}\,\delta_{mn} \\ &+ \sqrt{2\cos\theta}\,\mathcal{X}'_{ij}\left[k\,\delta_{mn} - \sin\theta\frac{1}{\sqrt{2\sigma}}\mathcal{Z}_{mn} - \frac{k\sin^2\theta}{\sin^2\theta+\alpha^2}\delta_{mn}\right] \\ &= \left(\lambda_j\cos\theta + (2m+1)\sqrt{\sin^2\theta+\alpha^2} + \frac{k^2\alpha^2}{\sin^2\theta+\alpha^2}\right)\delta_{ij}\,\delta_{mn} \\ &+ \sqrt{2\cos\theta}\,\mathcal{X}'_{ij}\left[\frac{k\alpha^2}{\sin^2\theta+\alpha^2}\delta_{mn} - \sin\theta\frac{1}{\sqrt{2\sigma}}\mathcal{Z}_{mn}\right]. \end{aligned}$$

It is seen that

$$\lim_{\alpha\to 0}\lim_{\theta\to 0}\langle j,m|\hat{L}|i,n\rangle = \left(\lambda_j + k^2\right)\delta_{ij}\,\delta_{mn} + \sqrt{2}\mathcal{X}'_{ij}k\delta_{mn}\,, \tag{B.42}$$

$$\begin{aligned}\lim_{\theta\to 0}\lim_{\alpha\to 0}\langle j,m|\hat{L}|i,n\rangle &= \lim_{\theta\to 0}[\lambda_j\cos\theta + (2m+1)\sin\theta]\;\delta_{ij}\,\delta_{mn} \\ &\quad - \sqrt{\sin\theta\cos\theta}\,\mathcal{X}'_{ij}\,\mathcal{Z}_{mn} \\ &= \lambda_j\,\delta_{mn}\,\delta_{ij}\,. \end{aligned} \tag{B.43}$$

That the two limits do not commute shows the non-analytical property of the eigenvalue equation.

The secular equation is given by

$$\det \left| \langle j, m | \hat{\mathcal{L}} | i, n \rangle - \varepsilon_\alpha \right| = 0 \tag{B.44}$$

Using this secular equation, we found that, provided a non-vanishing $\alpha \sim 0$ is included, the minimum eigenvalue, $\varepsilon(k, \theta)$, obtained from our numerical calculation showed explicit k dependence and continuously maps to $\varepsilon(k^*, 0)$ as $\theta \to 0$, where k^* denotes the nucleation center found in parallel field case. Nevertheless, in the case of $\alpha = 0$, $\varepsilon(k, \theta)$ maps to $\varepsilon(0, 0)$ as $\theta \to 0$ which is correct only in the thin film case corresponding to $k^* = 0$. For the thick film case, it gives rise to a higher eigenvalue found at $k = 0$ and the surface superconducting state case corresponding to $k^* \neq 0$ cannot be recovered.

Appendix C

C.1 Evaluation of the Eigenvalue of Small H

In this Appendix, we derive a rescaled eigenvalue equation, Eq. (C.16), in the limit $H \to 0$ for a multilayer system. This equation allows us to treat the multilayer system as a homogeneous superconductor with an effective coherence length $\xi_{eff} = \sqrt{\xi_N \xi_S} \propto \sqrt{D_S D_N}$ and obtain the eigenvalues for a superlattice and a semi-infinite superlattice given in Eq. (4.20) and Eq. (4.25).

Let's consider the no-node solution which gives rise to the lowest eigenvalue, we define the function R as

$$R(x) = \rho(x) \frac{d}{dx} \ln f_\lambda(x) . \tag{C.1}$$

The eigenvalue equation (3.19) becomes

$$\frac{d}{dx} R(x) = -R^2(x) + \frac{1}{4}x^2 - \frac{1}{2} - \lambda \quad x \in N \tag{C.2}$$

$$\frac{d}{dx} R(x) = -\frac{1}{\rho} R^2(x) + \frac{1}{4}\rho x^2 - \frac{1}{2} - \lambda \quad x \in S . \tag{C.3}$$

We wish to show how Eqs. (C.2) and (C.3) may be solved, subject to the appropriate boundary conditions, in the limit $H \to 0$, and the minimum eigenvalue λ^* obtained.

In the limit $H \to 0$ the magnetic coherence length ξ_H goes to infinity hence the reduced thickness of the layers, $\delta = d/\xi_H$, with d being the physical thickness of an N or S layer, becomes vanishingly small. In this limit Eqs. (C.2) and (C.3) are well approximated by the linearized difference equations

$$R(x_i) = R(x_{i+1}) - \delta\left[\frac{1}{4}x_{i+1}^2 - \frac{1}{2}\lambda - R^2(x_{i+1})\right] \qquad x \in N \qquad \text{(C.4)}$$

$$R(x_i) = R(x_{i+1}) - \delta\left[\frac{1}{4}\rho x_{i+1}^2 - \frac{1}{2}\lambda - \frac{1}{\rho}R^2(x_{i+1})\right] \qquad x \in S. \qquad \text{(C.5)}$$

To solve these linearized equations in the limit $\delta \to 0$ we apply the coarse graining procedure developed in the analysis of self similar multilamellar lattice structures[50]. The technique considers the superlattice as an alternating sequence of S (SNS) and N (NSN) trilayers. Using the continuity of the logarithmic derivative g at the interface between the layers, together with Eqs. (C.4) and (C.5), it is possible to obtain a set of rescaled equations for the superlattice composed of alternating trilayers, namely

$$R(x_i) = R(x_{i+1}) - D(1)\left[\frac{1}{4}\beta(1)x_{i+1}^2 - \frac{1}{2}\lambda - \frac{\alpha(1)}{\rho}R^2(x_{i+1})\right] \qquad x \in N \qquad \text{(C.6)}$$

$$R(x_i) = R(x_{i+1}) - D(1)\left[\frac{1}{4}\alpha(1)x_{i+1}^2 - \frac{1}{2}\lambda - \frac{\beta(1)}{\rho}R^2(x_{i+1})\right] \qquad x \in S \qquad \text{(C.7)}$$

with

$$\begin{cases} D(1) = 3\delta \\ \alpha(1) = \frac{1}{3}(2\rho + 1) \\ \beta(1) = \frac{1}{3}(2 + \rho) \end{cases} . \qquad \text{(C.8)}$$

Repeating the procedure m times yields the equations

$$R(x_L) = R(x_R) - D(m)\left[\frac{1}{4}\beta(m)x_R^2 - \frac{1}{2}\lambda - \frac{\alpha(m)}{\rho}R^2(x_R)\right] \qquad x \in N \qquad \text{(C.9)}$$

$$R(x_L) = R(x_R) - D(m)\left[\frac{1}{4}\alpha(m)x_R^2 - \frac{1}{2}\lambda - \frac{\beta(m)}{\rho}R^2(x_R)\right] \qquad x \in S \qquad \text{(C.10)}$$

with

$$\begin{cases} D(m) = 3D(m-1) \\ \alpha(m) = \frac{1}{3}\left(2\alpha(m-1) + \beta(m-1)\right) \\ \beta(m) = \frac{1}{3}\left(2\beta(m-1) + \alpha(m-1)\right) \end{cases} . \qquad \text{(C.11)}$$

The above equations may be solved and the explicit form for $D(m), \alpha(m)$ and $\beta(m)$ obtained. We find that $\lim_{m\to\infty}[\alpha(m)-\beta(m)]=0$ so that the above difference equations reduce to a single difference equation

$$R(x_L)=R(x_R)-D(m)\left[\frac{1}{4}\gamma x_R^2-\frac{1}{2}\lambda-\frac{\gamma}{\rho}R^2(x_R)\right] \qquad x\in N \text{ or } S, \tag{C.12}$$

where γ is defined as

$$\gamma=\lim_{m\to\infty}\alpha(m)=\lim_{m\to\infty}\beta(m)=\frac{1}{2}(1+\rho). \tag{C.13}$$

Provided $D(m)$ is sufficiently small we can approximate the above difference equation by the differential equation

$$\frac{dR(x)}{dx}=-\frac{\gamma}{\rho}R^2(x)+\frac{1}{4}\gamma x^2-\frac{1}{2}\lambda. \tag{C.14}$$

By defining

$$R_R(x)=\frac{\sqrt{\gamma}}{\sqrt[4]{\rho^3}}R(x), \qquad x_R=\frac{\sqrt{\gamma}}{\sqrt[4]{\rho}}x, \qquad \lambda_R=\frac{1}{\sqrt{\rho}}\lambda, \tag{C.15}$$

we can rescale the equation (C.14) as

$$\frac{dR_R(x_R)}{dx_R}=-R_R^2(x_R)+\frac{1}{4}x_R^2-\frac{1}{2}\lambda_R. \tag{C.16}$$

Applying Eq. (C.16) to a superlattice geometry yields the result $\lambda_R=1$ and thus $\lambda=\sqrt{\rho}$. For the semi-infinite superlattice $(NSN\cdots)$ or $(SNS\cdots)$ with the boundary condition at free surface $R_R(0)=0$, the eigenvalue can be readily calculated to give [66]

$$\begin{cases} x_R=\sqrt{0.59010} \\ \lambda_R=0.59010 \end{cases} \qquad H\to 0 \tag{C.17}$$

and hence

$$x=\sqrt{\frac{0.59010\sqrt{\rho}\,(1+\rho)}{2}} \qquad H\to 0 \tag{C.18}$$

while

$$\lambda=0.59010\sqrt{\rho} \qquad H\to 0. \tag{C.19}$$

Bibliography

[1] H. K. Onnes. *Commun. Phys. Lab. Univ. Leiden*, **120b**:120b, 1911.

[2] W. Meissner and R. Ochsenfeld. *Naturwiss.*, **34**:787, 1933.

[3] D. E. Mapother, *IBM J. of Res. Develop.*, **6**:77, 1962.

[4] V. L. Ginzburg and L. D. Landau. *Zh. Eksperim. i Teor. Fiz.*, **20**:1064, 1950.

[5] R. P. Huebener. *Magnetic Flux Structures in Superconductors*. Springer-Verlag, Berlin, 1979.

[6] F. London. *Superfluids*. Vol. I, Dover Publications Inc. New York, 1961.

[7] A. A. Abrikosov. *Soviet Phys. JETP*, **5**:1174, 1957.

[8] L. P. Gor'kov. *Sov. Phys. JETP*, **9**:1364, 1959.

[9] J. Bardeen, L. N. Cooper, and J. R. Schrieffer. *Phys. Rev.*, **108**:1175, 1957.

[10] Kazumi Maki. *Physics*, **1**:21, 1964.

[11] P. G. De Gennes. *Physik Kondensierten Materie*, **3**:79, 1964.

[12] E. Helfand and N. R. Werthamer. *Phys. Rev. Letters*, **13**:686, 1964.

[13] E. Helfand and N. R. Werthamer. *Phys. Rev.*, **147**:288, 1966.

[14] K. Maki and T. Tsuzuki. *Phys. Rev.*, **153**:584, 1967.

[15] G. Eilenberger. *Phys. Rev.*, **139**:A868, 1965.

[16] A. L. Fetter and P. C. Hohenberg. *Superconductivity* Vol. 2 Chapter 14, edited by R. D. Parks. Marcel Dekker, Inc, New York, (1969).

[17] I. S. Khukhareva. *Soviet Phys. JETP*, **14**:526, 1962.

[18] N. R. Werthamer. *Superconductivity*, Vol. 1 Chapter 6, edited by R. D. Parks. Marcel Dekker, Inc, New York, (1969).

[19] D. Saint-James and P. G. de Gennes. *Phys. Lett.*, **7**:306, 1963.

[20] M. Tinkham. *Phys. Rev.*, **172**:441, 1968.

[21] D. Saint-James. *Phys. Lett.*, **16**:218, 1966.

[22] J. P. Burger, G. Deutscher, and E. Guyon et A. Martinet. *Phys. Rev.*, **137**:A853, 1965.

[23] H. R. Hart Jr. and P. S. Swartz. *Phys. Lett.*, **10**:40, 1964.

[24] R. S. Thompson. *Sov. Phys.-JETP*, **42**:1144, 1976.

[25] B. Y. Jin and J. B. Ketterson. *Advances in Phys.*, **38**:189 366, 1989.

[26] P. G. De Gennes. *Rev. Mod. Phys.*, **36**:225, 1964.

[27] L. N. Cooper. *Phys. Rev. Lett.*, **6**:689, 1961.

[28] N. R. Werthamer. *Phys. Rev.*, **132**:2440, 1963.

[29] P. R. Auvil and J. B. Ketterson. *Jpn. J. Appl. Phys.*, **61**:1957, 1987.

[30] M. Menon and G. B. Arnold. *Commun. Phys. Lab. Univ. Leiden. Suppl.*, **34b**, 1913.

[31] Cornell S. L. Chun, Guo-Guang Zheng, Jose L. Vincent, and I. K. Schuller. *Phys. Rev. B*, **29**:4915, 1984.

[32] P. R. Broussard and T. H. Geballe. *Phys. Rev. B.*, **35**:1664, 1987.

[33] Kevin R. Biagi, Vladimir G. Kogan, and R. Clem. *Phys. Rev. B*, **32**:7165, 1985.

[34] Klaus D. Usadel. *Phys. Rev. Lett*, **25**:507, 1970.

[35] G. Eilenberger. *Z. Phys.*, **214**:195, 1968.

[36] S. Takahashi and M. Tachiki. *Phys. Rev. B*, **33**:4620, 1986.

[37] M. G. Karkut, V. Matiasevic, L. Antognazza, J. M. Triscone, N. Missert, M. R. Beasley, and Ø. Fischer. *Phys. Rev. Lett.*, **60**:1751, 1988.

[38] Y. Kuwasawa, U. Hayano, T. Tosaka, S. Nakano, and S.Matuda. *Physica C*, **165**:173, 1990.

[39] J. Aarts, K. Korver, W. Maj, and P. H. Kes. *Physica B*, **165-166**:475, 1990.

[40] J. Aarts, K. Korver, and P. H. Kes. *Europhysics Letters*, **12**:447, 1990.

[41] W. Maj and J. Aarts. *Phys. Rev. B*, **44**:7745, 1991.

[42] P. R. Auvil, J. B. Ketterson, and S. N. Song. *J. Low Temp.*, **74**:103, 1989.

[43] P. R. Auvil, J. B. Ketterson, and S. N. Song. *Jpn. J. Appl. Phys.*, **26**:1461, 1987.

[44] H. K. Wong, B. Y. Jin, H. Q. Yang, J. B. Ketterson, and J. E. Hilliard. *J. Low Temp.*, **63**:307, 1986.

[45] H. K. Wong, H. Q. Yang, B. Y. Jin, Y. H. Shen, W. Z. Chao, J. B. Ketterson, and J. E. Hilliard. *J. Appl. Phys.*, **55**:2494, 1984.

[46] H. K. Wong and J. B. Ketterson. *J. Low Temp.*, **63**:139, 1986.

[47] B. Davis, J. Q. Zheng, P.R. Auvil, J. B. Ketterson, and J. E. Hilliard. *Superlattices Microstructures*, **4**:465, 1988.

[48] Z. Radović, L. Dobrosavljević-Grujić, A. I. Buzdin, and John R. Clem. *Phys. Rev. B*, **38**:2388, 1988.

[49] Z. Radović, M. Ledvij, L. Dobrosavljević-Grujić, A. I. Buzdin, and John R. Clem. *Phys. Rev. B*, **43**:8613, 1991.

[50] B. J. Yuan and J. P. Whitehead. *Phys. Rev. B*, **44**:6943, 1991.

[51] B. J. Yuan and J. P. Whitehead. *Phys. Rev. B*, **47**:3308, 1993.

[52] A. Lodder and R. T. W. Koperdraad. *Physica C*, **212**:81, 1993.

[53] S. Takahashi and M. Tachiki. *Phys. Rev. B*, **34**:3162, 1986.

[54] K. Yamafuji, T. Kawashima, and F. Irie. *Phys. Lett.*, **20**:122, 1966.

[55] K. Yamafuji, E. Kusayanagi, and F. Irie. *Phys. Lett.*, **21**:11, 1966.

[56] Kenji Takanaka. *J. Phys. Soc. Japan*, **58**:668, 1989.

[57] H. Fröhlich. *Proc. Roy. Soc. London*, **A215**:291, 1952.

[58] L. P. Gorkov. *Sov. Phys. JETP*, **7**:505, 1958.

[59] A. B. Migdal. *Sov. Phys. JETP*, **7**:996, 1958.

[60] L. N. Cooper. *Phys. Rev.*, **104**:1189, 1956.

[61] A. L. Fetter and J. D. Walecka. *Quantum Theory of Many-Particle Systems*. McGraw-Hill, (1971).

[62] F. J. Dyson. *Phys. Rev.*, **75**:486, 1949.

[63] F. J. Dyson. *Phys. Rev.*, **75**:1736, 1949.

[64] J. P. Burger and D. Saint-James. *Superconductivity*, Vol. 2 Chapter 16, edited by R. D. Parks. Marcel Dekker, Inc., New York, 1969.

[65] P. G. de Gennes and D. Saint-James. *Phys. Lett.*, **4**:151, 1963.

[66] D. Saint-James and E. J. Thomas and G. Sarma *Type II Superconductivity.* Pergamon Press Ltd., London, 1969.

[67] Kazumi Maki. *Physics*, **1**:127, 1964.

[68] M. Tinkham. *Introduction to Superconductivity.* McGraw-Hill, New York, 1975.

[69] F. E. Harper and M. Tinkham. *Phys. Rev.*, **172**:441, 1968.

[70] Milton Abramowitz and Irene A. Stegun. *Handbook of Mathematical Functions.* Dover Publications, Inc., New York, 1972.

[71] J. P. Burger, G. Deutscher, and E. Guyon et A. Martinet. *Phys. Lett.*, **16**:220, 1965.

[72] W. J. Tomasch and A. S. Joseph. *Phys. Rev. Lett.*, **12**:148, 1964.

[73] C. M. Falco and I. K. Schuller. *Proceedings of the fourth conference on superconductivity in d- and f-band metals.* Kernforschungsanlage, Karlsruhe, 1982.

[74] H. Homma, C.S.L. Chun, G.G.Zheng, and I.K.Schuller. *Bull. Am. Phys. Soc.*, **30**:350, 1986.

[75] Y. Kuwasawa, T. Tosaka, A. Uchiyama, S. Matuda, and S.Nakano. *Physica C*, **175**:187, 1991.

[76] W. E. Lawrence and S. Doniach. *Proceedings of the sixteenth international conference on low temperature physics.* page 361. Academic Press of Japan, Kyoto, 1971.

[77] V. I. Dediu, A. G. Sandler, and A. S. Sidorenko. *Physica C*, **162-164**:425, 1989.

[78] J. Aarts, W. Maj, K. J. d. Korver, P. Koorevar, and P. H. Kes. *Physica C*, **185-189**:2071, 1991.

[79] A. M. Clogston. *Phys. Rev. Lett.*, **9**:266, 1962.

[80] B. S. Chandrasekhar. *App. Phys. Lett.*, **1**:7, 1962.

[81] N. R. Werthamer, E. Helfand, and P. C. Hohenberg. *Phys. Rev.*, **147**:295, 1966.

[82] Y. Kuwasawa. *Private Communication.*